**Encoding Cell Cycle Regulatory Information in the Genome**

by

Elli M. Buchert

A dissertation submitted in partial fulfillment
of the requirements for the degree of
Doctor of Philosophy
(Molecular, Cellular and Developmental Biology)
in The University of Michigan
2024

Doctoral Committee:

Professor Laura A. Buttitta, Chair
Professor Scott Barolo
Professor Kenneth Cadigan
Professor Patricia Wittkopp

Elli M. Buchert

ellimeri@umich.edu

ORCID iD: 0000-0003-2413-8146

*To my family and friends for supporting me throughout this journey,*

*especially Sebastian for building me up when I needed it most.*

**Acknowledgements**

There are so many people that have supported me throughout my PhD journey. First, I would like to thank my parents for encouraging me to pursue my interest in science and supporting me in all of my academic endeavors.

I would like to thank my mentor, Laura Buttitta, for helping me navigate the doctoral program as a first-generation college graduate. Thank you for supporting me when the project ran into problems, as they always do, and helping me think critically about how to address those problems. I appreciate your rigorous approach to science, and for teaching me to hold my science to the same standards. I would also like to thank the past and present Buttitta Lab members – Shyama, Ajai, Allison, Jaimian, Liz, Deena and Navya, as well as undergraduates Joe and Ava. I appreciate the help and feedback that you all have given over the years. Liz, thank you for teaching me how to perform the bioinformatic analysis that was vital to the success of this work.

Thank you to Drs Scott Barolo, Ken Cadigan and Trisha Wittkopp for serving on my committee all these years. I appreciate all of your feedback on the project, and making sure I gained the necessary skills to complete this body of work. And thank you to Dr. Cheng-yu Lee for your feedback and advice over the years in our fortnightly joint lab meetings.

I was fortunate enough to join the Genetics Training Program at the University of Michigan in my second year. My previous career was focused on biochemistry and

immunology, so the program was a fantastic opportunity for me to learn more about genetics and foster my interest in genetics. Thank you to John Moran for overseeing the program, and checking in with me every now and then to see how I was doing.

I have lived in and around Ann Arbor since 2008, so I was very lucky to have a network of friends in the area before starting graduate school. That network has grown over the last few years, and I cannot thank them enough for not only celebrating with me during the high points, but also for being there when I was unhappy with how the work was going.

Finally, thank you to my husband Sebastian. We started dating right after I accepted my spot at Michigan, and I'm not sure you knew what you were signing up for. But we have made it, through preliminary exams, a pandemic, an engagement and getting married, buying a home, adopting the cutest cats, and now a PhD program. You have been there day in and day out, especially when I wasn't sure how I was going to finish this program. I would not have reached this point without your unwavering support. I love you and I am so excited to see where life takes us.

## Table of Contents

## List of Tables

## List of Figures

Abstract

The timing of cell cycle exit and initiation of terminal differentiation must be precisely coordinated to ensure proper development of many tissues. Additional cell cycles during development can disrupt, but not necessarily prevent, progression of terminal differentiation programs, leading to tissues with incorrect cell numbers and morphology. The mechanisms that coordinate the transition from a proliferative state to a fully differentiated post-mitotic state are not well understood, and even less is understood about how a non-cycling postmitotic state is maintained in terminally differentiated cells. The eyes and wings of the fruit fly *Drosophila melanogaster* are excellent tissues to study this phenomenon, as both tissues undergo a relatively synchronous final cell cycle before exiting the cell cycle permanently at 24h after the start of metamorphosis, coincident with visible progression of terminal differentiation programs.

Cell cycle exit in *Drosophila* wings and eyes involves the transcriptional silencing of hundreds of cell cycle genes. However, maintaining cell cycle exit relies on preventing the re-activation of three rate-limiting cell cycle genes, the G1-S cyclin, Cyclin E, the cell cycle transcriptional activator, E2F1 and the regulator of mitotic entry, cdc25c, termed String in flies. Our prior work established that after cell cycle exit, chromatin accessibility is reduced at potential regulatory elements for these three genes, leading to a hypothesis that closing chromatin maintains cell cycle exit by

preventing activation of the rate-limiting cell cycle genes. In this thesis I examine this hypothesis by developing new techniques to allow for more detailed assays of chromatin accessibility changes and chromatin modifications (Chapter 2). I also test and validate several regulatory elements for the *e2f1* and *string* loci, to determine which elements are tissue specific vs. shared for the wing and eye and examine their shut off dynamics during chromatin accessibility changes after cell cycle exit (Chapter 3). Finally, I identify a chromatin remodeler responsible for the closing of chromatin accessibility at the *string* locus, and determine that it works together with a transcription factor expressed during metamorphosis to coordinate chromatin accessibility changes that decommission enhancers at cell cycle genes and early differentiation genes, to maintain cell cycle exit as terminal differentiation progresses (Chapter 4). Altogether this work examines how complex cell cycle regulatory events can be encoded in the genome, to ensure the proper coordination of cell cycle control with cellular differentiation.

# Chapter 1: Introduction

Development of multicellular organisms begins with a period of cell growth and division, as well as patterning of the body plan, to eventually give rise to the fully formed organism. For many tissues, a precise number of cells are required to form the final functional tissue. Therefore, the number of cell divisions must be controlled and coordinated with terminal differentiation programs. It is also necessary that postmitotic tissues maintain a non-cycling state, because re-entering the cell cycle can result in tumor formation and cancer. Some aspects of how the cell cycle is shut off, for example through repression of important cell cycle genes, are understood. The mechanisms that maintain a non-cycling, postmitotic state in long-lived tissues however are still unclear. Particularly, how crucial cell cycle genes become refractory to re-activation in postmitotic, terminally differentiated tissues is not well understood.

## 1.1 The Cell Cycle

Actively proliferating cells progress through four stages of the cell cycle to achieve the goal of fully replicating their DNA and forming two daughter cells with equal numbers of chromosomes. The four stages of the cell cycle are Gap 1 (G1) phase, Synthesis (S) phase, Gap 2 (G2) phase, and Mitosis (M) phase (Figure 1.1A). Both Gap phases (G1 and G2) are periods of growth where proteins and other components necessary for growth are produced. In G1 the purpose is to ensure that the cell is ready

to fully replicate its DNA in S phase, while the purpose of G2 is to make sure that the cell is prepared to divide into two daughter cells during mitosis. There are checkpoints in G1 and G2 that confirm the cell is prepared to continue into S phase or M phase, respectively. The G1/S checkpoint, also called the restriction point, is where the cell irreversibly commits to entering S phase (Pardee, 1974).

For cells to pass the G1/S restriction point and undergo DNA synthesis, it is necessary that they have hyperphosphorylated Retinoblastoma protein (Rb), do not have DNA damage, and have inactivated anaphase-promoting complex/cyclosome and adaptor protein CDH1 (APC-C/CDH-1) (Hume et al., 2020). Rb is a cell cycle inhibitor that blocks E2F activity, the major transcription factor that drives the cell cycle. Hyperphosphorylation of Rb prevents it from inhibiting E2F activity, allowing the cell cycle to proceed (Hume et al., 2020). APC-C/CHD-1 triggers the degradation of several S phase and M phase proteins, so its inhibition is also necessary for cells to enter S phase (Hume et al., 2020).

The purpose of the G2/M checkpoint is to ensure that DNA was fully and correctly replicated during S phase, and detection of DNA damage blocks cells from entering mitosis. The G2/M checkpoint is dependent upon the activity of cyclin-dependent kinase Cdc2 (also called Cdk1) (O'Connell et al., 1997). Cdk1 only has kinase activity when bound by a cyclin, and for mitosis entry it forms a complex with Cyclin B (O'Connell et al., 1997). An inhibitory phosphorylation prevents Cdk1/Cyclin B from being active, and this site is dephosphorylated by the phosphatases Cdc25a, b, or c, giving rise to the active form (O'Connell et al., 1997). Once Cdk1/Cyclin B is active, cells will enter mitosis and divide, completing a round of cell division. Thus, activity of

cdc25 is rate-limiting for entry to mitosis. Interestingly, cdc25 activity is primarily regulated at the level of transcription for activation (Edgar et al., 1994) and it is degraded by the APC/C for its destruction (Schaeffer et al., 2004).

Proliferation of developing *Drosophila* tissues is patterned through transcriptional control of cell cycle genes by developmental signaling pathways. The *Drosophila* embryonic cell cycles are synchronized through transcriptional control of *string* (Cdc25c), so that cells destined for the same cell fate express *string* at the same time, causing them to undergo mitosis coordinately (Edgar and Lehner, 1996). In the imaginal eye disc, the final cell cycle is synchronized by a temporary G1 arrest that occurs due to expression of Decapentaplegic (Dpp) and Hedgehog (Hh) (Baker, 2007). In the larval imaginal wing disc, Dpp is expressed along the anterior-posterior boundary, and is able to trigger cell proliferation in cell autonomous and non-autonomous manners (Baker, 2007). Ectopic expression of Dpp in the anterior or posterior compartments of the developing wing causes duplications in the respective compartment, further indicating that Dpp can drive cell proliferation (Edgar and Lehner, 1996). Conversely, loss of Dpp signaling in the wing results in a severe reduction of cell proliferation, and the wing does not fully develop (Edgar and Lehner, 1996). Another developmental pathway called Wingless (Wg) is also known to be correlated with spatial cell cycle synchronization in the imaginal eye and wing discs (Edgar and Lehner, 1996). These examples indicate that signaling pathways can affect cell proliferation in different ways in different tissues, and transcriptional activation of cell cycle gene expression must be precisely controlled for proper tissue formation.

### 1.2 Transcriptional Activation

Many factors must work together to activate transcription of genes. In general, the first step of initiating transcription is for a transcriptional activator to bind the promoter of the target gene. If necessary, nucleosomes are moved by chromatin remodeling complexes to allow for other general transcription factors to bind. A large transcriptional activator complex called the Mediator binds to general transcription factors, aiding in the formation of the preinitiation complex, followed by recruitment of RNA Polymerase II (Pol II) (Krasnov et al., 2016). Transcription is initiated once the C-terminal serine 5 of Pol II is phosphorylated, followed by pausing (Krasnov et al., 2016). The Mediator complex must then dissociate from the preinitiation complex, otherwise Pol II will not transition to the elongation phase (Krasnov et al., 2016). Once the Mediator dissociates, Pol II is phosphorylated at the C-terminal serine 2, allowing for transcription to progress to the elongation phase (Krasnov et al., 2016). This indicates that in some instances, transcriptional activators are only bound for a short period of time and can actually interfere with the transcriptional process, while others are engaged for longer periods of time. Understanding how transcriptional activation occurs is necessary to understand how dynamic expression of rate-limiting cell cycle genes drives the cell cycle.

### 1.3 Rate-limiting Cell Cycle Genes

There are three rate-limiting cell cycle genes that must be transcribed at the appropriate time for the cell cycle to progress and successfully produce two daughter cells with equal DNA content. E2F is a transcription factor that regulates the overall

speed of the cell cycle. In mammals there are nine E2F proteins produced from eight genes (*e2f1 – e2f8*), with various activator and repressor functions (DeGregori and Johnson, 2006). *Drosophila* have only two E2Fs, the activator form E2F1 and the repressor form E2F2. The *Drosophila* E2Fs dimerize with their binding partner DP before they bind DNA to affect gene expression. E2F is known to regulate the expression of hundreds of cell cycle and other genes including proteins that are necessary for DNA synthesis as well as important cell cycle regulators such as the Cyclins and Cyclin-Dependent Kinases (Cdks) themselves (Asano et al., 1996). E2F protein levels increase dramatically during G1, and they rapidly decrease in S phase (Asano et al., 1996). E2F1 has been shown to primarily regulate progression of the cell cycle rather than cell growth because wing imaginal disc cells null for *e2f1* grow larger in size than controls, even though they are progressing through the cell cycle more slowly (Neufeld et al., 1998). Overexpression of *e2f1* shortens the doubling time of the cell cycle, and this is because overexpression of *e2f1* results in upregulation of Cyclin E (CycE, the G1/S regulator) and String (the G2/M regulator) (Neufeld et al., 1998). To corroborate this observation, overexpression of *cycE* + *string* together had a similar effect on doubling time, and E2F has also been shown to regulate *cycE* expression levels (Duronio and O'Farrell, 1995; Neufeld et al., 1998). Ectopic *e2f1* expression is also able to induce quiescent, or non-cycling, cells to re-enter S phase (Johnson et al., 1993). After cell cycle exit in the *Drosophila* eye disc, some expression of *e2f1* is necessary to maintain cell cycle exit, due to derepression of E2F1 target genes in *e2f1* mutant eyes (Bradley-Gill et al., 2016). The *Drosophila* retinoblastoma protein Rbf binds E2F1 and suppresses its ability to activate gene expression (Bradley-Gill et al., 2016).

In this instance, it is likely that E2F1 remains bound to its target genes, and recruits Rbf and possibly other repressors to maintain inactivity of E2F1 target genes after cell cycle exit (Bradley-Gill et al., 2016) (Figure 1.1B). Increased APC/C activity after cell cycle exit in pupal eyes and wings is thought to inhibit cycling in cells with ectopic overexpression of *e2f1*, due to APC/C degradation of String and other G2/M cyclin-Cdks (Buttitta et al., 2010). *e2f1* is unique compared to most other cell cycle genes because the regulatory region of *Drosophila e2f1* is quite large, ~40kb, and in Chapter 3 I examine fragments of this region. I show that they act as modular enhancers of *e2f1* expression in *Drosophila* larval and pupal eyes and wings.

Cyclin E is a G1-specific cyclin that is rate-limiting for the G1/S phase transition. The function of CycE is to bind and activate Cdk2, a cyclin-dependent kinase. In mammalian cell lines, overexpression of *cycE* has been shown to decrease the length of G1 phase and increase the speed of the G1/S transition (Ohtsubo and Roberts, 1993; Resnitzky et al., 1994). However, in actively proliferating cells, this shortening of G1 does not result in a faster cell cycle speed, but rather the S and G2 phases are elongated in a compensatory manner (Ohtsubo and Roberts, 1993; Resnitzky et al., 1994). In *Drosophila*, there are two Cyclin E isoforms. Type II is maternally supplied and drives the early syncytial nuclear division cycles before it is degraded (Richardson et al., 1993). Type I is expressed from the zygotic genome when it becomes active and is the main form of CycE for the rest of development (Richardson et al., 1993). *cycE* is expressed in pulses throughout the cell cycle that correlate with S phases, and expression begins in late G1 (Richardson et al., 1993). Similarly to mammals, *Drosophila* CycE is rate-limiting for entry for the G1/S transition, with expression of *cycE*

closely overlapping with S phases, and ectopic expression of *cycE* can push G1 cells to enter S phase (Richardson et al., 1995, 1993). Constitutive expression of *cycE* in imaginal wing discs greatly reduces the proportion of cells in G1, providing further evidence that CycE induces cells to exit G1 and enter S phase (Neufeld et al., 1998). Like *e2f1*, *cycE* has a large *cis*-regulatory region, and fragments of that region have been shown to drive *cycE* expression in different tissues (Jones et al., 2000). Therefore, the function of CycE to regulate the G1/S transition is evolutionarily conserved, and *cycE* expression is dynamic during the cell cycle.

String (Stg) is a rate-limiting phosphatase in *Drosophila* that regulates the G2/M phase transition. The mammalian homolog of Stg is Cdc25c, and both homologs function to activate Cdk1 (Cdc2), the mitotic kinase that forms a complex with Cyclin B, by dephosphorylation (Lehman et al., 1999). Stg is known to be rate-limiting for entry into mitosis because mutant alleles of *stg* lacking activity result in G2 arrest in embryos and imaginal wing discs (Edgar and O'Farrell, 1989; Neufeld et al., 1998). Ectopic expression of *stg* in larval imaginal wing discs promotes premature mitoses (Kylsten and Saint, 1997). Overexpression of *stg* in embryos results in early mitosis entry, and truncated G2 phases have been observed in imaginal wing discs (Edgar and O'Farrell, 1990; Neufeld et al., 1998). Even though time in G2 is truncated with overexpression of *stg*, the overall doubling time of the cell cycle is comparable to wild type, and this is accomplished by extending the time spent in G1 (Neufeld et al., 1998; Reis and Edgar, 2004). Interestingly, the *cis*-regulatory region of *stg* is much larger than that of most cell cycle genes and extends ~50kb upstream of the promoter. About 40kb of the *cis*-regulatory region has been shown to act as modular enhancers of *stg* in the embryo and

multiple stages of the neural lineages (Lehman et al., 1999). In the case of *Drosophila* embryos, different regions within the 40kb analyzed were found to drive expression of *stg* in different germ layers and mitotic domains (Lehman et al., 1999). A 15kb region was also found to drive *stg* expression in neuroblasts in a modular fashion (Lehman et al., 1999). In Chapter 3 I show that the ~50kb *cis*-regulatory region acts as modular enhancers of *stg* in larval and pupal eyes and wings. In human fibroblasts, it has been shown that Cdc25c levels are low in G1, the levels increase during the S and G2 phases, reaching a maximum amount in late G2/M phase, followed by a rapid decrease during G1 (Turowski et al., 2003). Altogether this tells us that the transcription of *stg* is not only controlled by modular enhancers, but Stg protein levels are also dynamic throughout the cell cycle.

### 1.4 Enhancers and how they contribute to gene expression

The complex regulatory regions for *e2f1, cycE* and *stg* are due to the presence of many modular enhancers. Enhancers are *cis*-regulatory DNA elements that can affect gene expression, regardless of their orientation or position, by increasing transcription levels of the target gene. Enhancers are bound by proteins, such as transcription factors, and this can occur in a sequence-specific or non-specific manner, and some of these factors can recruit other complexes like chromatin remodelers, chromatin modifiers or transcriptional machinery (Arnosti and Kulkarni, 2005). Typically, binding of one factor is not sufficient to activate an enhancer, and enhancers usually contain multiple clustered binding sites (Arnosti and Kulkarni, 2005). There are multiple models for how enhancers may function to incorporate binding of multiple factors to affect gene

expression levels. One model is the “enhanceosome” model, where there is cooperativity between transcription factors, and a complex forms from these interacting factors (Arnosti and Kulkarni, 2005). Substitution of any of the factors will drastically affect the activity of these enhancers (Arnosti and Kulkarni, 2005). Another model is the billboard model, and in this model the individual factors do not act as one large complex, but rather as more discrete groups of factors that can affect gene expression separately (Arnosti and Kulkarni, 2005).

It is thought that enhancers affect transcription by “looping”, so that the enhancer comes into physical contact with the promoter-bound basal transcriptional machinery (Figure 1.2A) (Small and Arnosti, 2020). The activity of enhancers can be cooperative, so they can be referred to as modular enhancers (Small and Arnosti, 2020). Microarrays performed in a time course of *Drosophila* pupa wings determined that genes expressed together temporally tended to have enrichment of shared enhancer motifs, suggesting that enhancers may play a role in temporal regulation of gene expression during metamorphosis (O’Keefe et al., 2012). In a study following mouse embryonic stem cells in their transition to epiblast-like cells, the *fibroblast growth factor 5* (*fgf5*) locus was found to have five enhancers that function together to drive expression of *fgf5* in a modular fashion (Thomas et al., 2021). Upon deletion, two of the enhancers reduced *fgf5* expression levels at the beginning of differentiation, while a third enhancer only reduced *fgf5* expression levels after 48 hours into differentiation (Thomas et al., 2021). The fourth enhancer appeared to be dispensable for activation of *fgf5* while the fifth enhancer was necessary to elevate *fgf5* levels at all times, indicating that it may work synergistically with the other necessary enhancers (Thomas et al., 2021). It is important

to note that because genes can have multiple enhancers, there are sometimes redundancies, where enhancers can drive expression of the same gene in the same region of a tissue, and the secondary enhancer functions as a ‘backup’ for the primary enhancer (Hong et al., 2008). These ‘backup’ enhancers were coined shadow enhancers (Hong et al., 2008). While the verification of shadow enhancers remains limited, there is extensive evidence for enhancer redundancy (Lorberbaum et al., 2016).

Enhancers have been shown to also mediate repression of gene expression, typically through the inclusion of binding sites for repressors (Small and Arnosti, 2020). Repressor binding can occur through a separate site so that both activators and repressors are bound, or they may compete with activators for an overlapping binding site (Small and Arnosti, 2020). There are two forms of repression that can occur, short-range and long-range repression. Short-range repression is when local chromatin marks are modified to prevent enhancer-promoter looping (Figure 1.2B) (Small and Arnosti, 2020). Long-range repression is thought to affect chromatin marks over a larger span of DNA as well as recruit other corepressors to not only prevent enhancer-promoter looping but to compact chromatin around the enhancer (Figure 1.2C) (Small and Arnosti, 2020). In addition, recent studies have revealed a class of elements termed “facilitators”, which do not fit the criteria for enhancers or repressors themselves, but are essential for the proper function of associated enhancers (Blayney et al., 2023).

### 1.5 Chromatin Organization

DNA compaction is necessary to fit large amounts of DNA into the nucleus, and to accomplish this goal, DNA is organized into chromatin. In eukaryotes, the

nucleosome is the smallest component of chromatin, comprised of a histone octamer consisting of two copies of histones H2A, H2B, H3 and H4, with 147 base pairs of DNA wrapped around the histone octamer. Nucleosomes are connected by linker DNA, which can vary in length, to form a “beads-on-a-string” structure that is also referred to as the 10-nm fiber. The next unit of compaction is the 30-nm chromatin fiber, where linker histones such as histone H1 bind to linker DNA, resulting in further compaction of nucleosomes (Li and Zhu, 2015). From there, chromatin is organized into higher order structures to give rise to heterochromatin, highly compacted and transcriptionally inactive regions, or euchromatin, less compacted and therefore more accessible DNA that is likely to be transcriptionally active. Certain histone marks, or modifications to histone tails, are associated with heterochromatin and euchromatin. In general, histone H3 lysine 9 (H3K9) methylation, histone H3 lysine 27 (H3K27) methylation, and histone H4 lysine 12 (H4K12) methylation are all associated with heterochromatic regions while histone H3 lysine 4 (H3K4) methylation, histone H3 lysine 36 (H3K36) methylation and histone tail acetylation are associated with euchromatin regions (Doenecke, 2014; Jenuwein and Allis, 2001). Histone phosphorylation can be associated with both heterochromatin and euchromatin (Jenuwein and Allis, 2001). This compaction of DNA into chromatin and the location of nucleosomes is not permanently fixed. Nucleosomes can be moved, edited, and ejected, and these functions are carried out by chromatin remodelers.

### 1.6 Chromatin remodelers that regulate chromatin accessibility and composition

There are four classes of ATP-dependent chromatin remodelers, the switching/sucrose non-fermenting (SWI/SNF), Imitation SWItch (ISWI), Chromodomain-Helicase-DNA binding (CHD), and Inositol requiring 80 (Ino80) families. These families contain a shared ATPase domain that is split into two lobes but have different N- and C-terminal components (Figure1.3A) (Clapier et al., 2017; Längst and Manelyte, 2015). SWI/SNF family remodelers slide and/or evict nucleosomes from DNA, and they contain a helicase-SANT (HSA) domain in their N terminus, which is able to bind actin or actin-related proteins, while the C terminus contains a bromodomain, which can bind histone acetylation marks (Längst and Manelyte, 2015). SWI/SNF remodelers slide or evict nucleosomes to create chromatin accessibility (Clapier et al., 2017). The ISWI family binds to DNA and unmodified histone tails through a HAND-SANT-SLIDE (HSS) domain located at the C terminus (Clapier et al., 2017; Längst and Manelyte, 2015). There are several remodeling complexes that fall into the ISWI family with varying roles. Some function to repress transcription by controlling nucleosome spacing and promoting chromatin compaction, while others disrupt nucleosome organization and spacing in order to promote transcriptional activation (Clapier et al., 2017; Längst and Manelyte, 2015). The CHD family of chromatin remodelers have two tandem chromodomains in the N terminus, and subclasses contain further varying domains (Längst and Manelyte, 2015). The Ino80 family are unique in that the two lobes that form the ATPase domain are spaced further apart, they also have nucleosome editing functions in that they can remove a histone from a nucleosome and replace it with a canonical or variant histone (Clapier et al., 2017; Längst and Manelyte, 2015).

### 1.7 DNA translocation mechanism of ATP-dependent chromatin remodelers

Because the ATP-dependent chromatin remodelers all have a shared ATPase domain, it is thought that they use a similar DNA translocation mechanism. Studies of monomeric DNA helicases-translocases have indicated that the two lobes of the ATPase domain, DExx (lobe 1) and HELICc (lobe2), bind to the same strand of DNA to form a DNA-binding cleft, with one lobe leading the other (Clapier et al., 2017). The space between the lobes is also a site where ATP can be bound and hydrolyzed to facilitate movement of DNA (Clapier et al., 2017). The lobes work together to bind and release DNA sequentially, moving the DNA 1-2 base pairs in one direction for each cycle of ATP binding and hydrolysis (Figure1.3B) (Clapier et al., 2017). In the case of SWI/SNF remodelers, the lobes move in the 3' to 5' direction while translocating DNA in the opposite direction (Clapier et al., 2017). This movement is more complicated however when moving DNA around nucleosomes, due to DNA-histone interactions and the twisting of DNA around nucleosomes.

The wave-ratchet-wave model is used to describe how DNA is translocated around histone octamers (Saha et al., 2005). This translocation mechanism begins with binding of the ATPase domain, also referred to as the translocase domain, to nucleosomes, at chromatin two helical turns away from the nucleosome dyad (Clapier et al., 2017). The nucleosome dyad is the center of nucleosomal DNA, where there are ~72 base pairs of nucleosomal DNA on either side (Zhou et al., 2019). DNA is then pulled towards the nucleosome dyad from the proximal entry site, approximately 50 base pairs from the translocase (Clapier et al., 2017; Saha et al., 2005). This movement is believed to utilize the sequential movement of DNA by the ATPase domain lobes as

described above. This pulling of DNA is considered the first “wave” in the model, with the additional base pair creating an under-twisted fragment of DNA and breaking DNA-histone interactions (Figure1.4) (Saha et al., 2005). This is then resolved by establishing new DNA-histone contacts, with a shift of 1bp (Saha et al., 2005). As DNA passes through the translocase domain, there is a second “wave” where the altered twisting of the DNA helix is resolved when the linker DNA is reached and DNA-histone contacts are reestablished at the end of the “wave” (Clapier et al., 2017; Saha et al., 2005). Therefore, “wave” indicates the movement of DNA through breaking and reestablishing DNA-histone interactions while “rachet” indicates the unidirectionality of the movement (Saha et al., 2005).

This mechanism has been demonstrated for the four classes of ATP-dependent chromatin remodelers, however the step sizes, or the length of DNA translocated at one time, vary. ISW2 has been shown to move smaller fragments of DNA, with a minimum of 9bp translocated in conjunction with hydrolysis of one ATP, while SWI/SNF appears to hydrolyze three to four ATP molecules to dissociate ~50bp of DNA, followed by translocation of the entire fragment and reestablishment of DNA-histone interactions (Zofall et al., 2006). Recombinant *Drosophila* Mi-2, a member of the CHD family of chromatin remodelers, has been shown to prefer a step size of 10-11 base pairs (van Vugt et al., 2009). And finally, the Ino80 family dissociates ~15 base pairs of DNA from Histone H2A to allow for nucleosome editing (Eustermann et al., 2018). Therefore, while a similar mechanism appears to be employed by the four families of ATP-dependent chromatin remodelers, the exact way that DNA is translocated varies as well as whether nucleosomes are moved, ejected, or edited.

### 1.8 Chromatin remodeling throughout the cell cycle

During the cell cycle, DNA must be fully replicated and organized into compacted chromatin so that the chromosomes can be properly separated into two daughter cells during mitosis. During S phase, when DNA is replicated, chromatin assembly factor 1 (CAF-1) is responsible for initiation nucleosome assembly, beginning with targeting the H3-H4 tetramer to newly synthesized DNA (Krude and Keller, 2001). This is followed by addition of two H2A/H2B dimers to form the nucleosome histone octamer, although this step is independent of CAF-1 function (Krude and Keller, 2001). These histones are thought to come from two sources: preexisting nucleosomes from the parental DNA strands and newly synthesized histones (Krude and Keller, 2001). Following this, CAF-1 is readily lost from euchromatin while it remains for a short time on heterochromatin (Krude and Keller, 2001). CAF-1 is known to associate with heterochromatin protein 1 (HP1), which is known to interact with nucleosomes, therefore likely having a role in heterochromatin formation (Krude and Keller, 2001). The ATP-utilizing chromatin assembly and remodeling factor (ACF) consists of an ISWI chromatin remodeler subunit and an Acf1 subunit, and ACF can act together with CAF-1 to facilitate arranging the exact and periodic positioning of nucleosomes (Krude and Keller, 2001). This establishment of initial, loosely packed nucleosomes is the first step in achieving densely packaged chromosomes that can be faithfully segregated to two daughter cells.

During mitosis, chromosomes must be condensed individually to allow for equal separation into daughter cells. Phosphorylation of histone H3 has been observed in conjunction with highly condensed chromosomes, with phosphorylation occurring at

several sites, most notably at serine 10 (Doenecke, 2014). Phosphorylation of histone H3 at serine 10 was found to recruit a histone deacetylase (HDAC), which deacetylates histone H4 at lysine 16 (Doenecke, 2014). This allows the histone H4 N-terminal tail to interact with an acidic patch of a neighboring nucleosome's H2A/H2B histone dimer, causing further condensation of the chromatin (Doenecke, 2014). From there, Structural Maintenance of Chromosomes (SMC) protein complexes such as cohesin and condensin aid in further compaction to prepare the chromosomes for mitosis (Aragon et al., 2013; Doenecke, 2014). Cohesin complexes bind DNA and maintain the paired sister chromatids, while condensins on the other hand control the shape of chromosomes by aiding in the folding of chromatin that is required to occur before mitosis (Aragon et al., 2013). Once condensed, mitotic chromosomes have formed, and mitosis can proceed, giving rise to two daughter cells with the appropriate number of chromosomes. One subclass of SWI/SNF chromatin remodelers, the BAP complex, is necessary for the *Drosophila* embryo S2 cell line to undergo mitosis, with knockdown of BAP giving rise to cells with abnormal chromosome numbers (Moshkin et al., 2007). It is also worth noting that almost no transcription takes place during mitosis, since transcription factors and other coactivators are unable to bind their target genes (Doenecke, 2014). This contrasts with other phases of the cell cycle, where many factors are produced to prepare for cell division. These chromatin remodelers not only aid in chromatin compaction throughout the cell cycle, but some have also been shown to have a role in coordinating cell cycle exit with terminal differentiation.

### 1.9 Chromatin remodelers and their role in cell cycle exit and terminal differentiation

SWI/SNF chromatin remodelers in particular have been identified as having a role in coordinating cell cycle exit and terminal differentiation. During *C. elegans* hermaphrodite development, the anchor cell (a uterine cell) must invade the gonad basement membrane in order to initiate contact of uterine-vulval cells to initiate development of the mature reproductive system (Sherwood and Sternberg, 2003). The *C. elegans* SWI/SNF chromatin remodelers BAF and PBAF regulate different aspects of this process, with BAF having a role in the G0 cell cycle arrest of the anchor cell, while PBAF works with *fos-1*, a transcription factor, in a cell cycle independent manner to affect anchor cell invasion (Smith et al., 2021). Specifically, PBAF and *fos-1* work together to regulate the invasion and attachment of the anchor cell to the basement membrane by activating pro-invasive genes that are necessary for this process to occur (Smith et al., 2021). It is also necessary for the anchor cell to exit the cell cycle before invasion of the basement membrane can occur (Smith et al., 2021). In *C. elegans* muscle precursor cells, SWI/SNF function is necessary for cell cycle exit, as knockdown of BAF components resulted in additional muscle lineage cell divisions (Ruijtenberg and van den Heuvel, 2015). Knockdown of BAF components resulted in prolonged expression of the HLH-8 Twist transcription factor, which is normally expressed only in undifferentiated muscle precursor cells (Ruijtenberg and van den Heuvel, 2015). SWI/SNF is also thought to regulate terminal differentiation of muscle because chromatin occupancy studies have shown overlap of SWI/SNF and the HLH-1 MyoD, the master regulator of muscle development, at muscle-specific genes and positive and

negative G1 regulators (Ruijtenberg and van den Heuvel, 2015). Similar over proliferation of muscle precursors has also been observed in SWI/SNF and HLH-1 MyoD knockouts (Ruijtenberg and van den Heuvel, 2015).

SWI/SNF remodelers have a role in cell cycle exit and terminal differentiation in mammalian tissues as well. SWI/SNF complexes cause upregulation of cell cycle inhibitors such as $p16^{INK4a}$ and $p15^{INK4b}$ in human rhabdoid tumor cells, initiating cell cycle arrest (Kia et al., 2008; Ruijtenberg and van den Heuvel, 2016; Wilson et al., 2010). In mouse embryos, Baf60c, a subunit of the SWI/SNF BAF complexes, is necessary for proper heart morphogenesis due to its role in targeting BAF remodeling complexes to heart-specific enhancers (Lickert et al., 2004). BAF60c has also been reported to interact with MyoD and is necessary for skeletal muscle differentiation in mammals (Ruijtenberg and van den Heuvel, 2016). These examples establish that some ATP-dependent chromatin remodelers are already known to play a role in the transition from actively proliferating cells to cell cycle exit, with a role in initiating terminal differentiation programs. While this has primarily been shown for SWI/SNF chromatin remodelers, it is possible that other ATP-dependent chromatin remodelers may serve a similar function in different organisms and tissues. In Chapter 4 I delineate a role for a CHD chromatin remodeler Mi-2 in coordinating cell cycle exit and terminal differentiation.

### 1.10 Mi-2, a CHD chromatin remodeler

*Drosophila* Mi-2 (dMi-2) is a member of the CHD family of ATP-dependent chromatin remodelers and is homologous to human CHD3 (Mi-2α) and CHD4 (Mi-2β)

(Kunert and Brehm, 2009). The dMi-2 protein is composed of 1982 amino acids and forms a 220kDa protein (Brehm et al., 2000; Kehle et al., 1998). It contains two plant homeodomain (PHD) finger motifs, two chromodomains, a high-mobility group (HMG) like domain, and SNF2-like ATPase domain (Kehle et al., 1998). dMi-2 has been shown to use ATP to slide “end” positioned nucleosomes more centrally on a DNA fragment, which is opposite of ISWI chromatin remodelers, which bind centrally located nucleosomes and mobilize them towards the ends of DNA fragments (Brehm et al., 2000). dMi-2 has been shown not to bind to free DNA or histones, and histone tails appear to be unnecessary for dMi-2 interaction with nucleosomes (Brehm et al., 2000). This is in contrast to mammalian Mi-2, as recombinant Mi-2β has been shown to be stimulated by naked DNA, although to a lesser extent than nucleosomes (Wang and Zhang, 2001). The chromodomains are necessary for nucleosome mobilization, so it is thought that dMi-2 interacts with nucleosomes and nucleosomal DNA through its chromodomains (Bouazoune et al., 2002). The exact binding motif that Mi-2 interacts with nucleosomes through is currently unknown. dMi-2 has been shown to regulate higher order chromatin structures in both larval salivary glands and imaginal wing discs, with overexpression of Mi-2 resulting in less compacted chromosomes (Fasulo et al., 2012). Overexpression of an ATPase-dead dominant-negative dMi-2 resulted in disrupted banding patterns of larval salivary gland polytene chromosomes, indicating that functional Mi-2 is necessary to regulate organization of these chromosomes (Fasulo et al., 2012). Point mutations in the ATPase domain, PHD motif, and chromodomains reduce dMi-2’s nucleosome remodeling activity, indicating that these regions are necessary for proper Mi-2 function (Kovač et al., 2018).

dMi-2 functions as the ATPase mobilization subunit for two *Drosophila* complexes, dNuRD (Nucleosome Remodeling and Deacetylase complex) and dMec. The NRD/NuRD/NURD complex was first reported in humans to have histone deacetylase and nucleosome mobilization activity as well as a role in transcriptional repression in 1998 (Tong et al., 1998; Xue et al., 1998; Zhang et al., 1998). An Mi-2 containing complex with histone deacetylase activity was identified in *Xenopus laevis* around the same time (Wade et al., 1998). The subunits of NuRD are CHD3/4 (ATPase domain), MTA1/2/3 (metastasis-associated), MBD2/3 (methyl-binding domain), HDAC1/2 (histone deacetylase), RBBP4/7 (RbAp46/48, retinoblastoma-binding proteins) and p66α/β (Dege and Hagman, 2014). In *Drosophila*, dNuRD is comprised of dMi-2, dMTA, dMBD2/3, RPD3 (also known as HDAC1), p55 (homolog of RbAp46/48) and p66/68 (Bouazoune and Brehm, 2006). It has been shown *in vitro* that NuRD complexes can bind to methylated DNA through their MBD subunits (Wade et al., 1999; Zhang et al., 1999). In *Drosophila* larval Type I neuroblasts, knockdown of Mi-2/NuRD components was found to increase Notch-induced hyperplasia, as well as enhance the expression levels of *E(spl)* genes when Mi-2 was knocked down in *Drosophila* cell lines (Zacharioudaki et al., 2019). Mi-2/NuRD was also found to have a vital role in decommissioning stem cell enhancers in the Type I lineages of neuroblast progeny and was recruited by the zinc finger repressor Zfh1 (Zacharioudaki et al., 2019).

dMec is a complex consisting of dMi-2 and dMEP-1, a zinc finger protein, and is highly expressed in early embryos, and lower levels of expression have been detected in the larval and adult stages (Kunert et al., 2009). dMec is expected to use a different mechanism to affect gene expression than dNuRD. Neither dMi-2 nor dMEP-1 have

deacetylase activities, and they have not been shown to interact with the histone deacetylase dRPD3 (Kunert et al., 2009). In *Drosophila* S2 cells, knockdown of both dMEP-1 and dMi-2 by RNAi resulted in derepression of four proneural genes of the *achaete-scute complex (AS-C)*: *achaete, scute, lethal-of-scute* and *asense* (Kunert et al., 2009). In *C. elegans*, the Mi-2 homolog LET-418 functions with MEP-1 to repress expression of germline-specific genes in somatic cells (Unhavaithaya et al., 2002). This has also been shown in the *Drosophila* larval neurons, where knockdown of dMi-2 resulted in ectopic germline gene expression, and this function was found to be a dNuRD-independent mechanism of dMi-2 (Aughey et al., 2023). There was greater overlap of dMec binding sites with upregulated genes compared to overlap with dNuRD binding sites, so this may be another function of the dMec complex (Aughey et al., 2023). Therefore, the dMec complex is suspected to repress gene expression through an HDAC-independent mechanism. These functions of Mi-2, as part of the NURD and dMec complexes, are important for repressing gene expression when necessary.

### 1.11 Other complexes regulating cell cycle exit and terminal differentiation

Several factors besides ATP-dependent chromatin remodelers have been shown to play a role in coordinating termination of the cell cycle with initiation of terminal differentiation programs. dREAM (*Drosophila* RBF, E2F and Myb) complex is a repressive complex that contains RBF1 or RBF2, dDP, dE2F2, the Myb-interacting proteins CAF1/p55, Mip40, Mip120, Mip130 (Twilight), and dMyb (Korenjak et al., 2004). While the individual components are different, similar repressive complexes have also been identified in *C. elegans* (DRM) and humans (DREAM) (Ruijtenberg and van den

Heuvel, 2016; Sadasivam and DeCaprio, 2013). The *C. elegans* DRM complex and mammalian DREAM complexes do not contain Myb, however both contain the MuvB core (Sadasivam and DeCaprio, 2013). The *C. elegans* MuvB core consists of LIN-9, LIN-37, LIN-52, LIN-53 and LIN-54 (Walston et al., 2021). The mammalian MuvB core consists of LIN9, LIN54, LIN37, LIN52 and RBBP4 (Sadasivam and DeCaprio, 2013). dREAM/DREAM has been shown to repress cell cycle genes during G0 and knockdown of some components resulted in derepression of E2F target genes (Ma et al., 2019; Sadasivam and DeCaprio, 2013). Mammalian DREAM localizes to many sites that have peak expression in early G1/S phase and late G2/M phase, indicating that it likely plays a role in cell cycle regulation (Sadasivam and DeCaprio, 2013). dREAM was found to localize to approximately one third of all promoters, indicating a possible broader function of dREAM in *Drosophila* (Sadasivam and DeCaprio, 2013). In a study performed in a human colorectal carcinoma cell line, DREAM was found to repress G1/S and G2/M cell cycle genes in response to activation of p53, a human tumor suppressor, to aid in cell cycle exit (Uxa et al., 2019). One of the late G2/M targets of DREAM is specifically Cdc25c (*stg* in *Drosophila*), where it binds the promoter in response to p53 (Sadasivam and DeCaprio, 2013). It is known to bind transcriptionally silent chromatin through non-acetylated histone H4 tails, and it does not possess any chromatin modifying enzymes such as histone deacetylases or methyltransferases (Korenjak et al., 2004). Therefore, dREAM/DRM/DREAM is an important transcriptional silencing complex that is necessary to repress cell cycle genes and cell cycle exit.

Polycomb group (PcG) and Trithorax group (TrxG) complexes have opposite effects in the genome, with PcG functioning to repress transcription while TrxG function

to maintain an active chromatin state (Ruijtenberg and van den Heuvel, 2016). TrxG possesses histone methylation abilities, and it methylates lysine 4 of histone H3 (H3K4me3), a marker of active chromatin (Schuettengruber et al., 2007). One class of TrxG proteins includes ATP-dependent chromatin remodelers such as SWI/SNF (Schuettengruber et al., 2007). PcG comprises two complexes, Polycomb Repressor Complex (PRC) 1 and 2, and PRC2 possesses the ability to methylate lysine 27 of histone H3 (H3K27me3), which is a known repressive chromatin mark (Schuettengruber et al., 2007). *Drosophila* contain known binding sequences for PcG, called PcG responsive elements (PREs). *Cyclin A* contains one such PRE site, which covers the promoter, first exon and first intron (Martinez and Cavalli, 2006). It is transcriptionally silenced by PcG in *Drosophila*, indicating a direct role for PcG in mediating cell cycle gene expression (Martinez and Cavalli, 2006). The functions of dREAM and PcG, in conjunction with ATP-dependent chromatin remodelers, contribute to the process of shutting down the cell cycle machinery to aid in cell cycle exit, and transitioning into a non-cycling G0 state.

### 1.12 States of G0

Cells that are no longer actively dividing are considered to be in a G0 state, but not all states of G0 are the same. At least three distinct G0 states have been described – reversible quiescence, terminal differentiation, and senescence (Sun and Buttitta, 2017). Reversible quiescence is the G0 state that stem cells inhabit, in that they are no longer proliferating but readily maintain the ability to re-enter the cell cycle when needed (Sun and Buttitta, 2017). Terminal differentiation occurs during development and usually

is permanent and involves chromatin changes, but in some cases, these cells can be induced to re-enter the cell cycle due to damage (Sugiura et al., 2016; Sun and Buttitta, 2017). This occurs in instances such as appendage amputation of axolotls, which triggers regeneration programs that require re-entry into the cell cycle (Sugiura et al., 2016). Senescence is another state of G0, which is an irreversible exit from the cell cycle, and this is often triggered by various types of cellular stress, aging and as a normal part of development (Sun and Buttitta, 2017). This raises the question of how cells make the decision to exit the cell cycle during development, and this is referred to as the proliferation-quiescence decision. Cells are thought to make this proliferation-quiescence decision based on the amount of Cdk2 activity after mitosis (Spencer et al., 2013). In a human breast cancer cell line, cells with an intermediate level of Cdk2 activity followed by an increase in Cdk2 activity were committed to the next cell cycle while those with a low level of Cdk2 activity after mitosis entered a G0-like state but maintained the ability to re-enter the cell cycle by increasing Cdk2 activity levels (Spencer et al., 2013). Control over the intermediate versus low levels of Cdk2 activity was ultimately found to be due to the cell cycle inhibitor p21 levels, with high p21 giving rise to “Cdk2-low” cells and low p21 giving rise to “Cdk2-intermediate” cells (Spencer et al., 2013).

Cell cycle exit is thought to involve repression of Cyclin/Cdk activity as well as Rb-mediated repression of E2F activity (Buttitta et al., 2007). Ectopic Cyclin/Cdk or E2F activity are not sufficient to maintain a cycling state however, ectopic expression of both can bypass cell cycle exit in *Drosophila* pupal tissues (Buttitta et al., 2007). The double assurance model for cell cycle exit suggests that differentiation signals prevent positive

feedback between E2F1 and CycE, to prevent proliferation when one factor is ectopically expressed, ensuring that cell cycle exit is maintained when terminal differentiation has been initiated (Buttitta et al., 2007). *Drosophila* pupal eyes and wings are excellent tissues to use as models to study how cell cycle exit is maintained in conjunction with the beginning of terminal differentiation programs. We know that in these tissues the steroid hormone ecdysone plays a role in the timing of cell cycle exit and terminal differentiation.

### 1.13 Cell cycle exit and Terminal Differentiation of the *Drosophila* eye and wing

There are three life stages for *Drosophila melanogaster*, the larval, pupal and adult stages. Each transition to the next life stage is triggered by pulses of the steroid hormone ecdysone (Niwa and Niwa, 2016). One of the largest developmental changes that corresponds to a pulse of ecdysone is the larval-to-puparium transition, when metamorphosis begins. The time spent in metamorphosis is counted in hours after puparium formation (APF), when the larvae become immobile and the epidermis begins to harden to form a pupa case. This initial transition point is considered to be 0h APF. During metamorphosis, many larval structures are degraded so that adult structures may form in their place. The exceptions to this degradation are the imaginal tissues, which include the eye and wing discs. Instead of degradation, these tissues remain, exit from the cell cycle, and undergo morphological changes to form the adult tissues. Ecdysone affects expression of many genes, and this is carried out through binding of its receptor, ecdysone receptor (EcR), which forms a heterodimer with Ultraspiracle (USP) before binding to DNA (Cranna and Quinn, 2009). Ecdysone signaling has been

tied to cell cycle regulation as well as differentiation and larval tissue cell death (Cranna and Quinn, 2009; Li and White, 2003; Rusconi et al., 2000). There is a large ecdysone pulse at ~24h APF, and this correlates with many changes in the pupal eyes and wings, most notably cell cycle exit and the initiation of terminal differentiation programs (Guo et al., 2016; O'Keefe et al., 2012).

The wing cells are known to exit the cell cycle at 24h APF, as no cycling cells have been observed beyond that time (Milán et al., 1996; O'Keefe et al., 2012). The final cell cycle is relatively synchronous because mitoses throughout the wing blade are observed between 12 and 24h APF, with very few mitoses and no S phases observed at 24h APF (Figure 1.5B) (Schubiger and Palka, 1987). During 12 – 16h APF, mitoses appear first in the anterior wing margin bristles, the posterior wing margin, and the distal ends of the L3 and L4 wing veins (Milán et al., 1996). From 16 – 24h APF, this is followed by mitoses appearing throughout the wing blade, in the wing margin, the wing veins and interveins (Milán et al., 1996).The final cell cycle is relatively synchronous due in part to the regulation of the rate-limiting cell cycle gene *stg.* It has been shown that the majority of the wing cells arrest in G2 around 6h APF, and we know that this is due to a drop in *stg* levels at this time, caused by transcriptional repression by the transcription factor Broad (Guo et al., 2016). Since Stg is rate-limiting for the G2/M transition, the drop in Stg protein levels at 6h APF means that the wing cells cannot enter mitosis, causing the G2 arrest. The transcriptional repressor Broad becomes expressed in response to the pulse of ecdysone at 0h APF, binding to regulatory elements of *stg* and causing a decrease in Stg protein levels (Guo et al., 2016). After ecdysone titers from the pulse drop, Broad protein levels drop, allowing *stg* to be re-

expressed (Guo et al., 2016). The presence of Stg means the cells can now exit the G2 arrest and proceed into mitosis, which is followed by the final cell cycle (Guo et al., 2016). Once the wing cells have exited the cell cycle at 24h APF, differentiation programs are initiated to form the final adult wing structure. Interestingly, wing vein pre-patterning begins during the late larval and early pupal stages, when the wing is initially divided into pre-vein and intervein regions (De Celis, 1998). However, the vein vs. intervein patterning and fate decisions can be re-established during pupal stages (O'Keefe et al., 2014, 2007) and wing vein cells only adopt their final cell shape beginning at 24h APF, with cell shape changes more clearly visible at 36h APF (O'Keefe et al., 2012). During this time, the intervein cells are adopting a hexagonal cell shape, aiding in the visualization of wing veins versus interveins (O'Keefe et al., 2012). At 24h APF, the wing cells have initiated formation of wing hairs, with defined wing hairs visible at 36h APF (O'Keefe et al., 2012; Ren et al., 2005). Delayed cell cycle exit in the pupal wing has been found to disrupt wing cuticle formation (Ma et al., 2019). This indicates that proper timing of cell cycle exit in the pupal wing is important for appropriate initiation of terminal differentiation programs.

While there are some differences in how the *Drosophila* eye exits the cell cycle relative to the wing, there are some similarities. The eye undergoes a final relatively synchronized cell cycle just like the wing, and cell cycle exit in the pupal eye also occurs at 24h APF (Buttitta et al., 2007). Also like the wing, the eye exits the cell cycle with the majority of cells in G1, with a 2N DNA content (Figure 1.5A) (Buttitta et al., 2007). The final cell cycle is similarly synchronized by a cell cycle arrest however the cells undergo a G1 arrest in the *Drosophila* eye (Ready et al., 1976). This arrest occurs just anteriorly

to and within the morphogenetic furrow (MF), which appears as an indentation that sweeps across the late larval eye disc from the posterior to the anterior. Cells anterior to the MF continue to proliferate asynchronously (Buttitta et al., 2007; Cagan, 2009). Similar to the wing, the G1 arrest in the morphogenetic furrow is due in part to the regulation of *stg*. Just anterior to the MF, there is a burst of *stg* expression, pushing cells in front of the MF to undergo mitosis, giving rise to cells with a G1 DNA content (Alphey et al., 1992; Thomas et al., 1994). While most cells in the MF temporarily arrest in G1, there are a few cells that exit the cell cycle. These cells that exit within the MF and begin differentiation are the first five photoreceptors, R2, R3, R4, R5, and R8, and they form the photoreceptor precluster within the MF (Cagan, 2009; Ready et al., 1976). The majority of remaining cells will exit the G1 arrest to undergo one more round of cell division, and this is referred to as the second mitotic wave (SMW) (Thomas et al., 1994). The passage of the MF and completion of the SMW occurs by ~12h APF, and most cells have exited the cell cycle with a G1 DNA content (Meserve and Duronio, 2017). The exceptions to this are the sensory organ precursor cells (SOPs) that arrest in G2 after the MF passes across the eye (Meserve and Duronio, 2017). The SOPs will undergo a final round of cell division between 12 – 24h APF, and this begins centrally in the eye and proceeds radially (Cagan and Ready, 1989; Meserve and Duronio, 2017). These extra cell divisions give rise to additional cells that can be recruited in a lineage-independent manner to form the final eye structure (Ready et al., 1976). The first unspecified cells to be recruited give rise to the remaining photoreceptors, R1, R6 and R7, followed by four cone cells, and two primary pigment cells, which form the 14-cell ommatidial core (Cagan, 2009). Finally, secondary and tertiary pigment cells as well as

mechanosensory bristle groups, which are made up of four-cell clusters, are formed around the ommatidial core to give rise to the final ommatidial structure (Cagan, 2009; Meserve and Duronio, 2017). In eyes containing mutated *retinoblastoma* (*rbf*) and *dacapo* (*dap*, a cell cycle inhibitor), the cells continued to proliferate posterior to the MF, and the resulting ommatidia contained pairs of smaller R8 photoreceptor cells, rather than a single R8 photoreceptor (Firth and Baker, 2005). This indicates that additional rounds of cell division beyond the normal cell cycle exit timing affects terminal differentiation, resulting in altered eye structure. Later on in development, apoptosis occurs to remove extra cells not included in the ommatidia (Baker, 2001). The first and largest wave of apoptosis occurs between 20 – 36h APF, and a smaller but prolonged second wave of apoptosis occurs between 36 – 100h APF (Cagan and Ready, 1989). From approximately 50 - 60h APF onwards, the photoreceptors form rhabdomeres, eye pigmentation develops, the corneal lens is secreted and bristles form (Cagan and Ready, 1989). The final *Drosophila* adult compound eye contains anywhere from 700 to 800 ommatidia, arranged in a precise and repeating hexagonal lattice structure (Cagan, 200; Jones and Moses, 2004).

### 1.14 Ecdysone signaling

As stated earlier, 20-hydroxyecdysone, or the active form of ecdysone, is a steroid hormone that is periodically pulsed throughout *Drosophila* development, and it triggers the transition to subsequent stages of the *Drosophila* life cycle and as well as cell cycle exit and terminal differentiation in the eye and wing. Studies were performed in *Drosophila* larval salivary glands by Ashburner and colleagues, where it was

observed that the large, polytene chromosomes undergo sequential puffing that corresponds to gene expression changes in response to ecdysone (Ashburner and Richards, 1976). In cultured salivary glands, the early puffs, or the first genes to be induced in response to ecdysone, include 23E, 74EF and 75B (Ashburner and Richards, 1976). These early puffs eventually regress and become refractory to reinduction by subsequent exposure to ecdysone, indicating that their expression is actively inhibited (Ashburner and Richards, 1976). The early late puffs include 62E and 78D, and these puffs regress in the absence of ecdysone, but remain re-inducible (Ashburner and Richards, 1976). The late puffs include 22C, 63E and 82F, and these puffs appear to be induced by the protein products of the early puffs and are ecdysone independent (Ashburner and Richards, 1976). This has led to the model that ecdysone initiates a cascade of gene expression and repression, that begins with ecdysone activating the early genes, which not only activate early-late genes but also late-late genes, and the early genes form a negative feedback loop to inhibit their own expression (Figure 1.6A) (Thummel, 2002). This signaling pathway induced by ecdysone and its receptor is most similar to the retinoic acid receptor signaling pathway in mammals (Laudet, 1997).

Ecdysone signaling has effects on development and terminal differentiation, and the ecdysone receptor (EcR) has been found to interact with other proteins and complexes to aid in the ecdysone response. EcR interacts with NURF, another *Drosophila* ATP-dependent chromatin remodeling complex, to affect expression of several ecdysone responsive genes, and larvae null for NURF do not undergo pupariation (Badenhorst et al., 2005). EcR was also found to interact with dMi-2 in

*Drosophila* S2 cells, and Mi-2 constrains activation of ecdysone induced genes such as *Broad-Complex* and *vrille* (Kreher et al., 2017). In line with this, ecdysone signaling has been shown to play a role in synchronizing the final cell cycle in the *Drosophila* pupal wing, as well as coordinating cell cycle exit timing with the initiation of terminal differentiation programs through a cascade of gene expression (Figure 1.6B) (Guo et al., 2016). Genome-wide DNA binding experiments around the time of the larval to puparium transition in *Drosophila* wings found that EcR localized to not only ecdysone-responsive genes but also to wing-specific genes (Uyehara and McKay, 2019). Furthermore, knockdown of EcR via RNAi was found to prevent wing disc eversion, suggesting that EcR and therefore ecdysone signaling is necessary for proper pupal wing development (Uyehara and McKay, 2019). Together these indicate that ecdysone signaling and EcR are important not only for activating the ecdysone cascade, but also other genes necessary to achieve properly formed *Drosophila* tissues.

### 1.15 Ecdysone-induced protein 93F

The ecdysone cascade of gene activation was originally studied in larval salivary glands. Further studies identified that several of these genes are re-induced in pupal salivary glands in response to the pulse of ecdysone that triggers the larval to puparium transition (Richards, 1976a, 1976b). In addition, some puffs not induced during larval development acquire competency to respond to ecdysone during the pupal stages, including E93 (Richards, 1976a). Ecdysone-induced protein 93F (Eip93/E93) is considered a stage-specific early puff of the ecdysone cascade and is directly induced by ecdysone hormone in most tissues, with the highest RNA titers observed between

12-18h APF (Baehrecke EH and Thummel CS, 1995). E93 is a transcription factor that is necessary to promote adult development in hemimetabolous insects, where metamorphosis affects only a few tissues, and holometabolous insects, where metamorphosis affects all tissues (Ureña et al., 2014). Strong loss of function alleles of E93 have been shown to result in late pupal stage lethality, as well as defects in cuticle development and pigmentation (Lam et al., 2022). In addition to being expressed in developing adult tissues, E93 is necessary for bract cell formation (single cell pigmented outgrowths next bristle cells) in pupal legs, allowing the gene *Distal-less* (*Dll*) to respond to epidermal growth factor receptor (EGFR) signaling, and restricting this activation to the pupal stage (Mou et al., 2012). E93 has also been found to affect chromatin accessibility. Chromatin accessibility data from pupal wings mutant for E93 found that loss of E93 function resulted in chromatin accessibility changes at thousands of peaks (Uyehara et al., 2017). These changes fell into three categories – failure to open late-stage peaks, failure to close early-stage peaks, and peaks where chromatin accessibility was unchanged (Uyehara et al., 2017). For some of these, peaks that failed to open had a corresponding loss of enhancer activity, peaks that failed to close had prolonged enhancer activity, and others with unchanged chromatin accessibility failed to activate enhancer activity (Uyehara et al., 2017). To corroborate this, precocious activity of E93 in larval wings was found to prematurely terminate some early-acting enhancer activity and premature activate some late-acting enhancers, and these enhancers showed corresponding premature closing and opening of chromatin, respectively (Nystrom et al., 2020). These factors indicate that not only is E93 necessary to complete the larval to pupal transition, but it is also necessary for proper

activation of genes involved in development of adult tissues as well as repression of larval genes. The mammalian ortholog of E93, LCORL, was found to interact with CHD4 (Mi-2β) in human cell lines (Sakaguchi et al., 2022). CHD4 and LCORL were found to regulate an overlapping subset of Notch-related genes, which were upregulated upon knockdown of CHD4 or LCORL (Sakaguchi et al., 2022). This combined with the chromatin accessibility changes due to E93 knockdown and precocious activity of E93 indicates that E93 may be able to interact with chromatin remodelers to regulate gene expression.

In my thesis, I sought to investigate how enhancers of cell cycle genes are remodeled and closed after cell cycle exit. To achieve this, I developed a tissue dissociation protocol, described in Chapter 2, that is compatible with *Drosophila* pupal eyes and wings so that we could perform enzymatic genome-wide studies such as ATAC-seq and CUT&RUN. I also verified that many fragments of the large *cis*-regulatory regions of *e2f1* and *stg* are modular eye and wing enhancers throughout metamorphosis in Chapter 3. Specifically in the *Drosophila* wing, we observed that the combination of enhancers is necessary to recapitulate the endogenous expression patterns of *e2f1* and *stg.* Finally, in Chapter 4, I use the tissue dissociation protocol to perform ATAC-seq in pupal eyes, to observe the effects of disrupted Mi-2 function on chromatin accessibility during the final cell cycle. I combined this ATAC-seq dataset with RNA-sequencing data from pupal eyes with disrupted Mi-2 function or knockdown of E93 during the final cell cycle. I observed that Mi-2 and E93 appear to co-regulate a subset of genes, including cell cycle genes and terminal differentiation genes.

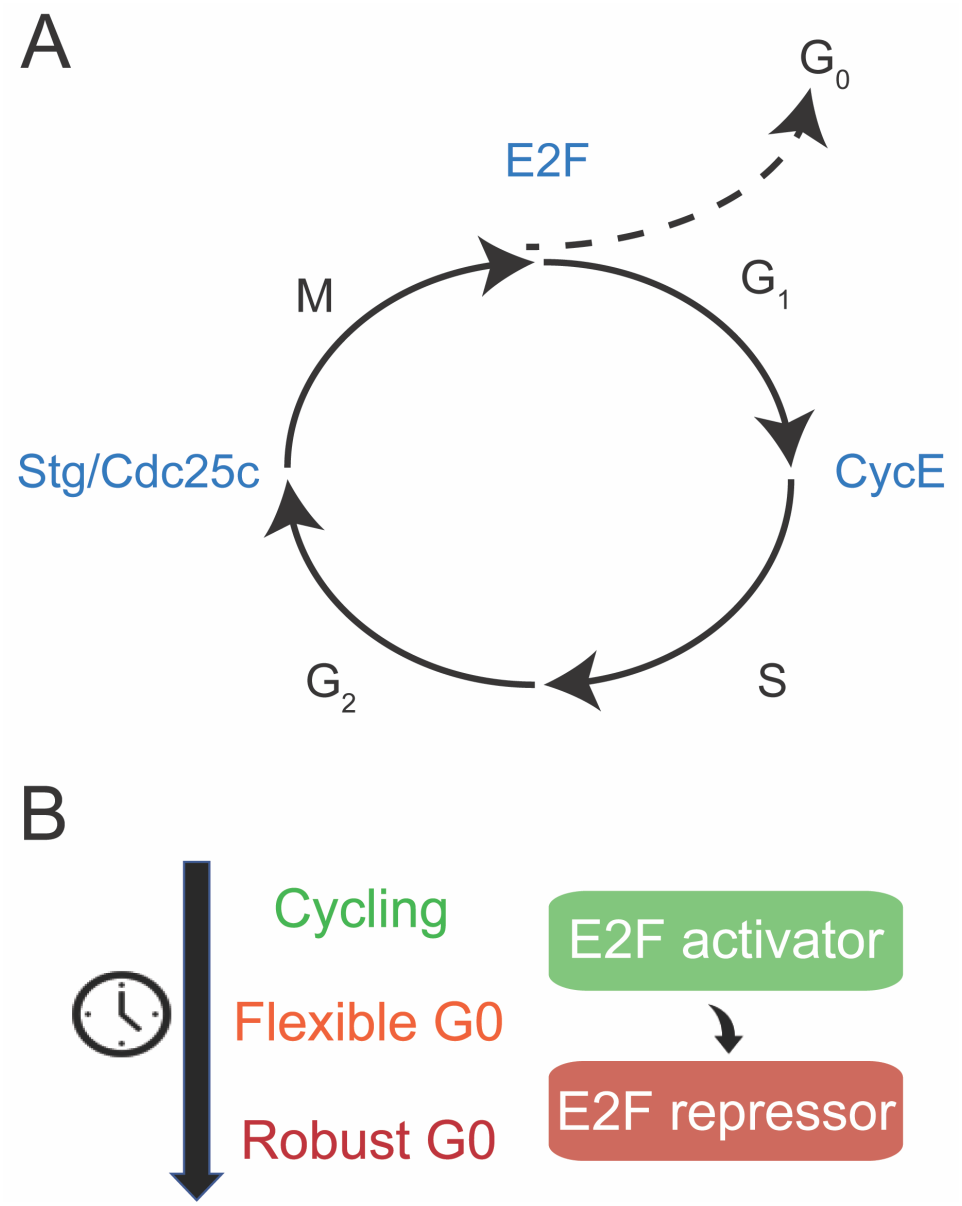


**Figure 1.1 Cell Cycle Diagram. (A)** Diagram of the cell cycle phases with depiction of where rate-limiting cell cycle genes function during the cell cycle. E2F affects the overall rate of the cell cycle, CycE is rate-limiting for the G1/S transition, and Stg is rate-limiting for the G2/M transition. **(B)** As cells transition from a cycling to a Robust G0 state, E2F complex also transitions from an activator E2F complex to a repressor E2F complex.

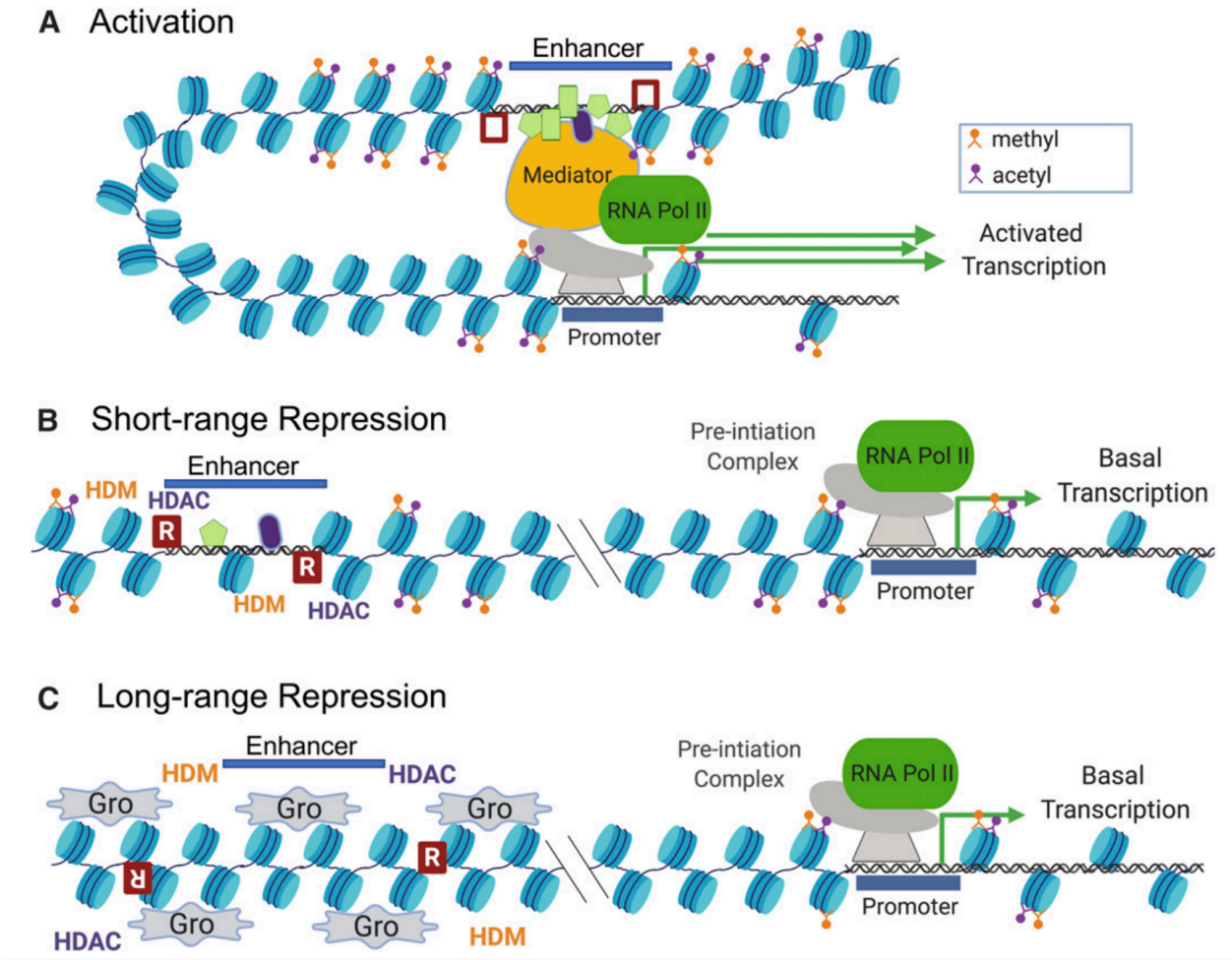


**Figure 1.2 Mechanism of Enhancer Activation and Repression.** Copied from Small and Arnosti, 2020. **(A)** Activator transcription factors can recruit histone methyltransferases and acety transferases to deposit active chromatin marks. This can be followed by enhancer-promoter looping, where enhancer and promoter are brought into close proximity to interact with transcription factors and RNA Pol II. **(B)** Short-range repression occurs when sequence specific repressors bind, recruiting histone demethylases and deacetylases. These prevent activator binding and enhancer-promoter looping. **(C)** Long-range repression occurs when corepressors (such as Groucho) bind along stretches of chromatin, recruiting additional histone demethylases and deacetylases to remove active chromatin marks from a larger region of chromatin.

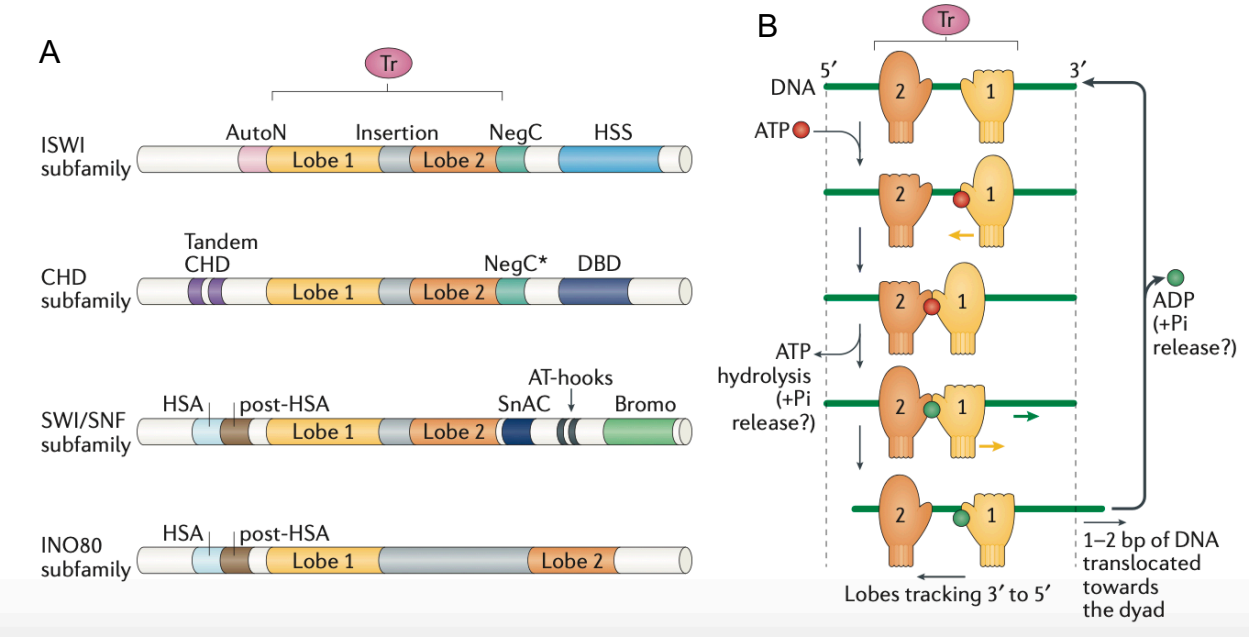


**Figure 1.3 ATP-dependent Chromatin Remodelers and Mechanism of Translocation.** Copied from Clapier et al., 2017. **(A)** Shows domains of ATP-dependent chromatin remodelers. **(B)** Simplified view of how the two lobes (depicted as mittens) function together in the translocase (Tr) domain to use and hydrolyze ATP in order to move DNA. Closed mittens indicate when the lobe has a high affinity for DNA, open mitten indicates low affinity for DNA. Yellow arrows indicate directional movement of chromatin remodelers, and green arrows represent the direction of DNA translocation.

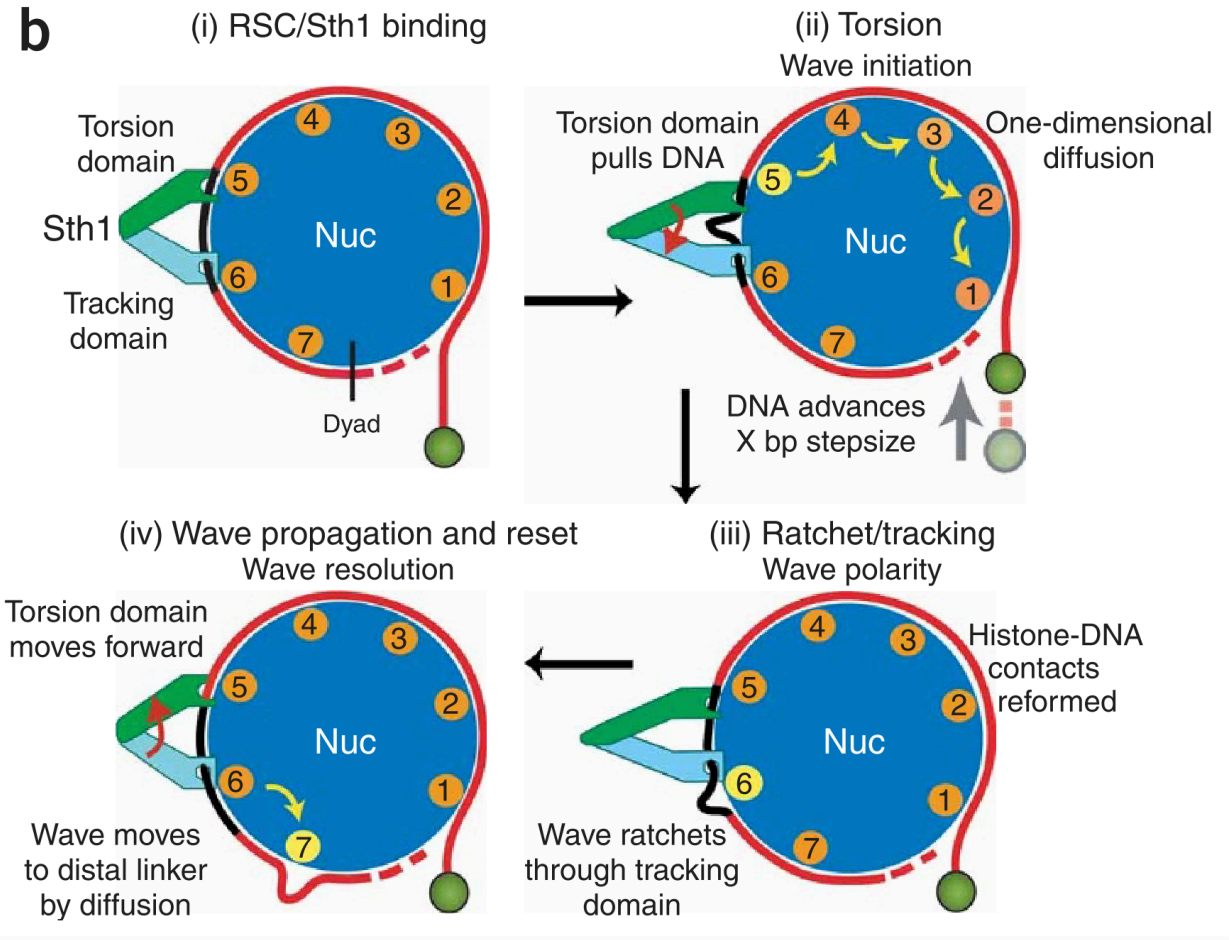


**Figure 1.4 Wave-Rachet-Wave Model of DNA Translocation.** Copied from Saha et al., 2005. Half nucleosome shown in blue from top view, DNA shown in red, orange/yellow circles indicate histone-DNA contacts (yellow indicates broken histone-DNA contact, while orange indicates intact histone-DNA contact), Sth1 torsion and tracking (translocase) domains shown in green and light blue, respectively. **(i)** RSC/Sth1 (a yeast SWI/SNF chromatin remodeler, Sth1 is the catalytic subunit) binds to nucleosome, **(ii)** torsion domain pulls DNA initiating a "wave" of breaking and reforming histone DNA-contacts beginning with position 5 (can also occur simultaneously at multiple histone-DNA contacts), **(iii)** the wave is pulled through the tracking domain, which causes breakage of the histone-DNA contact at position 6, **(iv)** the second "wave" of breaking and reforming histone-DNA contacts moves distally from the translocase domain

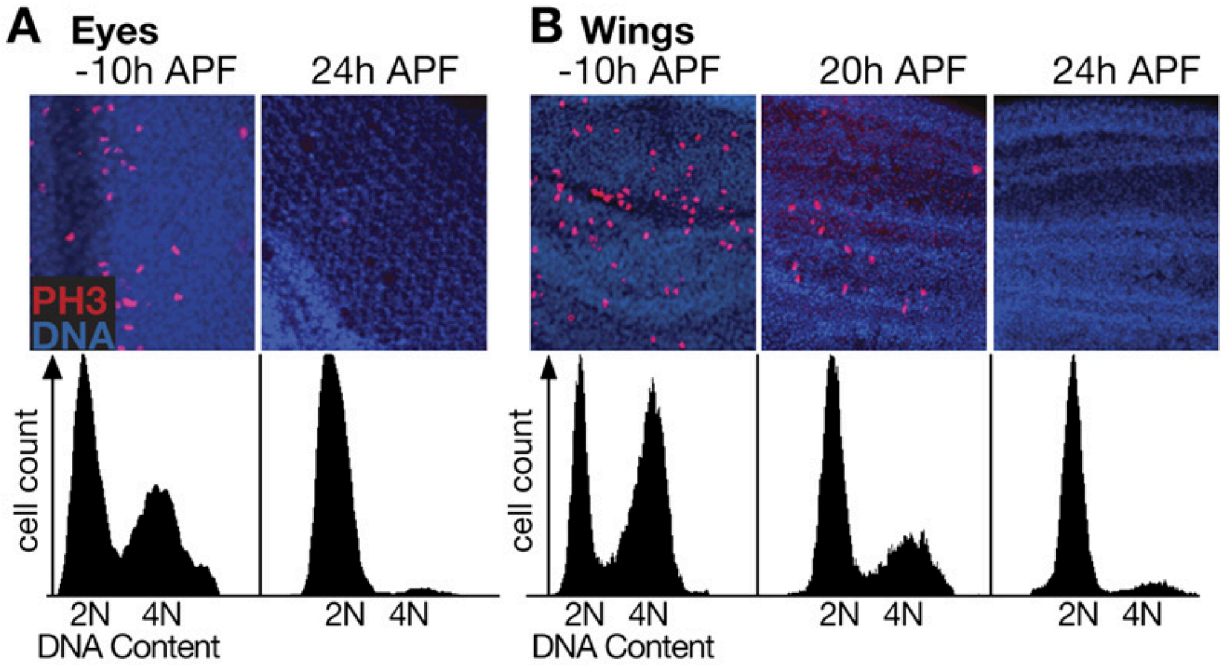


**Figure 1.5 Cell Cycle Exit in *Drosophila* eyes and wings.** Copied from Buttitta et al., 2007. **(A)** Phosphorylated histone H3 (PH3) staining in -10h (3rd instar larvae) and 24h APF wild-type eyes. Below are fluorescence-activated cell sorting (FACS) plots showing the proportion of cells with a 2N (G1) and 4N (G2) DNA content. **(B)** Same as (A) but for wild-type wings at -10h, 20h and 24h APF.

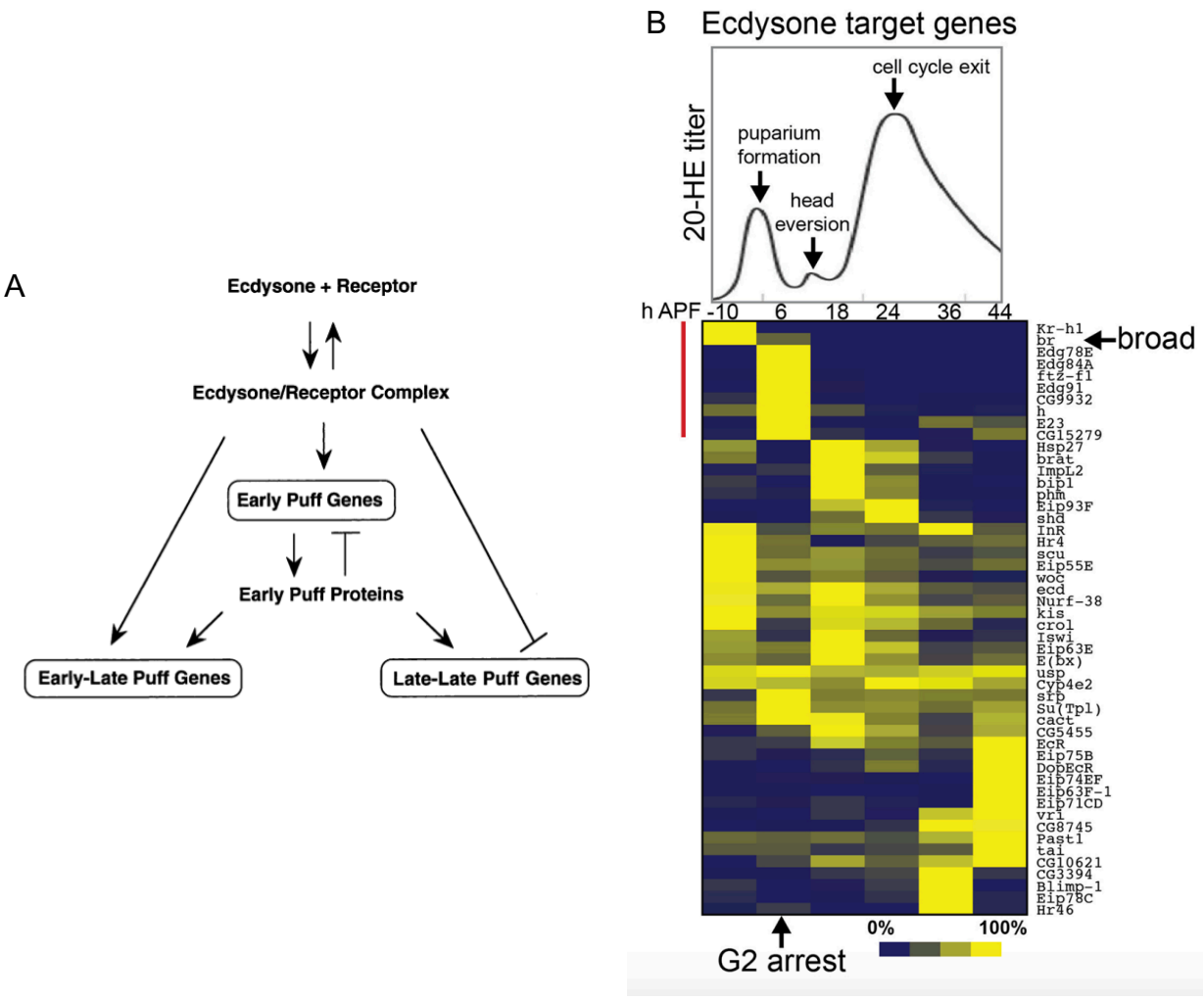


**Figure 1.6 Ecdysone Cascade Model.** A) Copied from Thummel, 2002. B) Copied from Guo et al., 2016. **(A)** Modification of the Ashburner model of the ecdysone puff gene expression cascade. Ecdysone directly activates early puffs, which in turn induce expression of late-late puffs while simultaneously repressing their own expression. The early-late puffs are induced by the early puffs as well as ecdysone directly, causing them to be expressed before the late-late puffs. **(B)** Chart showing ecdysone titers throughout metamorphosis with notable developmental events indicated. Below is showing known ecdysone targets clustered based on their gene expression changes in the *Drosophila* wing throughout metamorphosis. Red vertical line indicates ecdysone targets induced around the time of cell cycle arrest

## 1.16 References


Ahringer, J., 2000. NuRD and SIN3 histone deacetylase complexes in development. Trends Genet 16, 351–356. https://doi.org/10.1016/S0168-9525(00)02066-7

Albini, S., Coutinho Toto, P., Dall'Agnese, A., Malecova, B., Cenciarelli, C., Felsani, A., Caruso, M., Bultman, S.J., Puri, P.L., 2015. Brahma is required for cell cycle arrest and late muscle gene expression during skeletal myogenesis. EMBO Rep 16, 1037–1050. https://doi.org/10.15252/EMBR.201540159

Alphey, L., Jimenez, J., White-Cooper, H., Dawson, L., Nurse, P., Glover, D.M., 1992. twine, a cdc25 Homolog That Functions in the Male and Female Germline of Drosophila, Cell. https://doi.org/10.1016/0092-8674(92)90616-k

Andrade-Zapata, I., Baonza, A., 2014. The bHLH factors extramacrochaetae and daughterless control cell cycle in Drosophila imaginal discs through the transcriptional regulation of the Cdc25 phosphatase string. PLoS Genet 10. https://doi.org/10.1371/JOURNAL.PGEN.1004233

Aragon, L., Martinez-Perez, E., Merkenschlager, M., 2013. Condensin, cohesin and the control of chromatin states. Curr Opin Genet Dev 23, 204–211. https://doi.org/10.1016/J.GDE.2012.11.004

Arnosti, D.N., Kulkarni, M.M., 2005. Transcriptional enhancers: Intelligent enhanceosomes or flexible billboards? J Cell Biochem. https://doi.org/10.1002/jcb.20352

Asano, M., Nevins, J.R., Wharton, R.P., 1996. Ectopic E2F expression induces S phase and apoptosis in Drosophila imaginal discs. Genes Dev 10, 1422–1428. https://doi.org/10.1101/GAD.10.11.1422

Ashburner, M., Richards, G., 1976. Sequential gene activation by ecdysone in polytene chromosomes of Drosophila melanogaster. III. Consequences of ecdysone withdrawal. Dev Biol 54, 241–255. https://doi.org/10.1016/0012-1606(76)90302-X

Aughey, G.N., Forsberg, E., Grimes, K., Zhang, S., Southall, T.D., 2023. NuRD-independent Mi-2 activity represses ectopic gene expression during neuronal maturation. EMBO Rep 24. https://doi.org/10.15252/embr.202255362

Badenhorst, P., Xiao, H., Cherbas, L., Kwon, S.Y., Voas, M., Rebay, I., Cherbas, P., Wu, C., 2005. The Drosophila nucleosome remodeling factor NURF is required for Ecdysteroid signaling and metamorphosis. Genes Dev 19, 2540–2545. https://doi.org/10.1101/gad.1342605

Baehrecke EH, Thummel CS, 1995. The Drosophila E93 Gene from the 93F Early Puff Displays Stage and Tissue Specific Regulation by 20-Hydroxyecdysone. Dev Biol 171, 85–97. https://doi.org/10.1006/dbio.1995.1262

Bai, Huiru, Lin, M., Meng, Y., Bai, Huiyuan, Cai, S., 2022. An improved CUT&RUN method for regulation network reconstruction of low abundance transcription factor. Cell Signal 96. https://doi.org/10.1016/J.CELLSIG.2022.110361

Baker, N.E., 2001. Cell proliferation, survival, and death in the Drosophila eye. Semin Cell Dev Biol 12, 499–507. https://doi.org/10.1006/scdb.2001.0274

Baker, N. E. 2007. Patterning signals and proliferation in Drosophila imaginal discs. *Current Opinion in Genetics & Development*, *17*(4), 287–293. https://doi.org/10.1016/J.GDE.2007.05.005

Blayney, J. W., Francis, H., Rampasekova, A., Camellato, B., Mitchell, L., Stolper, R., Cornell, L., Babbs, C., Boeke, J. D., Higgs, D. R., & Kassouf, M. 2023. Super-enhancers include classical enhancers and facilitators to fully activate gene expression. *Cell*, *186*(26). https://doi.org/10.1016/J.CELL.2023.11.030

Bouazoune, K., Brehm, A., 2006. ATP-dependent chromatin remodeling complexes in Drosophila. Chromosome Res 14, 433–449. https://doi.org/10.1007/S10577-006-1067-0

Bouazoune, K., Mitterweger, A., Längst, G., Imhof, A., Akhtar, A., Becker, P.B., Brehm, A., 2002. The dMi-2 chromodomains are DNA binding modules important for ATP-dependent nucleosome mobilization. EMBO J 21, 2430–2440. https://doi.org/10.1093/emboj/21.10.2430

Bradley-Gill, M.R., Kim, M., Feingold, D., Yergeau, C., Houde, J., Moon, N.S., 2016. Alternate transcripts of the Drosophila “activator” E2F are necessary for maintenance of cell cycle exit during development. Dev Biol 411, 195–206. https://doi.org/10.1016/j.ydbio.2016.02.004

Brehm, A., Längst, G., Kehle, J., Clapier, C.R., Imhof, A., Eberharter, A., Müller, J., Becker, P.B., 2000. dMi-2 and ISWI chromatin remodeling factors have distinct nucleosome binding and mobilization properties. EMBO J 19, 4332–4341. https://doi.org/10.1093/emboj/19.16.4332

Buttitta, L.A., Edgar, B.A., 2007. Mechanisms controlling cell cycle exit upon terminal differentiation. Curr Opin Cell Biol 19, 697–704. https://doi.org/10.1016/J.CEB.2007.10.004

Buttitta, L.A., Katzaroff, A.J., Edgar, B.A., 2010. A robust cell cycle control mechanism limits E2F-induced proliferation of terminally differentiated cells in vivo. Journal of Cell Biology 189, 981–996. https://doi.org/10.1083/jcb.200910006

Buttitta, L.A., Katzaroff, A.J., Perez, C.L., de la Cruz, A., Edgar, B.A., 2007. A Double-Assurance Mechanism Controls Cell Cycle Exit upon Terminal Differentiation in Drosophila. Dev Cell 12, 631–643. https://doi.org/10.1016/j.devcel.2007.02.020

Cagan, R., 2009. Chapter 5 Principles of Drosophila Eye Differentiation, in: Current Topics in Developmental Biology. pp. 115–135. https://doi.org/10.1016/S0070-2153(09)89005-4

Cagan, R.L., Ready, D.F., 1989. The emergence of order in the Drosophila pupal retina. Dev Biol 136, 346–362. https://doi.org/10.1016/0012-1606(89)90261-3

Clapier, C.R., Iwasa, J., Cairns, B.R., Peterson, C.L., 2017. Mechanisms of action and regulation of ATP-dependent chromatin-remodelling complexes. Nat Rev Mol Cell Biol 18, 407–422. https://doi.org/10.1038/nrm.2017.26

Cranna, N., Quinn, L., 2009. Impact of steroid hormone signals on Drosophila cell cycle during development. Cell Div 4. https://doi.org/10.1186/1747-1028-4-3

De Celis, J.F., 1998. Positioning and differentiation of veins in the Drosophila wing. International Journal of Developmental Biology 42, 335–343. https://doi.org/10.1387/ijdb.9654017

Dege, C., Hagman, J., 2014. Mi-2/NuRD chromatin remodeling complexes regulate B and T-lymphocyte development and function. Immunol Rev 261, 126–140. https://doi.org/10.1111/imr.12209

DeGregori, J., Johnson, D., 2006. Distinct and Overlapping Roles for E2F Family Members in Transcription, Proliferation and Apoptosis. Curr Mol Med 6, 739–748. https://doi.org/10.2174/1566524010606070739

Dimova, D.K., Stevaux, O., Frolov, M. V., Dyson, N.J., 2003. Cell cycle-dependent and cell cycle-independent control of transcription by the Drosophila E2F/RB pathway. Genes Dev 17, 2308–2320. https://doi.org/10.1101/GAD.1116703

Djiane, A., Krejci, A., Bernard, F., Fexova, S., Millen, K., Bray, S.J., 2013. Dissecting the mechanisms of Notch induced hyperplasia. EMBO J 32, 60. https://doi.org/10.1038/EMBOJ.2012.326

Dobin, A., Davis, C.A., Schlesinger, F., Drenkow, J., Zaleski, C., Jha, S., Batut, P., Chaisson, M., Gingeras, T.R., 2013. STAR: Ultrafast universal RNA-seq aligner. Bioinformatics 29, 15–21. https://doi.org/10.1093/bioinformatics/bts635

Doenecke, D., 2014. Chromatin dynamics from S-phase to mitosis: contributions of histone modifications. Cell Tissue Res 356, 467–475. https://doi.org/10.1007/S00441-014-1873-1

Duronio, R.J., O'Farrell, P.H., 1995. Developmental control of the G1 to S transition in Drosophila: cyclin E is a limiting downstream target of E2F. Genes Dev 9, 1456–1468. https://doi.org/10.1101/GAD.9.12.1456

Edgar, B.A., Lehman, D.A., O'Farrell, P.H., 1994. Transcriptional regulation of string (cdc25): a link between developmental programming and the cell cycle. Development 120, 3131–3143. https://doi.org/10.1242/DEV.120.11.3131

Edgar, B. A., Lehner, C. F. 1996. Developmental control of cell cycle regulators: a fly's perspective. *Science (New York, N.Y.)*, *274*(5293), 1646–1652. https://doi.org/10.1126/SCIENCE.274.5293.1646

Edgar, B.A., O'Farrell, P.H., 1990. The Three Postblastoderm Cell Cycles of Drosophila Embryogenesis Are Regulated in G2 by string. Cell 62, 469. https://doi.org/10.1016/0092-8674(90)90012-4

Edgar, B.A., O'Farrell, P.H., 1989. Genetic control of cell division patterns in the Drosophila embryo. Cell 57, 177–187. https://doi.org/10.1016/0092-8674(89)90183-9

Elfring, L.K., Daniel, C., Papoulas, O., Deuring, R., Sarte, M., Moseley, S., Beek, S.J., Ross Waldrip, W., Daubresse, G., Depace, A., Kennison, J.A., Tamkun, J.W., Tamkun, J., 1998. Genetic Analysis of brahma : The Drosophila Homolog of the Yeast Chromatin Remodeling Factor SWI2/SNF2. Genetics 148, 251–265. https://doi.org/10.1093/genetics/148.1.251

Eustermann, S., Schall, K., Kostrewa, Di., Lakomek, K., Strauss, M., Moldt, M., Hopfner, K.P., 2018. Structural basis for nucleosome remodeling by the INO80 complex. Nature 556, 386. https://doi.org/10.1038/S41586-018-0029-Y

Evans, C.J., Olson, J.M., Ngo, K.T., Kim, E., Lee, N.E., Kuoy, E., Patananan, A.N., Sitz, D., Tran, P.T., Do, M.T., Yackle, K., Cespedes, A., Hartenstein, V., Call, G.B., Banerjee, U., 2009. G-TRACE: Rapid Gal4-based cell lineage analysis in Drosophila. Nat Methods 6, 603–605. https://doi.org/10.1038/nmeth.1356

Fasulo, B., Deuring, R., Murawska, M., Gause, M., Dorighi, K.M., Schaaf, C.A., Dorsett, D., Brehm, A., Tamkun, J.W., 2012. The Drosophila Mi-2 Chromatin-Remodeling Factor Regulates Higher-Order Chromatin Structure and Cohesin Dynamics In Vivo. PLoS Genet 8. https://doi.org/10.1371/journal.pgen.1002878

Firth, L.C., Baker, N.E., 2005. Extracellular signals responsible for spatially regulated proliferation in the differentiating Drosophila eye. Dev Cell 8, 541–551. https://doi.org/10.1016/j.devcel.2005.01.017

Flegel, K., Grushko, O., Bolin, K., Griggs, E., Buttitta, L., 2016. Roles for the Histone Modifying and Exchange Complex NuA4 in Cell Cycle Progression in Drosophila melanogaster. Genetics 203, 1265–1281. https://doi.org/10.1534/GENETICS.116.188581

Freeman, M., 1996. Reiterative use of the EGF receptor triggers differentiation of all cell types in the Drosophila eye. Cell 87, 651–660. https://doi.org/10.1016/S0092-8674(00)81385-9

Gelbart, M.E., Bachman, N., Delrow, J., Boeke, J.D., Tsukiyama, T., 2005. Genome-wide identification of Isw2 chromatin-remodeling targets by localization of a catalytically inactive mutant. Genes Dev 19, 942–954. https://doi.org/10.1101/GAD.1298905

Graves, B.J., Schubiger, G., 1982. Cell cycle changes during growth and differentiation of imaginal leg discs in Drosophila melanogaster. Dev Biol 93, 104–110. https://doi.org/10.1016/0012-1606(82)90243-3

Guo, Y., Flegel, K., Kumar, J., McKay, D.J., Buttitta, L.A., 2016. Ecdysone signaling induces two phases of cell cycle exit in Drosophila cells. Biol Open 5, 1648–1661. https://doi.org/10.1242/bio.017525

Hay, B.A., Wolff, T., Rubin, G.M., 1994. Expression of baculovirus P35 prevents cell death in Drosophila. Development 120, 2121–2129. https://doi.org/10.1242/DEV.120.8.2121

Hong, J.-W., Hendrix, D.A., Levine, M.S., 2008. Shadow Enhancers as a Source of Evolutionary Novelty. Science 321, 1314. https://doi.org/10.1126/science.ll60631

Hume, S., Dianov, G.L., Ramadan, K., 2020. A unified model for the G1/S cell cycle transition. Nucleic Acids Res 48, 12483–12501. https://doi.org/10.1093/NAR/GKAA1002

Jenett, A., Rubin, G.M., Ngo, T.T.B., Shepherd, D., Murphy, C., Dionne, H., Pfeiffer, B.D., Cavallaro, A., Hall, D., Jeter, J., Iyer, N., Fetter, D., Hausenfluck, J.H., Peng, H., Trautman, E.T., Svirskas, R.R., Myers, E.W., Iwinski, Z.R., Aso, Y., DePasquale, G.M., Enos, A., Hulamm, P., Lam, S.C.B., Li, H.H., Laverty, T.R., Long, F., Qu, L., Murphy, S.D., Rokicki, K., Safford, T., Shaw, K., Simpson, J.H., Sowell, A., Tae, S., Yu, Y., Zugates, C.T., 2012. A GAL4-Driver Line Resource for Drosophila Neurobiology. Cell Rep 2, 991–1001. https://doi.org/10.1016/j.celrep.2012.09.011

Jenuwein, T., Allis, C.D., 2001. Translating the histone code. Science 293, 1074–1080. https://doi.org/10.1126/SCIENCE.1063127

Johnson, D.G., Schwarz, J.K., Cress, W.D., Nevins, J.R., 1993. Expression of transcription factor E2F1 induces quiescent cells to enter S phase. Nature 365, 349–352. https://doi.org/10.1038/365349A0

Jones, C., Moses, K., 2004. Cell-cycle regulation and cell-type specification in the developing Drosophila compound eye. Semin Cell Dev Biol 15, 75–81. https://doi.org/10.1016/j.semcdb.2003.09.002

Jones, L., Richardson, H., Saint, R., 2000. Tissue-specific regulation of cyclin E transcription during Drosophila melanogaster embryogenesis. Development 127, 4619–4630. https://doi.org/10.1242/dev.127.21.4619

Kehle, J., Beuchle, D., Treuheit, S., Christen, B., Kennison, J.A., Bienz, M., 1998. dMi-2, a hunchback-interacting protein that functions in polycomb repression. Science 282, 1897–1900. https://doi.org/10.1126/SCIENCE.282.5395.1897

Kia, S.K., Gorski, M.M., Giannakopoulos, S., Verrijzer, C.P., 2008. SWI/SNF Mediates Polycomb Eviction and Epigenetic Reprogramming of the INK4b-ARF-INK4a Locus. Mol Cell Biol 28, 3457. https://doi.org/10.1128/MCB.02019-07

Kim, J., Lu, C., Srinivasan, S., Awe, S., Brehm, A., Fuller, M.T., 2017. Blocking promiscuous activation at cryptic promoters directs cell type-specific gene expression. Science 356, 717–721. https://doi.org/10.1126/SCIENCE.AAL3096

Korenjak, M., Taylor-Harding, B., Binné, U.K., Satterlee, J.S., Stevaux, O., Aasland, R., White-Cooper, H., Dyson, N., Brehm, A., 2004. Native E2F/RBF Complexes Contain Myb-Interacting Proteins and Repress Transcription of Developmentally Controlled E2F Target Genes. Cell 119, 181–193. https://doi.org/10.1016/J.CELL.2004.09.034

Kovač, K., Sauer, A., Mačinković, I., Awe, S., Finkernagel, F., Hoffmeister, H., Fuchs, A., Müller, R., Rathke, C., Längst, G., Brehm, A., 2018. Tumour-associated missense mutations in the dMi-2 ATPase alters nucleosome remodelling properties in a mutation-specific manner. Nat Commun 9. https://doi.org/10.1038/s41467-018-04503-2

Krasnov, A.N., Mazina, M.Y., Nikolenko, J. V., Vorobyeva, N.E., 2016. On the way of revealing coactivator complexes cross-talk during transcriptional activation. Cell Biosci 6. https://doi.org/10.1186/s13578-016-0081-y

Kreher, J., Kovač, K., Bouazoune, K., MačInković, I., Ernst, A.L., Engelen, E., Pahl, R., Finkernagel, F., Murawska, M., Ullah, I., Brehm, A., 2017. EcR recruits dMi-2 and increases efficiency of dMi-2-mediated remodelling to constrain transcription of hormone-regulated genes. Nat Commun 8. https://doi.org/10.1038/ncomms14806

Krude, T., Keller, C., 2001. Chromatin assembly during S phase: contributions from histone deposition, DNA replication and the cell division cycle. Cell Mol Life Sci 58, 665–672. https://doi.org/10.1007/PL00000890

Kunert, N., Brehm, A., 2009. Novel Mi-2 related ATP-dependent chromatin remodelers. Epigenetics 4, 209–211. https://doi.org/10.4161/epi.8933

Kunert, N., Wagner, E., Murawska, M., Klinker, H., Kremmer, E., Brehm, A., 2009. dMec: A novel Mi-2 chromatin remodelling complex involved in transcriptional repression. EMBO Journal 28, 533–544. https://doi.org/10.1038/emboj.2009.3

Kvon, E.Z., Kazmar, T., Stampfel, G., Yáñez-Cuna, J.O., Pagani, M., Schernhuber, K., Dickson, B.J., Stark, A., 2014. Genome-scale functional characterization of Drosophila developmental enhancers in vivo. Nature 512, 91–95. https://doi.org/10.1038/nature13395

Kylsten, P., Saint, R., 1997. Imaginal tissues of Drosophila melanogaster exhibit different modes of cell proliferation control. Dev Biol 192, 509–522. https://doi.org/10.1006/DBIO.1997.8770

Lam, G., Nam, H.J., Velentzas, P.D., Baehrecke, E.H., Thummel, C.S., 2022. Drosophila E93 promotes adult development and suppresses larval responses to ecdysone during metamorphosis. Dev Biol 481, 104–115. https://doi.org/10.1016/j.ydbio.2021.10.001

Längst, G., Manelyte, L., 2015. Chromatin remodelers: From function to dysfunction. Genes (Basel) 6, 299–324. https://doi.org/10.3390/genes6020299

Laudet, V. 1997. Evolution of the nuclear receptor superfamily: early diversification from an ancestral orphan receptor. *Journal of Molecular Endocrinology*, *19*(3), 207–226. https://doi.org/10.1677/JME.0.0190207

Lehman, D.A., Patterson, B., Johnston, L.A., Balzer, T., Britton, J.S., Saint, R., Edgar, B.A., 1999. Cis-regulatory elements of the mitotic regulator, string/Cdc25. Development 126, 1793–803.

Li, G., Zhu, P., 2015. Structure and organization of chromatin fiber in the nucleus. FEBS Lett 589, 2893–2904. https://doi.org/10.1016/J.FEBSLET.2015.04.023

Li, T.R., White, K.P., 2003. Tissue-Specific Gene Expression and Ecdysone-Regulated Genomic Networks in Drosophila. Dev Cell 5, 59–72. https://doi.org/10.1016/S1534-5807(03)00192-8

Lickert, H., Takeuchi, J.K., Von Both, I., Walls, J.R., McAuliffe, F., Adamson, S.L., Henkelman, R.M., Wrana, J.L., Rossant, J., Bruneau, B.G., 2004. Baf60c is

essential for function of BAF chromatin remodelling complexes in heart development. Nature 432, 107–112. https://doi.org/10.1038/NATURE03071

Lopes, C.S., Casares, F., 2015. Eye Selector Logic for a Coordinated Cell Cycle Exit. PLoS Genet 11, 1–22. https://doi.org/10.1371/journal.pgen.1004981

Lorberbaum, D. S., Ramos, A. I., Peterson, K. A., Carpenter, B. S., Parker, D. S., De, S., Hillers, L. E., Blake, V. M., Nishi, Y., McFarlane, M. R., Chiang, A. C. Y., Kassis, J. A., Allen, B. L., McMahon, A. P., & Barolo, S. 2016. An ancient yet flexible cis-regulatory architecture allows localized Hedgehog tuning by patched/Ptch1. *ELife*, *5*(MAY2016). https://doi.org/10.7554/ELIFE.13550

Ma, Y., 2018. Chromatin Structure Changes During Terminal Differentiation and Cell Cycle Exit in Drosophila melanogaster. University of Michigan - Ann Arbor.

Ma, Y., Buttitta, L., 2017. Chromatin organization changes during the establishment and maintenance of the postmitotic state. Epigenetics Chromatin 10. https://doi.org/10.1186/S13072-017-0159-8

Ma, Y., Kanakousaki, K., Buttitta, L., 2015. How the cell cycle impacts chromatin architecture and influences cell fate. Front Genet 6. https://doi.org/10.3389/FGENE.2015.00019

Ma, Y., McKay, D.J., Buttitta, L., 2019. Changes in chromatin accessibility ensure robust cell cycle exit in terminally differentiated cells. PLoS Biol 17, e3000378. https://doi.org/10.1371/journal.pbio.3000378

Martin, B.J.E., Ablondi, E.F., Goglia, C., Mimoso, C.A., Espinel-Cabrera, P.R., Adelman, K., 2023. Global identification of SWI/SNF targets reveals compensation by EP400. Cell 186. https://doi.org/10.1016/J.CELL.2023.10.006

Martinez, A.M., Cavalli, G., 2006. The role of polycomb group proteins in cell cycle regulation during development. Cell Cycle 5, 1189–1197. https://doi.org/10.4161/cc.5.11.2781

McKay, D.J., Lieb, J.D., 2013. A Common Set of DNA Regulatory Elements Shapes Drosophila Appendages. Dev Cell 27, 306–318. https://doi.org/10.1016/j.devcel.2013.10.009

Meserve, J.H., Duronio, R.J., 2017. A population of G2-arrested cells are selected as sensory organ precursors for the interommatidial bristles of the Drosophila eye. Dev Biol 430, 374–384. https://doi.org/10.1016/J.YDBIO.2017.06.023

Meyer, C.A., Jacobs, H.W., Datar, S.A., Du, W., Edgar, B.A., Lehner, C.F., 2000. Drosophila Cdk4 is required for normal growth and is dispensable for cell cycle progression. EMBO J 19, 4533–4542. https://doi.org/10.1093/EMBOJ/19.17.4533

Milán, M., Campuzano, S., García-Bellido, A., 1996. Cell cycling and patterned cell proliferation in the Drosophila wing during metamorphosis. Proc Natl Acad Sci U S A 93, 11687–11692. https://doi.org/10.1073/PNAS.93.21.11687

Moshkin, Y.M., Mohrmann, L., van Ijcken, W.F.J., Verrijzer, C.P., 2007. Functional Differentiation of SWI/SNF Remodelers in Transcription and Cell Cycle Control. Mol Cell Biol 27, 651–661. https://doi.org/10.1128/mcb.01257-06

Mou, X., Duncan, D.M., Baehrecke, E.H., Duncan, I., 2012. Control of target gene specificity during metamorphosis by the steroid response gene E93. Proc Natl Acad Sci U S A 109, 2949–2954. https://doi.org/10.1073/pnas.1117559109

Neufeld, T.P., De La Cruz, A.F.A., Johnston, L.A., Edgar, B.A., 1998. Coordination of growth and cell division in the Drosophila wing. Cell 93, 1183–1193. https://doi.org/10.1016/S0092-8674(00)81462-2

Neufeld, T.P., Edgar, B.A., 1998. Connections between growth and the cell cycle. Curr Opin Cell Biol 10, 784–790. https://doi.org/10.1016/S0955-0674(98)80122-1

Ninov, N., Manjón, C., Martín-Blanco, E., 2009. Dynamic control of cell cycle and growth coupling by ecdysone, EGFR, and PI3K signaling in Drosophila histoblasts. PLoS Biol 7, 0892–0903. https://doi.org/10.1371/JOURNAL.PBIO.1000079

Niwa, Y.S., Niwa, R., 2016. Transcriptional regulation of insect steroid hormone biosynthesis and its role in controlling timing of molting and metamorphosis. Dev Growth Differ. https://doi.org/10.1111/dgd.12248

Nystrom, S.L., Niederhuber, M.J., McKay, D.J., 2020. Expression of E93 provides an instructive cue to control dynamic enhancer activity and chromatin accessibility during development. Development (Cambridge) 147. https://doi.org/10.1242/dev.181909

O'Connell, M.J., Raleigh, J.M., Verkade, H.M., Nurse, P., 1997. Chk1 is a wee1 kinase in the G2 DNA damage checkpoint inhibiting cdc2 by Y15 phosphorylation. EMBO J 16, 545–554. https://doi.org/10.1093/EMBOJ/16.3.545

Ohtsubo, M., Roberts, J.M., 1993. Cyclin-dependent regulation of G1 in mammalian fibroblasts. Science 259, 1908–1912. https://doi.org/10.1126/SCIENCE.8384376

O'Keefe, D.D., Prober, D.A., Moyle, P.S., Rickoll, W.L., Edgar, B.A., 2007. Egfr/Ras signaling regulates DE-cadherin/Shotgun localization to control vein morphogenesis in the Drosophila wing. Dev Biol 311, 25–39. https://doi.org/10.1016/J.YDBIO.2007.08.003

O'Keefe, D.D., Thomas, S., Edgar, B.A., Buttitta, L., 2014. Temporal regulation of Dpp signaling output in the Drosophila wing. Dev Dyn 243, 818–832. https://doi.org/10.1002/DVDY.24122

O'Keefe, D.D., Thomas, S.R., Bolin, K., Griggs, E., Edgar, B.A., Buttitta, L.A., 2012. Combinatorial control of temporal gene expression in the Drosophila wing by enhancers and core promoters. BMC Genomics 13. https://doi.org/10.1186/1471-2164-13-498

Pardee, A.B., 1974. A restriction point for control of normal animal cell proliferation. Proc Natl Acad Sci U S A 71, 1286–1290. https://doi.org/10.1073/PNAS.71.4.1286

Polo, S.E., Kaidi, A., Baskcomb, L., Galanty, Y., Jackson, S.P., 2010. Regulation of DNA-damage responses and cell-cycle progression by the chromatin remodelling factor CHD4. EMBO J 29, 3130–3139. https://doi.org/10.1038/EMBOJ.2010.188

Pulianmackal, A.J., Kanakousaki, K., Flegel, K., Grushko, O.G., Gourley, E., Rozich, E., Buttitta, L.A., 2022. Misregulation of Nucleoporins 98 and 96 leads to defects in protein synthesis that promote hallmarks of tumorigenesis. Dis Model Mech 15. https://doi.org/10.1242/DMM.049234

Ready, D.F., Hanson,' And, T.E., Benzer, S., 1976. Development of the Drosophila Retina, a Neurocrystalline Lattice. Dev Biol 53, 217–240.

Reis, T., Edgar, B.A., 2004. Negative regulation of dE2F1 by cyclin-dependent kinases controls cell cycle timing. Cell 117, 253–264. https://doi.org/10.1016/S0092-8674(04)00247-8

Ren, N., Zhu, C., Lee, H., Adler, P.N., 2005. Gene expression during Drosophila wing morphogenesis and differentiation. Genetics 171, 625–638. https://doi.org/10.1534/genetics.105.043687

Resnitzky, D., Gossen, M., Bujard, H., Reed, S.I., 1994. Acceleration of the G1/S phase transition by expression of cyclins D1 and E with an inducible system. Mol Cell Biol 14, 1669. https://doi.org/10.1128/MCB.14.3.1669

Richards, G., 1976a. Sequential gene activation by ecdysone in polytene chromosomes of Drosophila melanogaster. IV. The mid prepupal period. Dev Biol 54, 256–263. https://doi.org/10.1016/0012-1606(76)90303-1

Richards, G., 1976b. Sequential gene activation by ecdysone in polytene chromosomes of Drosophila melanogaster. V. The late prepupal puffs. Dev Biol 54, 264–275. https://doi.org/10.1016/0012-1606(76)90304-3

Richardson, H., O'Keefe, L. V., Marty, T., Saint, R., 1995. Ectopic cyclin E expression induces premature entry into S phase and disrupts pattern formation in the

Drosophila eye imaginal disc. Development 121, 3371–3379. https://doi.org/10.1242/DEV.121.10.3371

Richardson, H.E., O'keefe, L. V., Reed, S., Saint, R., 1993. A Drosophila G1-specific cyclin E homolog exhibits different modes of expression during embryogenesis. Development 119, 673–690. https://doi.org/10.1242/DEV.119.3.673

Robinson, M.D., McCarthy, D.J., Smyth, G.K., 2010. edgeR: a Bioconductor package for differential expression analysis of digital gene expression data. Bioinformatics 26, 139. https://doi.org/10.1093/BIOINFORMATICS/BTP616

Ruijtenberg, S., van den Heuvel, S., 2016. Coordinating cell proliferation and differentiation: Antagonism between cell cycle regulators and cell type-specific gene expression. Cell Cycle 15, 196–212. https://doi.org/10.1080/15384101.2015.1120925

Ruijtenberg, S., van den Heuvel, S., 2015. G1/S Inhibitors and the SWI/SNF Complex Control Cell-Cycle Exit during Muscle Differentiation. Cell 162, 300–313. https://doi.org/10.1016/j.cell.2015.06.013

Rusconi, J.C., Hays, R., Cagan, R.L., 2000. Programmed cell death and patterning in Drosophila. Cell Death Differ 7, 1063–1070. https://doi.org/10.1038/SJ.CDD.4400767

Sadasivam, S., DeCaprio, J.A., 2013. The DREAM complex: Master coordinator of cell cycle-dependent gene expression. Nat Rev Cancer 13, 585–595. https://doi.org/10.1038/nrc3556

Saha, A., Wittmeyer, J., Cairns, B.R., 2005. Chromatin remodeling through directional DNA translocation from an internal nucleosomal site. Nat Struct Mol Biol 12, 747–755. https://doi.org/10.1038/NSMB973

Sakaguchi, C., Ichihara, K., Nita, A., Katayama, Y., Nakayama, K.I., 2022. Identification and characterization of novel proteins associated with CHD4. Genes Cells 27, 61–71. https://doi.org/10.1111/GTC.12909

Schaeffer, V., Althauser, C., Shcherbata, H.R., Deng, W.M., Ruohola-Baker, H., 2004. Notch-dependent Fizzy-related/Hec1/Cdh1 expression is required for the mitotic-to-endocycle transition in Drosophila follicle cells. Curr Biol 14, 630–636. https://doi.org/10.1016/J.CUB.2004.03.040

Schubiger, M., Palka, J., 1987. Changing Spatial Patterns of DNA Replication in the Developing Wing of Drosophila. Dev Biol 123, 145–153.

Schuettengruber, B., Chourrout, D., Vervoort, M., Leblanc, B., Cavalli, G., 2007. Genome Regulation by Polycomb and Trithorax Proteins. Cell 128, 735–745. https://doi.org/10.1016/J.CELL.2007.02.009

Sherwood, D.R., Sternberg, P.W., 2003. Anchor cell invasion into the vulval epithelium in C. elegans. Dev Cell 5, 21–31. https://doi.org/10.1016/S1534-5807(03)00168-0

Skene, P.J., Henikoff, S., 2017. An efficient targeted nuclease strategy for high-resolution mapping of DNA binding sites. Elife 6, 1–35. https://doi.org/10.7554/eLife.21856

Small, S., Arnosti, D.N., 2020. Transcriptional enhancers in Drosophila. Genetics 216, 1–26. https://doi.org/10.1534/genetics.120.301370

Smith, J.J., Xiao, Y., Parsan, N., Medwig-Kinney, T.N., Martinez, M.A.Q., Moore, F.E.Q., Palmisano, N.J., Kohrman, A.Q., Reyes, M.C.D., Adikes, R.C., Liu, S., Bracht, S.A., Zhang, W., Wen, K., Kratsios, P., Matus, D.Q., 2021. The SWI/SNF chromatin remodeling assemblies BAF and PBAF differentially regulate cell cycle exit and cellular invasion in vivo. PLoS Genet 18. https://doi.org/10.1371/journal.pgen.1009981

Spencer, S.L., Cappell, S.D., Tsai, F.C., Overton, K.W., Wang, C.L., Meyer, T., 2013. The proliferation-quiescence decision is controlled by a bifurcation in CDK2 activity at mitotic exit. Cell 155, 369. https://doi.org/10.1016/j.cell.2013.08.062

Sugiura, T., Wang, H., Barsacchi, R., Simon, A., Tanaka, E.M., 2016. MARCKS-like protein is an initiating molecule in axolotl appendage regeneration. Nature 531, 237–240. https://doi.org/10.1038/NATURE16974

Sun, D., Buttitta, L., 2017. States of G0 and the proliferation-quiescence decision in cells, tissues and during development. International Journal of Developmental Biology 61, 357–366. https://doi.org/10.1387/ijdb.160343LB

Thacker, S.A., Bonnette, P.C., Duronio, R.J., 2003. The Contribution of E2F-Regulated Transcription to Drosophila PCNA Gene Function. Current Biology 13, 53–58.

Thomas, B.J., Gunning, D.A., Cho, J., Lawrence Zipursky, S., 1994. Cell Cycle Progression in the Developing Drosophila Eye: roughex Encodes a Novel Protein Required for the Establishment of GI, Cell.

Thomas, H.F., Kotova, E., Jayaram, S., Pilz, A., Romeike, M., Lackner, A., Penz, T., Bock, C., Leeb, M., Halbritter, F., Wysocka, J., Buecker, C., 2021. Temporal dissection of an enhancer cluster reveals distinct temporal and functional contributions of individual elements. Mol Cell 81, 969-982.e13. https://doi.org/10.1016/j.molcel.2020.12.047

Thummel, C.S., 2002. Ecdysone-regulated puff genes 2000. Insect Biochem Mol Biol 32, 113–120.

Thummel, C.S., 1990. Puffs and gene regulation--molecular insights into the Drosophila ecdysone regulatory hierarchy. Bioessays 12, 561–568. https://doi.org/10.1002/BIES.950121202

Tong, J.K., Hassig, C.A., Schnitzler, G.R., Kingston, R.E., Schreiber, S.L., 1998. Chromatin deacetylation by an ATP-dependent nucleosome remodelling complex. Nature 395, 917–921. https://doi.org/10.1038/27699

Treisman, J.E., 2013. Retinal differentiation in Drosophila. Wiley Interdiscip Rev Dev Biol 2, 545–557. https://doi.org/10.1002/WDEV.100

Turowski, P., Franckhauser, C., Morris, M.C., Vaglio, P., Fernandez, A., Lamb, N.J.C., 2003. Functional cdc25C dual-specificity phosphatase is required for S-phase entry in human cells. Mol Biol Cell 14, 2984–2998. https://doi.org/10.1091/mbc.E02-08-0515

Unhavaithaya, Y., Shin, T.H., Miliaras, N., Lee, J., Oyama, T., Mello, C.C., 2002. MEP-1 and a Homolog of the NURD Complex Component Mi-2 Act Together to Maintain Germline-Soma Distinctions in C. elegans. Cell 111, 991–1002.

Ureña, E., Manjón, C., Franch-Marro, X., Martín, D., 2014. Transcription factor E93 specifies adult metamorphosis in hemimetabolous and holometabolous insects. Proc Natl Acad Sci U S A 111, 7024–7029. https://doi.org/10.1073/PNAS.1401478111

Uxa, S., Bernhart, S.H., Mages, C.F.S., Fischer, M., Kohler, R., Hoffmann, S., Stadler, P.F., Engeland, K., Müller, G.A., 2019. DREAM and RB cooperate to induce gene repression and cell-cycle arrest in response to p53 activation. Nucleic Acids Res 47, 9087–9103. https://doi.org/10.1093/NAR/GKZ635

Uyehara, C.M., McKay, D.J., 2019. Direct and widespread role for the nuclear receptor EcR in mediating the response to ecdysone in Drosophila. Proc Natl Acad Sci U S A 116, 9893–9902. https://doi.org/10.1073/pnas.1900343116

Uyehara, C.M., Nystrom, S.L., Niederhuber, M.J., Leatham-Jensen, M., Ma, Y., Buttitta, L.A., McKay, D.J., 2017. Hormone-dependent control of developmental timing through regulation of chromatin accessibility. Genes Dev 31, 862–875. https://doi.org/10.1101/gad.298182.117

van Vugt, J.J.F.A., de Jager, M., Murawska, M., Brehm, A., van Noort, J., Logie, C., 2009. Multiple Aspects of ATP-Dependent Nucleosome Translocation by RSC and Mi-2 Are Directed by the Underlying DNA Sequence. PLoS One 4. https://doi.org/10.1371/JOURNAL.PONE.0006345

Vázquez, M., Moore, L., Kennison, J.A., 1999. The trithorax group gene osa encodes an ARID-domain protein that genetically interacts with the Brahma chromatin-remodeling factor to regulate transcription. Development 126, 733–742. https://doi.org/10.1242/DEV.126.4.733

Verma, P., Cohen, S.M., 2015. miR-965 controls cell proliferation and migration during tissue morphogenesis in the Drosophila abdomen. Elife 4. https://doi.org/10.7554/ELIFE.07389

Wade, P.A., Gegonne, A., Jones, P.L., Ballestar, E., Aubry, F., Wolffe, A.P., 1999. Mi-2 complex couples DNA methylation to chromatin remodelling and histone deacetylation. Nat Genet 23, 62–66. https://doi.org/10.1038/12664

Wade, P.A., Jones, P.L., Vermaak, D., Wolffe, A.P., 1998. A multiple subunit Mi-2 histone deacetylase from Xenopus laevis cofractionates with an associated Snf2 superfamily ATPase. Curr Biol 8, 843–848. https://doi.org/10.1016/S0960-9822(98)70328-8

Walston, H., Iness, A.N., Litovchick, L., 2021. DREAM On: Cell Cycle Control in Development and Disease. Annu Rev Genet 55, 309–329. https://doi.org/10.1146/ANNUREV-GENET-071819-103836

Wang, H., Morrison, C.A., Ghosh, N., Tea, J.S., Call, G.B., Treisman, J.E., 2022. The Blimp-1 transcription factor acts in non-neuronal cells to regulate terminal differentiation of the Drosophila eye. Development 149. https://doi.org/10.1242/DEV.200217

Wang, H.-B., Zhang, Y., 2001. Mi2, an auto-antigen for dermatomyositis, is an ATP-dependent nucleosome remodeling factor, Nucleic Acids Research.

Wilson, B.G., Wang, X., Shen, X., McKenna, E.S., Lemieux, M.E., Cho, Y.J., Koellhoffer, E.C., Pomeroy, S.L., Orkin, S.H., Roberts, C.W.M., 2010. Epigenetic antagonism between polycomb and SWI/SNF complexes during oncogenic transformation. Cancer Cell 18, 316–328. https://doi.org/10.1016/J.CCR.2010.09.006

Xin, S., Weng, L., Xu, J., Du, W., 2002. The role of RBF in developmentally regulated cell proliferation in the eye disc and in Cyclin D/Cdk4 induced cellular growth. Development 129, 1345–1356. https://doi.org/10.1242/DEV.129.6.1345

Xue, Y., Wong, J., Moreno, G.T., Young, M.K., Cô, J., Wang, W., 1998. NURD, a Novel Complex with both ATP-Dependent Chromatin-Remodeling and Histone Deacetylase Activities. Mol Cell 2, 851–861.

Zacharioudaki, E., Sanjuan, J.F., Bray, S., 2019. Mi-2/NuRD complex protects stem cell progeny from mitogenic Notch signaling. Elife. https://doi.org/10.7554/eLife.41637.001

Zambanini, G., Nordin, A., Jonasson, M., Pagella, P., Cantù, C., 2022. A new CUT&RUN low volume-urea (LoV-U) protocol optimized for transcriptional co-factors uncovers Wnt/β-catenin tissue-specific genomic targets. Development 149. https://doi.org/10.1242/DEV.201124

Zhang, Y., LeRoy, G., Seelig, H.P., Lane, W.S., Reinberg, D., 1998. The dermatomyositis-specific autoantigen Mi2 is a component of a complex containing histone deacetylase and nucleosome remodeling activities. Cell 95, 279–289. https://doi.org/10.1016/S0092-8674(00)81758-4

Zhang, Y., Ng, H.H., Erdjument-Bromage, H., Tempst, P., Bird, A., Reinberg, D., 1999. Analysis of the NuRD subunits reveals a histone deacetylase core complex and a connection with DNA methylation. Genes Dev 13, 1924–1935. https://doi.org/10.1101/GAD.13.15.1924

Zhou, K., Gaullier, G., Luger, K., 2019. Nucleosome structure and dynamics are coming of age. Nat Struct Mol Biol 26, 3–13. https://doi.org/10.1038/s41594-018-0166-x

Zofall, M., Persinger, J., Kassabov, S.R., Bartholomew, B., 2006. Chromatin remodeling by ISW2 and SWI/SNF requires DNA translocation inside the nucleosome. Nat Struct Mol Biol 13, 339–346. https://doi.org/10.1038/nsmb1071

## Chapter 2: A Tissue Dissociation Method for ATAC-seq and CUT&RUN in *Drosophila* Pupal Tissues

This chapter was published in:

Elli M Buchert, Elizabeth A Fogarty, Christopher M Uyehara, Daniel J McKay, Laura A Buttitta

*Fly* 17(1), 28 April 2023. https://doi.org/10.1080/19336934.2023.2209481

EMB developed the dissociation protocol described in Figure 1 and used throughout the paper. EMB contributed to the original writing and final revisions, and created results shown in Figure 4

### 2.1 Abstract

Chromatin accessibility, histone modifications and transcription factor binding are highly dynamic during *Drosophila* metamorphosis and drive global changes in gene expression as larval tissues differentiate into adult structures. Unfortunately, the presence of pupa cuticle on many *Drosophila* tissues during metamorphosis prevents enzyme access to cells and has limited the use of enzymatic *in situ* methods for assessing chromatin accessibility and histone modifications. Here, we present a dissociation method for cuticle-bound pupal tissues that is compatible for use with ATAC-Seq and CUT&RUN to interrogate chromatin accessibility and histone modifications. We show this method provides comparable chromatin accessibility data

to the non-enzymatic approach FAIRE-seq, with only a fraction of the amount of input tissue required. This approach is also compatible with CUT&RUN, which allow genome-wide mapping of histone modifications with less than 1/10$^{th}$ of the tissue input required for more conventional approaches such as Chromatin Immunoprecipitation Sequencing (ChIP-seq). Our protocol makes it possible to use newer, more sensitive enzymatic *in situ* approaches to interrogate gene regulatory networks during *Drosophila* metamorphosis.

## 2.2 Introduction

The study of global gene regulatory networks during development requires observational data describing changes in chromatin accessibility, histone modifications and transcription factor binding over time, in a manner coordinated with cellular differentiation. Molecular studies of developmental gene regulatory networks *in vivo* have often involved pooling of embryos, dissection of tissues and/or sorting of specific cell types to isolate nuclei or chromatin, followed by nuclease assays or Chromatin ImmunoPrecipitation (ChIP) (Wilczynski and Furlong, 2010). Newer enzymatic methods to examine the molecular underpinnings of gene regulation such as Assay for Transposase-Accessible Chromatin with high-throughput sequencing (ATAC-seq) and Cleavage Under Targets and Release Using Nuclease (CUT&RUN) have made it possible to assay chromatin accessibility and histone modifications or transcription factor binding with a fraction of the input required for more traditional assays (Ahmad and Spens, 2019; Davie et al., 2015), making them ideal tools for experiments that require tissue dissection or cell sorting (Uyehara and McKay, 2019). But these assays

can be challenging in tissue types where the cells are heavily embedded in the extracellular matrix, or in the case of insects, enclosed within a tough cuticle, which limits nuclear isolation by homogenization and enzyme access to cells.

We previously customized a flow cytometry protocol for cuticle-encased tissues such as *Drosophila* pupal wings, to measure DNA content and fluorescent transgene expression (Flegel et al., 2013). Our protocol was designed to dissociate the wing after pupa cuticle deposition, but optimized cell recovery, viability and access to vital DNA dyes for DNA content quantification. We therefore reasoned that with further optimization, our dissociation approach could provide enzyme access to live cells from these tissues to take advantage of newer chromatin profiling techniques toward the study of chromatin dynamics in the fly wing during metamorphosis.

Here, we describe a dissociation method for cuticle-bound pupal tissues such as the *Drosophila* wing, that is compatible for use with subsequent ATAC-Seq or CUT&RUN applications to interrogate chromatin accessibility and histone modifications.

## 2.3 Methods

### *Drosophila* genotypes and staging

*Drosophila* tissues were dissected from $w^{1118}/y,w,hsflp^{122}$ *; +;* + female animals for all samples except the CUT&RUN 24h APF 45 and 75 wing samples, which were a mixture of *y,w* males and females. Animals were raised at 25°C on Bloomington Cornmeal media without malt extract (bdsc.indiana.edu/information/recipes/bloomfood.html). Larval samples were dissected from wandering larvae isolated from uncrowded vials. Vials with more than ~100 larvae were diluted into fresh vials to keep larvae uncrowded.

Pupa were collected from vials at the White Pre-pupa stage (WPP) as described (Flegel *et al.*, 2013), which was taken as 0h After Puparium Formation (APF) and reared on damp Kimwipes at 25°C to the indicated hours APF.

**Tissue Isolation and Dissociation**

We use Collagenase/Dispase from Sigma (cat# 10269638001), which is $Ca^{2+}$ dependent and acts at low temperatures such as 4°C. Collagenase/Dispase is not inhibited by serum, but is compatible with the wash solutions for ATAC-Seq and CUT&RUN and is inhibited by EDTA.

Reconstitute Collagenase/Dispase mixture:

Collagenase/Dispase comes as 100mg lyophilized powder. To reconstitute, dissolve powder in 1mL dH2O to make 100mg/mL concentrated stock. This can be stored at -20°C, but we suggest making aliquots of 2mg/mL 2X working stock to avoid repeated freeze/thaw cycles. To make the 2X working stock, dilute the concentrated 100mg/mL stock 1:50 in Wash solution (20 mM HEPES, pH 7.5, 150 mM NaCl, 0.1% BSA). Aliquot 100µL per tube to make multiple aliquots of 2X working stock to avoid repeated freeze thaw cycles.

Dissociation:

We dissect tissues in glass embryo dishes (Electron Microscopy Sciences) in Wash+ solution (Wash solution supplemented with 0.5 mM Spermidine and Roche complete Protease Inhibitor Tablet 1 tablet per 50 mL). Videos of pupal wing dissections are published (Flegel *et al.*, 2013) and also available upon request. In brief for pupa wing

dissection, we use forceps to hold the pupa at the anterior operculum and use microdissection scissors (Fine Science Tools, Vannas Tubingen spring scissors) to perform a posterior cut across the pupa to release fat body and hemolymph. We then perform a second, longitudinal cut on the ventral side of the pupa, extending from the posterior edge to the head region. Forceps can now be used to remove the fileted pupa from the tanned cuticle. The shiny, clear pupa cuticle will now be evident, and we use a glass Pasteur pipet to gently flow dissection solution throughout the opened pupa to remove any remaining fat body. We then pull wings off from the cleaned pupa at the hinge, using sharp forceps (Fine Science Tools, Dumont #5). For some CUT&RUN experiments here (those with 24h APF wings), we also dissected and added 4 *Drosophila virilis* 3$^{rd}$ larval instar wing discs to the dissociation mixture, to use as a spike-in control to verify similar fragment recovery rates across dissociated samples with varying inputs from 20-75 pupal wings.

We use 10 larval wing discs or pupal wings for ATAC-Seq and 20-75 discs or wings for CUT&RUN. The amount of tissue used for CUT&RUN depends on the antibody and must be determined empirically. Keep track of how many tissues you add per sample, particularly when optimizing the protocol and preparing samples for flow cytometry. This will allow for calculations of viable cells released per tissue. Pre-coat a cutoff P200 tip by pipetting up and down in histolyzed fat body from dissected pupa or larva carcasses (to avoid tissue sticking). Pipet 100µl of dissected tissues in Wash+ solution directly into 100µL 2X Collagenase/Dispase solution. Incubate in a thermomixer at 23°C for 30 minutes, shaking at 500 rpm. Vortex for 10 seconds at setting 6 (about 60% of max speed). Incubate another 10 minutes at 23°C, shaking at 500 rpm. Vortex

again for 10 seconds at 60% speed. At this point you may see the empty, clear pupa wing cuticle floating at the top of the solution. Proceed to downstream protocols as described for ATAC-seq, CUT&RUN or flow cytometry.

**Flow Cytometry**

In pilot experiments used to assess and optimize the dissociation protocol, we measured cell number and viability by flow cytometry. A live cell DNA stain is used to count cells and propidium iodide is used to differentiate live from dead or dying cells. After dissection but before beginning the incubations at 23°C with shaking, add an additional 300 µL of Wash+ solution for a total volume of 500µL. Add 0.5µL of live cell DNA stain (Vybrant DyeCycle Violet DNA Stain, Invitrogen or Hoechst 33342, Sigma) and 1.2 µL of 10mg/mL Propidium Iodide (PI, Sigma). Proceed with shaking at 23°C and vortexing as described above. After the final 10 second vortex, add 500 µL of 1X PBS + 0.1% BSA bringing final sample volume to 1mL. Do not pipet to mix, as cells will stick to the plastic pipet; adding the solution will sufficiently mix the sample. Run sample immediately through a flow cytometer to measure cell number per tissue (gating on diploid 2N and 4N cells stained with live DNA dye) and cell viability (PI positive cells are permeable dead or dying cells, PI negative cells are viable). Our flow cytometry was performed using an Attune NxT at a flow rate of 100µL/min. We consider samples with >95% of PI negative diploid cells to be successful.

**ATAC-Seq**

We use the Omni-ATAC Protocol described in (Corces et al., 2017). Dissect and dissociate larval or pupal tissues (10 wings per sample) as described above. After the final 10 second vortex, spin down tissues at 800 x g, for 5 minutes, at 4°C. Remove supernatant and wash in 200 µL $Ca^{2+}$ free 1X PBS. Repeat 4°C spin and remove supernatant. Resuspend cell pellet in 50 µl cold ATAC-RSB (10mM Tris-HCl pH 7.4, 10 mM NaCl, 3mM $MgCl_2$) supplemented with 0.1% NP40, 0.1% Tween-20, and 0.01% Digitonin for cell lysis. Pipette up and down 3 times. Incubate on ice 3 minutes. Quench lysis by adding 1 mL cold ATAC-RSB containing 0.1% Tween-20 without NP40 or Digitonin. Invert tube 3 times to mix. Spin down at 800 x g for 10 minutes, 4°C. Discard supernatant and immediately continue to transposition reaction. Note that the pellet can be quite loose at this point. We often remove 1 mL of supernatant, then spin down again for 5 minutes to re-pellet and remove the final 50 µL.

Transposition reaction and purification- To make the transposition reaction mix, combine the following per sample: 25 µl 2x TDE1 Buffer (Illumina Cat #20034197), 3.5 µl Tn5 Enzyme (100nM final, Illumina Cat #20034197), 16.5 µl PBS, 0.5 µL 1% Digitonin, 0.5 µL 10% Tween-20, 5 µL water. Resuspend nuclei in 50 µL transposition reaction mix. The transposition reaction is carried out at 37°C for 30 minutes shaking at 1000 rpm. Following transposition reaction, the sample is purified using a Qiagen MinElute kit according to manufacturer's protocol. Elute transposed DNA in 21 µl Elution Buffer (10 mM Tris buffer pH 8.0). Purified DNA can be stored at -20°C.

**CUT&RUN**

Our pupal CUT&RUN protocol is adapted from (Uyehara and McKay, 2019). Dissect tissues (20 wings per sample) in cold CUT&RUN Wash+ buffer, and proceed with Collagenase/Dispase dissociation as described above.

Binding dissociated cells to Concanavalin A (ConA) beads: Aliquot 15 µL of Concanavalin A (ConA) beads (Polysciences cat#86057-3) and bind to magnet for 5 minutes, then remove supernatant. Wash beads 2X with 1mL Binding Buffer (20mM HEPES-KOH, pH 7.9, 10mM KCl, 1mM $CaCl_2$, 1mM $MnCl_2$), then resuspend in 15 µL Binding Buffer. Transfer dissociated wings to ConA beads and mix with gentle pipetting, then add 1mL DBE (Digitonin Block EDTA: 2mM EDTA, 0.1 % Digitonin in Wash + buffer) and pipette to mix. Incubate for 10 minutes on ice. Bind cells and beads to magnet for 2 minutes. Remove buffer and replace with 100µL DBE supplemented with primary antibody of interest (data presented here: rabbit anti-H3K27Me3 antibody C36B11, Cell Signaling, 1:100). Incubate cells plus antibody angled sideways on orbital shaker, set to low, overnight at 4°C. Bind beads to magnet for 2 minutes at 4°C. Remove supernatant and wash 2 X with 500µL DBE, inverting tube back & forth ~10X to mix.

We used two sources of protein A/G-MNase in this study. For larval wings (L3) and 24h pupal samples with 20 wings, we used protein A/G-MNase from Epicypher. For 24h pupal samples with 40 and 75 wings, we used protein A/G-MNase kindly provided by Dr. Steven Henikoff (Meers et al., 2019). For experiments using pA/G Mnase from Epicypher, dilute pA/G Mnase 1:20 into DBE and keep on ice until ready for use. Bind

samples to magnet for 2 minutes then remove supernatant and resuspend in 100 µL Protein A/G-MNase solution. Incubate for 10 minutes at room temperature on an orbital shaker, set to low, at an angle. At 4°C, bind samples to magnet for 2 minutes, then remove supernatant. Resuspend beads in 500 µL Wash+ and incubate for 2 minutes. Bind samples to magnet for 2 minutes, then repeat wash once. Remove the supernatant and resuspend samples in 75 µL Digitonin Buffer (Wash + solution with 0.1% Digitonin). Add 75 µL 2x Rxn Buffer (Wash + buffer with 4mM $CaCl_2$) to samples. Digest for 2 hours at 4°C on orbital shaker. Add 150 µL 2xSTOP buffer (20 mM HEPES, pH7.5, 200 mM NaCl, 20 mM EDTA, 4 mM EGTA) + 60 µg/ml RNAseA to stop digestion reaction and pipette to mix. For L3 wing samples, a spike-in control was used of *E. Coli* DNA (Epicypher cat# 18-1401) at 5.25 pg per sample. For experiments using pA/G Mnase provided by the Henikoff lab we made the following modifications to the above process; cells were incubated with pA/G Mnase for 1h at 4°C prior to adding Rxn buffer. Digestion was performed in Rxn buffer for 30 min at 4°C.

Fragment Release and purification: Incubate samples in thermomixer set to 37°C without shaking for 30 minutes, then bind sample on magnet for 2 minutes. Transfer supernatant to low retention tube labeled “S” (for supernatant). Resuspend the remaining pellet in 150 µL Pellet Buffer (Wash + buffer with an equal volume of 2xSTOP + 10% SDS and 6.89 µL proteinase K 20mg/mL). Add 2 µL 10% SDS and 2.5 µL proteinase K (20mg/mL) to supernatant samples. Mix by briefly vortexing. Incubate supernatant and pellet samples in thermomixer set 50°C without shaking for 2 hours. Place tubes on magnet for 2 minutes, then transfer supernatant to new low retention

tube. Fragments were selected using SPRI beads and library preparation was performed using Takara ThruPLEX DNA-seq kits.

Sequencing platforms and read depth: Library quality was assessed with an Agilent Tape Station. H3K27me3 CUT&RUN 24h APF 20 wings sample was sequenced using Illumina NextSeq 100 Cycles HO, paired-end 50bp reads, at a target depth of 15 million reads. 45 and 75 wings samples were sequenced on an Illumina NovaSeq SP 100 cycle flow cell for 50 bp paired-end reads, at a target depth of 10 million reads per sample. L3 H3K27me3 Cut&Run samples were sequenced on an Illumina NovaSeq S4 300 cycle flow cell for 150 bp paired-end reads, at a target depth of 50 million reads per sample. L3 wing disc ATAC-Seq libraries were sequenced on an Illumina NextSeq MO 150 cycle flow cell for 75bp paired end reads, with a target depth of 16 million reads per sample. Pupal wing ATAC-Seq libraries were sequenced on an Illumina NovaSeq SP 100 cycle flow cell for 50bp paired end reads, at a target depth of 90 million reads per sample.

Data Analysis: Raw sequencing files were assessed using FastQC (https://www.bioinformatics.babraham.ac.uk/projects/fastqc/), then adaptors and low-quality bases were trimmed using Trimmomatic-0.39 (Bolger et al., 2014) for Cut&Run libraries, or cutadapt 1.18 (Martin, 2011) for ATAC-Seq libraries. Reads were aligned to DM6 using Bowtie2.4.1 (Langmead and Salzberg, 2012) using --local --very-sensitive parameters and max fragment size set to 1000.  PCR duplicates were marked using picard-tools 2.8.1 MarkDuplicates (“Picard Toolkit.” 2019. Broad Institute, GitHub Repository. https://broadinstitute.github.io/picard/; Broad Institute). BAM files were

generated using samtools 1.5 (Danecek et al., 2021), and peaks were called using macs2 version 2.1.2 (Zhang et al., 2008). ATAC-Seq fragments spanning less than 120bp (sub-nucleosomal fragments) were used for analysis. Within each analysis (dissociated vs non-dissociated L3 ATAC, ATAC vs FAIRE, etc) library depth was normalized by downsampling larger datasets prior to peak calling. Only peaks that were identified in all replicates for a given timepoint or condition were used in downstream analyses. Bigwig tracks and CUT&RUN heatmaps, Pearson correlation plots, and PCA plots were generated using DeepTools utilities (Ramirez et al., 2016). ATAC-Seq and FAIRE heatmaps were generated using R package pheatmap version 1.0.12. ATAC-Seq and FAIRE peaks mapping to blacklist regions (Amemiya et al., 2019) and LINE/LTR repeat regions (Karolchik et al., 2004) were excluded from analyses. Read coverage within peaks was calculated using featureCounts from subread version 1.6.0 (Liao et al., 2014). Peaks were assigned to genomic features using R package ChIPpeakAnno (Zhu et al., 2010). Conservation scores for ATAC-Seq and FAIRE peaks were extracted from the UCSC Genome Browser dm6 124-way PhastCons data file (Kent et al., 2002) using a publicly available custom script written by Dr. Ian Donaldson, University of Manchester (https://www.biostars.org/p/16724/#16731).

Data Access:

Data generated in these studies is available in GEO at GSE211269.
Previously published larval and pupal wing FAIRE data can be accessed from GEO GSE131981.

Previously published L3 wing H3K27Me3 ChIP data was accessed from GEO GSE74080.

### 2.4 Results & Discussion

**A wing dissociation protocol to release cells from cuticle that minimizes cell death and loss.**

During *Drosophila* metamorphosis, tissues that make the head, notum, wings, halteres, abdomen and legs are covered by a pupal cuticle secreted by the imaginal epithelium beginning at 6-10 hours after puparium formation (APF) (Reed et al., 1975). To study these tissues after 6h APF, the cuticle is typically removed by hand dissection after fixation, to allow access for antibodies and stains for immunofluorescence on these tissues. We previously attempted to perform ATAC-seq on dissected pupal tissues, but found the pupa cuticle inhibited access to the transposase enzyme. We therefore used a chemical approach with fixation and sonication, FAIRE-seq, to interrogate chromatin accessibility changes in pupal wings (Ma et al., 2019). This chemical approach required at least 40 wings per sample, which involved significant manual dissection and limited the resolution of our timecourse. This prompted us to reinvestigate whether ATAC-seq may work on smaller numbers of unfixed pupal tissues that have been dissociated, to release them from the pupa cuticle.

We started from a well-established protocol for flow cytometry that was developed to study cell cycle changes in developing *Drosophila* wings (de la Cruz and Edgar, 2008) and adapted it for various pupal tissues, from stages 18-44 h APF for cell cycle analysis (Flegel *et al.*, 2013). We tested tissue dissociation with various enzymes

including trypsin-based digestion, collagenase, dispase and chitinase, as chitin is a major component of the pupa cuticle (Fristrom et al., 1982). In our hands, dispase alone and several concentrations of chitinase failed to dissociate cells from pupal wings. We found that digestion with a commercially available Collagenase/Dispase mixture (see methods) for about 40 minutes at room temperature with gentle shaking optimized cell recovery from unfixed, hand-dissected tissues and minimized cell death (Figure 2.1). Key steps to optimize cell recovery and improve consistency from sample to sample include: 1. pre-coating pipet tips (both glass and plastic) with histolyzed fat body from dissected pupa before using them to transfer dissected tissues in order to avoid sticking and tissue loss, 2. transferring tissues from dissection dishes in a Hepes-based wash buffer with minimal solution carryover, and 3. consistent shaking during dissociation. We prefer to use a temperature and speed-controlled Thermomixer (available from Eppendorf) for this purpose. For performing ATAC-seq after tissue dissociation, we gently pellet the cells and wash once with $Ca^{2+}$ free 1X PBS to remove enzymes. For CUT&RUN, the mixture of cells and enzymes can be directly added to prepared Concanavalin A beads, since solutions used in cell permeabilization for CUT&RUN contain EDTA, which inhibits the activity of collagenase and dispase enzymes.

To assess whether our tissue dissociation protocol is compatible with chromatin accessibility assays via ATAC-seq, we first compared ATAC-seq data we obtained from 3 replicates of 10 dissociated wings across L3, 24h and 44h APF timepoints to our previously published FAIRE-seq data on 3 replicates of 40 wings across the same timepoints (Figure 2.2). We see good agreement of the ATAC-seq data on dissociated wings with 58% of identified accessible peaks overlapping with peaks in our previous

FAIRE-seq data on wings and most peaks exhibiting similar opening and closing dynamics over time. This demonstrates that after tissue dissociation, comparable chromatin accessibility profiles can be obtained with ¼ of the input used for FAIRE-seq. We also observe that ATAC-seq picks up more accessible peaks within gene coding regions, while FAIRE peaks are more likely to be at promoters, which was also previously observed in a direct comparison of FAIRE-seq and ATAC-seq signals in the *Drosophila* larval eye (Davie *et al.*, 2015).

While tissue dissociation is essential for ATAC-seq on pupa wings after pupa cuticle formation (after 6h APF), ATAC-seq without tissue dissociation has been previously employed on larval wings, which are not yet enclosed within cuticle (Harris et al., 2020; Vizcaya-Molina et al., 2018). We therefore compared ATAC-seq profiles on dissociated larval wings with undissociated larval wings to assess how the dissociation process may impact chromatin accessibility assays (Figure 2.3). In general, we find good agreement between datasets from dissociated and undissociated tissues of the same stage. However, we noted ATAC-seq libraries prepared from dissociated wings required fewer PCR cycles of amplification, exhibited fewer reads from mitochondria and *Wolbachia* and better rates of reads mapping to the *Drosophila* genome, suggesting improved sensitivity of the assay after tissue dissociation. We suggest this may be due to improved access of the transposase enzyme to all nuclei of the tissue after dissociation, rather than just those on the surface of undissociated tissues. We therefore propose that dissociation may also assist with improving sensitivity and recovery from enzyme-based chromatin assays in thick tissues, in addition to allowing access to those with significant extracellular matrix or cuticle deposition. We have

successfully performed this assay with dissociation on larval and pupal eyes and brains with similar sensitivity. Since tissue dissociation is essential for ATAC-seq on pupal tissues, we suggest that whenever comparisons between larval and pupal tissues are performed, larval tissues must also be dissociated.

We next tested whether our dissociation protocol was compatible with the enzyme-based CUT&RUN assay to examine histone modification distribution in larval and pupal wings. To date, the only approach to examine the genome-wide localization of chromatin binding proteins or histone modification distribution in pupal wings after 6h APF has been Chromatin IP, which required a massive dissection of 700-1,000 pupa wings (Uyehara et al., 2017). We performed wing dissociation followed by CUT&RUN to localize the repressive histone mark Histone H3 Lysine 27 trimethylation (H3K27Me3) on L3 larval and 24h APF pupal wings with inputs ranging from 20-75 wings per sample (Figure 2.4). Even with an input of only 20 wings (~1 million cells), we readily detect regions of broad H3K27Me3 that are consistent with known H3K27Me3 signals identified by ChIP in larval wings (Loubiere et al., 2016). Unfortunately, there are no published H3K27Me3 ChIP datasets from the *Drosophila* pupal wing available for comparison, but when we examine known temporally stable, wing-specific regions of H3K27Me3 enrichment (e.g. the Bithorax Complex), we observe the expected patterns of this histone mark across inputs ranging from 20-75 wings at both larval and pupal stages (Papp and Muller, 2006).

**Summary:** The tissue dissociation protocol described here provides sufficient cell recovery and viability for use with subsequent ATAC-seq and CUT&RUN assays. This

protocol will greatly facilitate genome-wide examinations of chromatin accessibility, histone modifications, and localization of chromatin binding proteins in tissues across metamorphosis at timepoints previously inaccessible to these assays.

## 2.5 Acknowledgements

Work in the Buttitta lab is supported by the NIH/NIGMS (R01) GM127367. Work in the McKay Lab is supported by NIH/NIGMS (R35) GM128851. EMB was supported by the U.Michigan Genetics Training Grant (T32GM007544). We thank Matt Niederhuber for kindly providing the illustration in Figure 2.1 adapted from (Niederhuber and McKay, 2021). We thank Dr. Steven Henikoff (FHCRC) for providing pA/G MNase. We thank Dr. Yiqin Ma for initial studies into ATAC-seq on pupal wings.

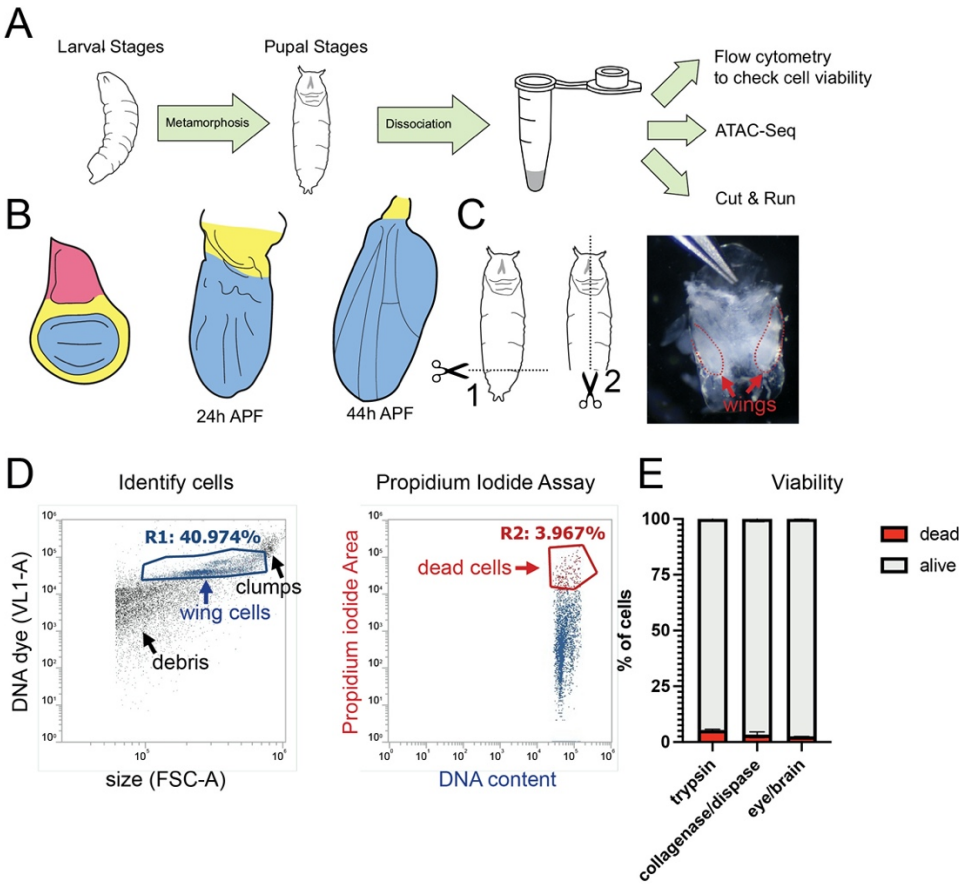


**Figure 2.1. A wing dissociation protocol to release cells from cuticle and minimize cell death and loss. (A)** Workflow diagram of assays compatible with gentle dissociation on larval and pupal tissues. Pupal tissues after 6h into metamorphosis are encased within pupa cuticle and require dissociation for the subsequent assays. **(B)** Diagrams of pupal wing morphogenesis during metamorphosis. Notum (pink) is present in larval wings but absent from dissected pupa wings after 18h APF. Larval and pupal wings contain hinge (yellow) and wing pouch (blue). **(C)** Diagram of pupa dissection (dotted lines) with image of 24h APF pupa removed from the tanned pupal case. Wings are enclosed in shiny, translucent pupa cuticle and are manually dissected from the body at the hinge for dissociation. **(D)** Example flow cytometry plot of dissociated 24h APF pupal wings. Cells were stained with a vital DNA dye (DyeCycleViolet) to discern cells from debris. Cell viability was assayed using a Propidium Iodide (PI) permeability assay and dead or dying cells were quantified based on gating of PI positive cells. **(E)** Quantifications of viable vs. dead/dying cells in trypsin-based dissociation vs. collagenase/dispase dissociation in 24h APF pupal wings and 24h APF pupal eye/brain complexes.

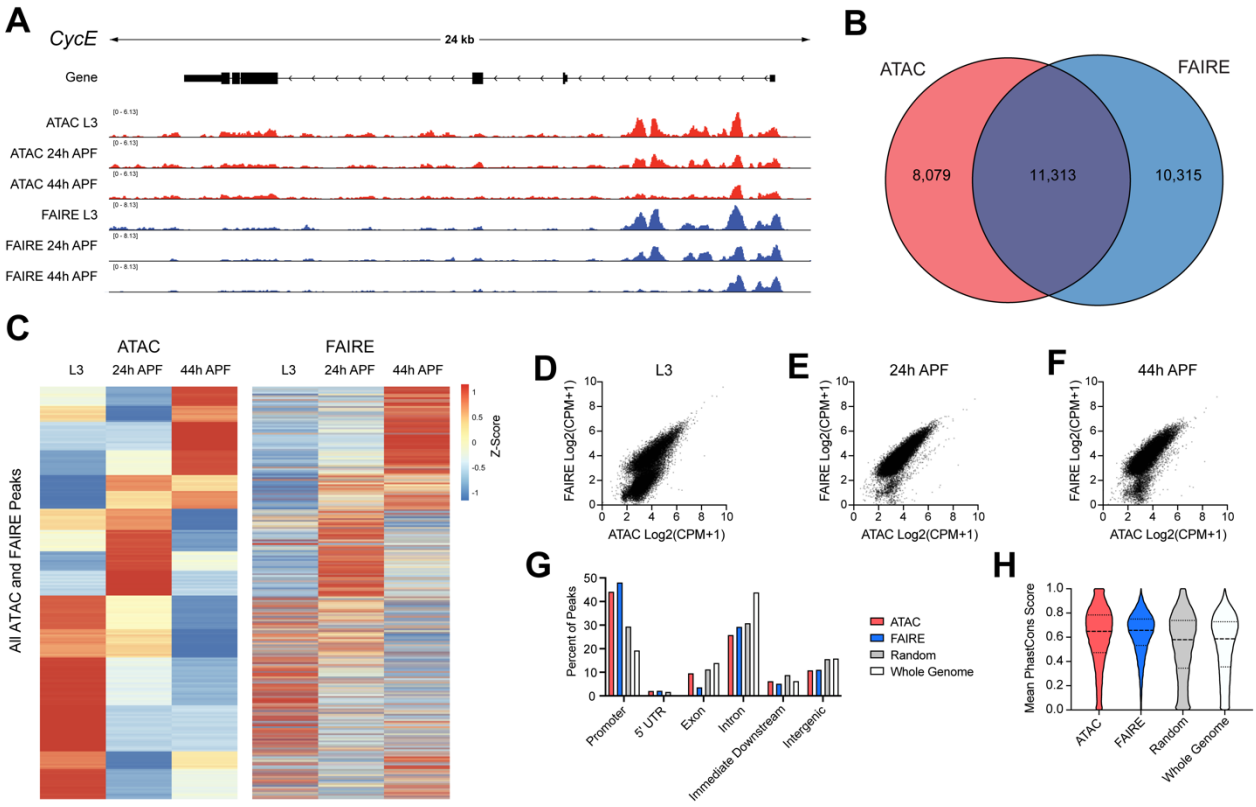


**Figure 2.2. ATAC-Seq libraries from larval and pupal wings strongly correlate with accessibility profiles generated using FAIRE-Seq**. (**A**) Accessibility profiles at the *cycE* gene locus generated using ATAC-Seq (red) and FAIRE-Seq (blue) from third larval instar (L3) wing discs and pupal wings at 24h and 44h after puparium formation (APF). Arrows on gene diagram indicate the direction of transcription. Y-axes for ATAC-Seq and FAIRE-Seq tracks: normalized read counts per million. (**B**) Venn diagram depicting the overlap between ATAC-Seq and FAIRE-Seq peaks called from any time point. (**C**) Heatmap depicting the average signal intensity dynamics at the union set of all peaks defined by ATAC-Seq and FAIRE-Seq. Data are scaled by Z-score and hierarchically clustered based on ATAC-Seq dynamics. (**D-F**) Scatter plots depicting the signal intensity (log2-transformed read counts per million) in FAIRE-Seq (y-axis) and ATAC-Seq (x-axis) libraries from L3 discs (D), 24h APF (E), and 44h APF (F) wings. Each plot includes the union set of peak regions called at the given time point. (**G-H**) Percent of peaks residing at various genomic elements (G) and distribution of mean PhastCons scores (H) from ATAC-Seq (red) or FAIRE-Seq (blue) libraries, as well as from randomized peak regions (grey) and 250 bp regions covering the entire genome (white). ATAC-Seq and FAIRE-Seq datasets include peaks called at any time point. Additional data including Pearson correlation coefficients for all samples and replicates are provided in Supplemental Fig. 1.

**A**

| ATAC Sample | Library Prep PCR Cycles | Raw Sequencing Read Pairs | Percent Mapping to Wolbachia | Percent Mapping to DM6 | Percent Duplicated Reads | Percent Mitochondrial Reads | Median Insert Size |
|---|---|---|---|---|---|---|---|
| L3 Wing Non-Dissociated 1 | 10 | 18,096,665 | 6.87 | 69.84 | 14.14 | 3.19 | 156 |
| L3 Wing Non-Dissociated 2 | 10 | 18,027,602 | 9.03 | 64.86 | 12.49 | 2.65 | 160 |
| L3 Wing Dissociated 1 | 7 | 20,004,289 | 2.41 | 94.89 | 7.53 | 0.42 | 167 |
| L3 Wing Dissociated 2 | 6 | 18,866,964 | 3.31 | 93.90 | 7.05 | 0.63 | 156 |

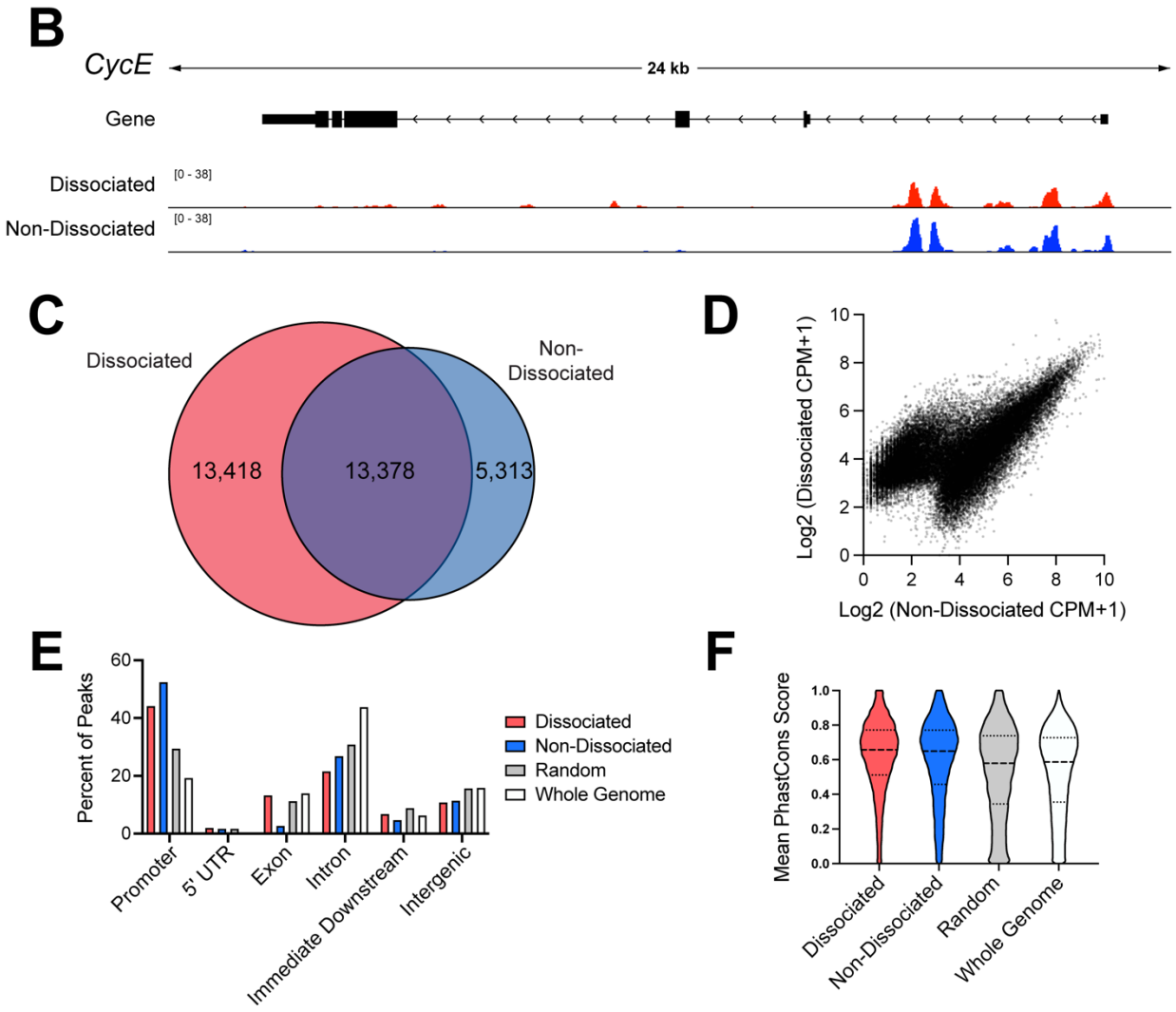


**Figure 2.3. Wing disc dissociation is compatible with generation of high-quality ATAC-Seq libraries.** (**A**) Table of quality metrics comparing ATAC-Seq libraries prepared from non-dissociated versus dissociated third larval instar (L3) wing discs. (**B**) ATAC-Seq reads at the *cycE* gene locus from dissociated (red) and non-dissociated (blue) L3 wing discs. Arrows on gene diagram indicate the direction of transcription. Y-

axes for ATAC-Seq tracks: normalized read counts per million. (**C**) Venn diagram depicting the overlap between ATAC-Seq peaks called from dissociated (red) and non-dissociated (blue) L3 wing discs. (**D**) Scatter plot depicting the average signal intensity (log2-transformed counts per million) in dissociated (y-axis) and non-dissociated (x-axis) L3 wing discs for the union set of peak regions called in each condition. (**E-F**) Percent of peaks residing at various genomic elements (E) and distribution of mean PhastCons scores (F) from dissociated (red) or non-dissociated (blue) L3 wing disc ATAC-Seq libraries, as well as from randomized peak regions (grey) and 250 bp regions covering the entire genome (white). Additional data including Pearson correlation coefficients for dissociated vs. non-dissociated wings are provided in Supplemental Fig. 2.

A

| Sample | Raw Sequencing Read Pairs | Percent Mapping to DM6 | Percent Duplicated Reads | Library Prep PCR Cycles | Peaks Called (MACS2) |
|---|---|---|---|---|---|
| 24h 20 wings | 38,569,506 | 82 | 39 | 16 | 2753 |
| 24h 45 wings | 8,882,230 | 98.4 | 15 | 16 | 4103 |
| 24h 75 wings | 8,061,809 | 98.2 | 9 | 14 | 2623 |
| L3 rep1 20 wings | 53,806,249 | 98.6 | 74 | 19 | 907 |
| L3 rep2 20 wings | 50,747,138 | 90.5 | 63 | 14 | 700 |

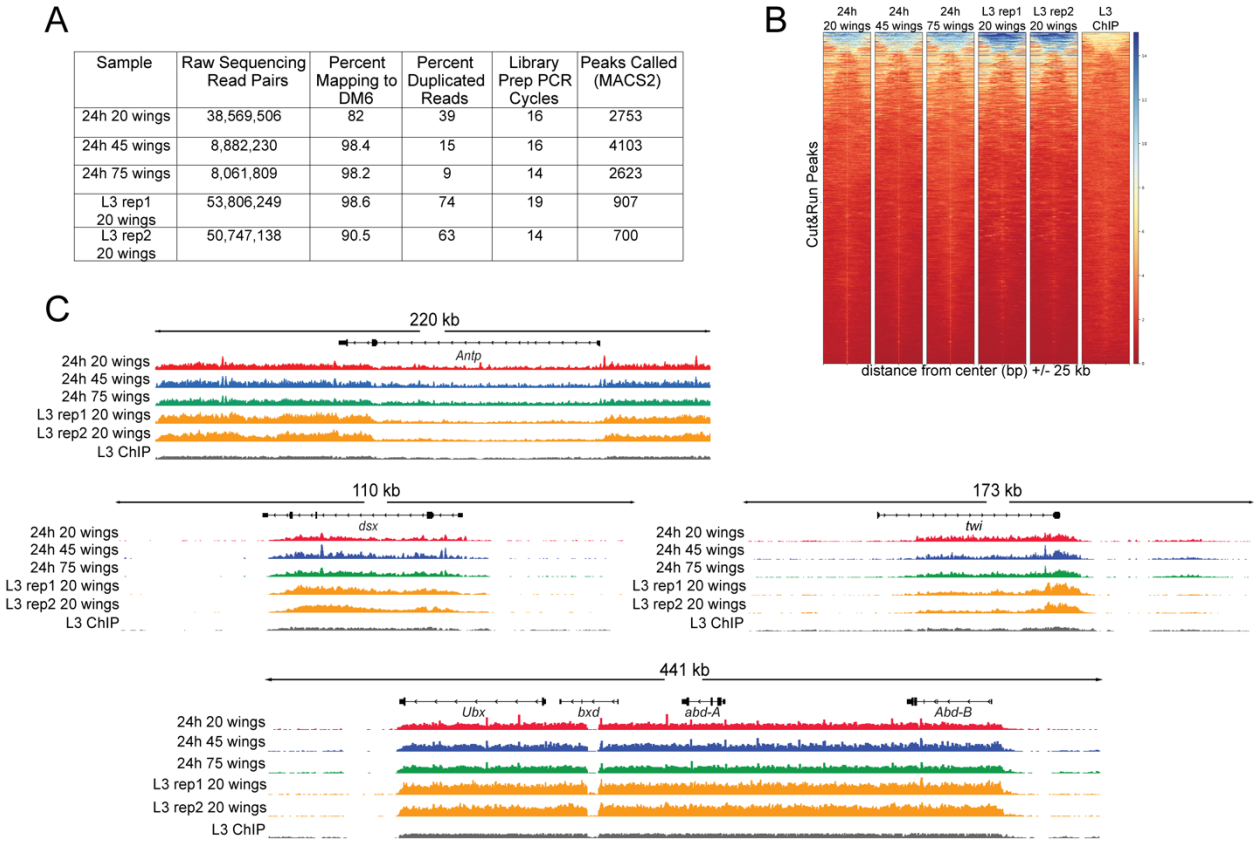


**Figure 2.4. H3K27me3 CUT&RUN on dissociated pupal wings identifies stable domains similar to H3K27me3 ChIP-seq on larval wings. (A**) Table of quality metrics comparing H3K27me3 CUT&RUN data prepared from 20 (red), 45 (blue) and 75 (green) dissociated 24h APF wings and third larval instar dissociated wings (gold) to H3K27me3 third larval instar wing ChIP-seq (black). Downsampling of the CUT&RUN 20 wings and third larval instar samples was performed to account for the varying sequencing depth; number of peaks shown reflects downsampled data. (**B**) Heatmaps showing signal intensity of peaks called from CUT&RUN dissociated 24h APF wings with differing sample input compared to peak signal intensity in third larval instar ChIP-seq. (**C**) Browser tracks showing H3K27me3 coverage at *Antp*, *dsx*, *twi*, and the bithorax complex containing *Ubx*, *bxd*, *abd-A* and *Abd-B* loci comparing CUT&RUN wing samples with third larval instar wing disc ChIP-seq. Browser tracks were group autoscaled with the following scales: *Antp* locus(scale 0-39), *dsx* locus (scale 0-45), *twi* locus (scale 0-33), and *Ubx* locus (scale 0-37).

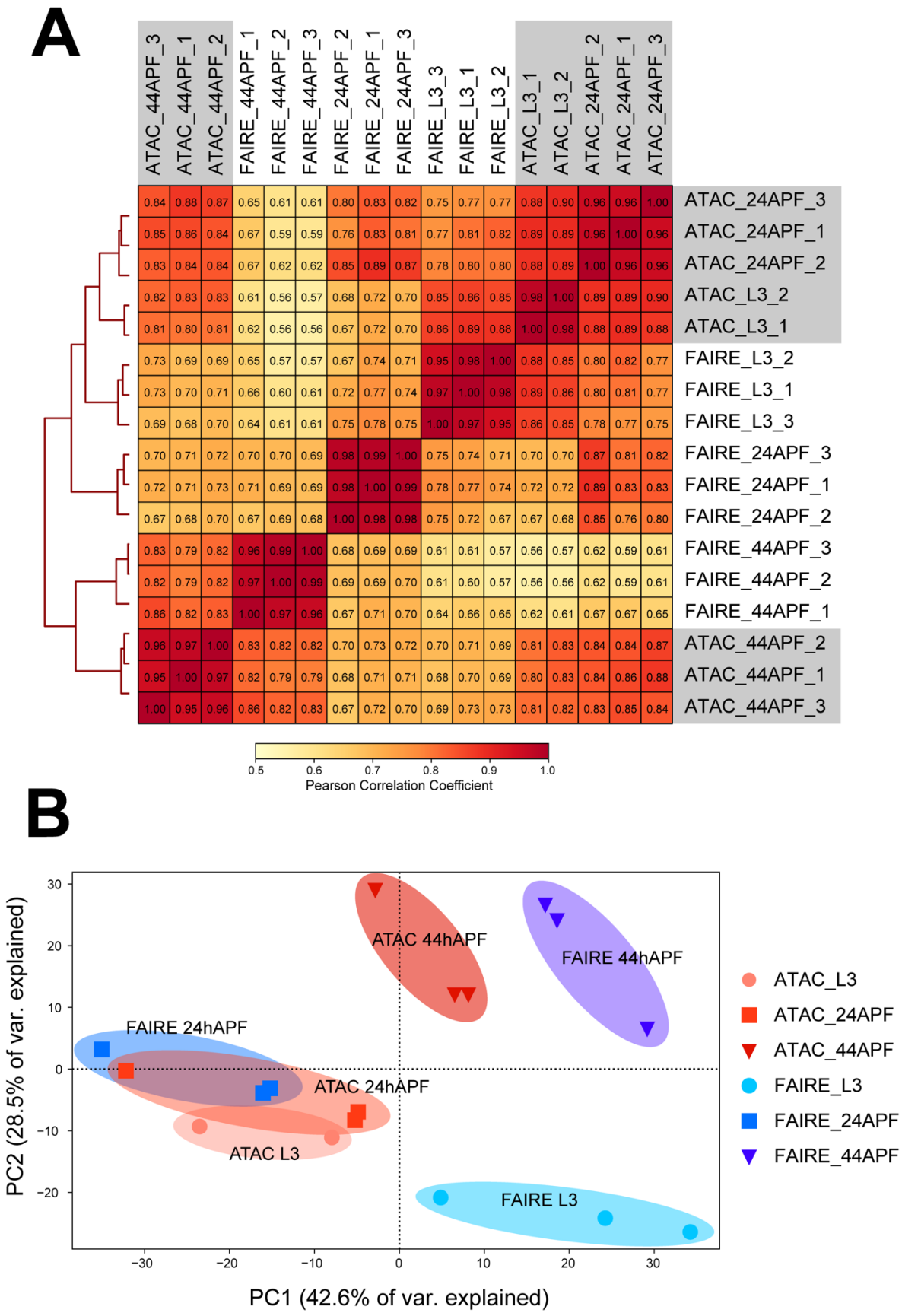
A
ATAC_44APF_3
ATAC_44APF_1
ATAC_44APF_2
FAIRE_44APF_1
FAIRE_44APF_2
FAIRE_44APF_3
FAIRE_24APF_2
FAIRE_24APF_1
FAIRE_24APF_3
FAIRE_L3_3
FAIRE_L3_1
FAIRE_L3_2
ATAC_L3_1
ATAC_L3_2
ATAC_24APF_2
ATAC_24APF_1
ATAC_24APF_3
ATAC_24APF_3
ATAC_24APF_1
ATAC_24APF_2
ATAC_L3_2
ATAC_L3_1
FAIRE_L3_2
FAIRE_L3_1
FAIRE_L3_3
FAIRE_24APF_3
FAIRE_24APF_1
FAIRE_24APF_2
FAIRE_44APF_3
FAIRE_44APF_2
FAIRE_44APF_1
ATAC_44APF_2
ATAC_44APF_1
ATAC_44APF_3
0.5
0.6
0.7
0.8
0.9
1.0
Pearson Correlation Coefficient
B
ATAC 44hAPF
FAIRE 44hAPF
FAIRE 24hAPF
ATAC 24hAPF
ATAC L3
FAIRE L3
PC2 (28.5% of var. explained)
PC1 (42.6% of var. explained)
ATAC_L3
ATAC_24APF
ATAC_44APF
FAIRE_L3
FAIRE_24APF
FAIRE_44APF

**Figure S2.1. Pearson Correlation and PCA Analysis comparing ATAC-Seq and FAIRE-Seq data from larval and pupal wings.** Pearson correlation and hierarchical clustering analysis (**A**) and principal component analysis (**B**) of ATAC-Seq and FAIRE-Seq data from third instar larval (L3) wing discs and pupal wings at 24 and 44 hours after puparium formation (APF). Each analysis was performed based on read coverage from individual replicates within the union set of peak regions for all conditions.

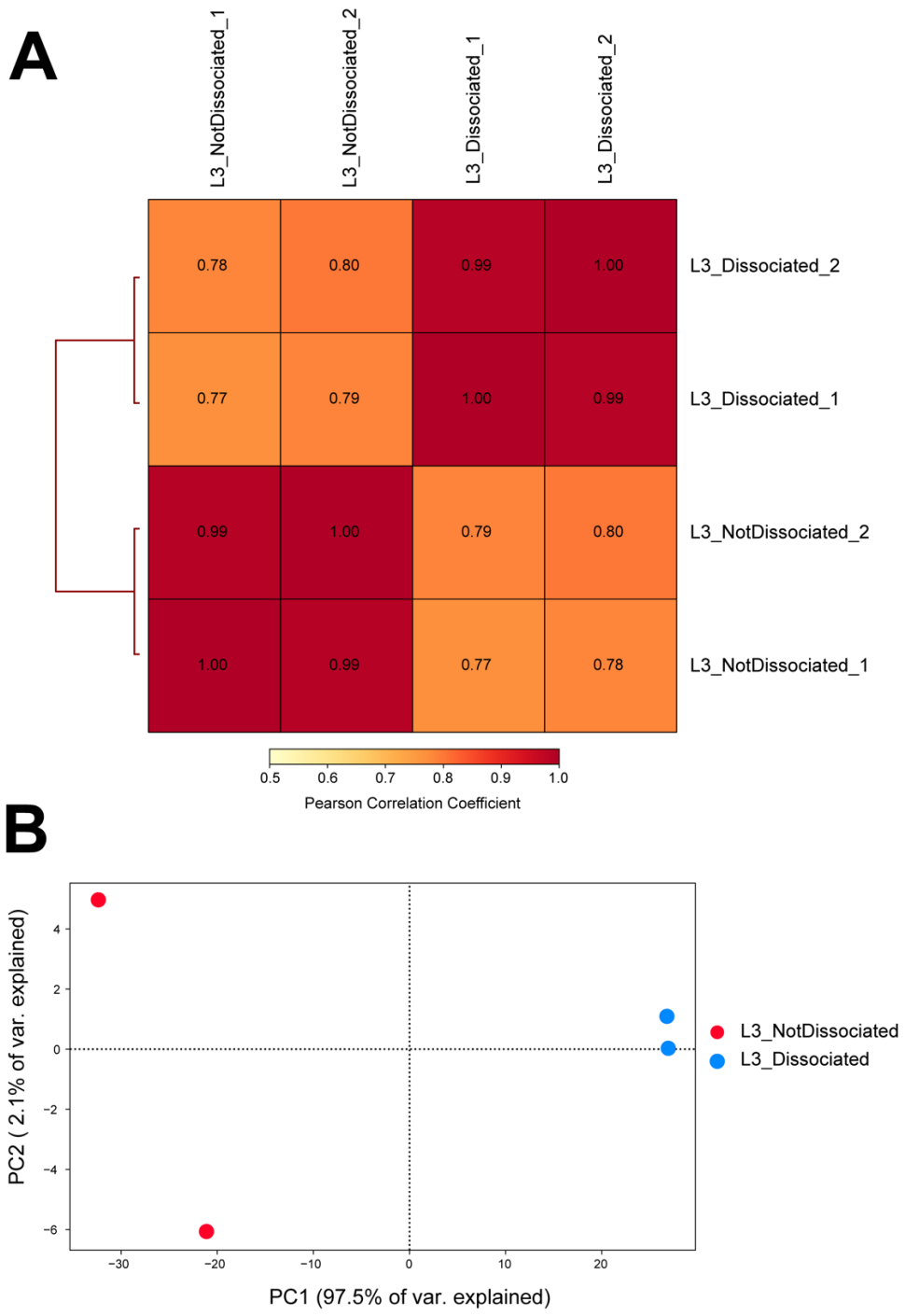


**Figure S2.2. Pearson Correlation and PCA Analysis comparing ATAC-Seq data from dissociated and non-dissociated larval wing discs.** Pearson correlation and hierarchical clustering analysis (**A**) and principal component analysis (**B**) of ATAC-Seq data from third instar larval (L3) wing discs that were dissociated or not dissociated prior to cell lysis. Each analysis was performed based on read coverage from individual replicates within the union set of peak regions for both conditions.

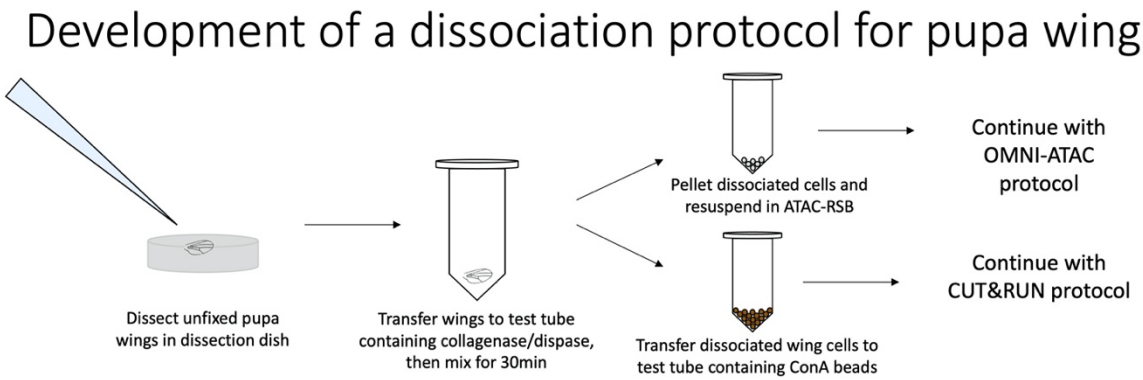


| Technique | Minimum wings/sample | Total cell estimate* |
|---|---|---|
| FAIRE-seq | 40 | 2,000,000 |
| ATAC-seq | 10 | 500,000 |
| ChIP-seq | 200** | 10,000,000 |
| Cut & Run | 20 | 1,000,000 |

*Note these cell number estimates are for dissected pupal wings lacking the hinge and notum
** Described in DOI: 10.21769/BioProtoc.2327

**Figure S2.3. Protocol overview and cell number estimates.** The diagram outlines the steps for dissociation prior to ATAC-Seq or Cut & Run. The table provides estimates of the minimum number of wings and cells for each approach compared in this paper.

## 2.6 References


Ahmad, K., and Spens, A.E. (2019). Separate Polycomb Response Elements control chromatin state and activation of the vestigial gene. PLoS Genet *15*, e1007877. 10.1371/journal.pgen.1007877.

Amemiya, H.M., Kundaje, A., and Boyle, A.P. (2019). The ENCODE Blacklist: Identification of Problematic Regions of the Genome. Sci Rep *9*, 9354. 10.1038/s41598-019-45839-z.

Bolger, A.M., Lohse, M., and Usadel, B. (2014). Trimmomatic: a flexible trimmer for Illumina sequence data. Bioinformatics *30*, 2114-2120. 10.1093/bioinformatics/btu170.

Corces, M.R., Trevino, A.E., Hamilton, E.G., Greenside, P.G., Sinnott-Armstrong, N.A., Vesuna, S., Satpathy, A.T., Rubin, A.J., Montine, K.S., Wu, B., et al. (2017). An improved ATAC-seq protocol reduces background and enables interrogation of frozen tissues. Nat Methods *14*, 959-962. 10.1038/nmeth.4396.

Danecek, P., Bonfield, J.K., Liddle, J., Marshall, J., Ohan, V., Pollard, M.O., Whitwham, A., Keane, T., McCarthy, S.A., Davies, R.M., and Li, H. (2021). Twelve years of SAMtools and BCFtools. Gigascience *10*. 10.1093/gigascience/giab008.

Davie, K., Jacobs, J., Atkins, M., Potier, D., Christiaens, V., Halder, G., and Aerts, S. (2015). Discovery of transcription factors and regulatory regions driving in vivo tumor development by ATAC-seq and FAIRE-seq open chromatin profiling. PLoS Genet *11*, e1004994. 10.1371/journal.pgen.1004994.

de la Cruz, A.F., and Edgar, B.A. (2008). Flow cytometric analysis of Drosophila cells. Methods Mol Biol *420*, 373-389. 10.1007/978-1-59745-583-1_24.

Flegel, K., Sun, D., Grushko, O., Ma, Y., and Buttitta, L. (2013). Live cell cycle analysis of Drosophila tissues using the Attune Acoustic Focusing Cytometer and Vybrant DyeCycle violet DNA stain. J Vis Exp, e50239. 10.3791/50239.

Fristrom, J.W., Doctor, J., Fristrom, D.K., Logan, W.R., and Silvert, D.J. (1982). The formation of the pupal cuticle by Drosophila imaginal discs in vitro. Dev Biol *91*, 337-350. 10.1016/0012-1606(82)90040-9.

Harris, R.E., Stinchfield, M.J., Nystrom, S.L., McKay, D.J., and Hariharan, I.K. (2020). Damage-responsive, maturity-silenced enhancers regulate multiple genes that direct regeneration in Drosophila. Elife *9*. 10.7554/eLife.58305.

Karolchik, D., Hinrichs, A.S., Furey, T.S., Roskin, K.M., Sugnet, C.W., Haussler, D., and Kent, W.J. (2004). The UCSC Table Browser data retrieval tool. Nucleic Acids Res *32*, D493-496. 10.1093/nar/gkh103.

Kent, W.J., Sugnet, C.W., Furey, T.S., Roskin, K.M., Pringle, T.H., Zahler, A.M., and Haussler, D. (2002). The human genome browser at UCSC. Genome Res *12*, 996-1006. 10.1101/gr.229102.

Langmead, B., and Salzberg, S.L. (2012). Fast gapped-read alignment with Bowtie 2. Nat Methods *9*, 357-359. 10.1038/nmeth.1923.

Liao, Y., Smyth, G.K., and Shi, W. (2014). featureCounts: an efficient general purpose program for assigning sequence reads to genomic features. Bioinformatics *30*, 923-930. 10.1093/bioinformatics/btt656.

Loubiere, V., Delest, A., Thomas, A., Bonev, B., Schuettengruber, B., Sati, S., Martinez, A.M., and Cavalli, G. (2016). Coordinate redeployment of PRC1 proteins suppresses tumor formation during Drosophila development. Nat Genet *48*, 1436-1442. 10.1038/ng.3671.

Ma, Y., McKay, D.J., and Buttitta, L. (2019). Changes in chromatin accessibility ensure robust cell cycle exit in terminally differentiated cells. PLoS Biol *17*, e3000378. 10.1371/journal.pbio.3000378.

Martin, M. (2011). Cutadapt removes adapter sequences from high-throughput sequencing reads. EMBnet.journal; Vol 17, No 1: Next Generation Sequencing Data Analysis. 10.14806/ej.17.1.200.

Meers, M.P., Bryson, T.D., Henikoff, J.G., and Henikoff, S. (2019). Improved CUT&RUN chromatin profiling tools. Elife *8*. 10.7554/eLife.46314.

Niederhuber, M.J., and McKay, D.J. (2021). Mechanisms underlying the control of dynamic regulatory element activity and chromatin accessibility during metamorphosis. Curr Opin Insect Sci *43*, 21-28. 10.1016/j.cois.2020.08.007.

Papp, B., and Muller, J. (2006). Histone trimethylation and the maintenance of transcriptional ON and OFF states by trxG and PcG proteins. Genes Dev *20*, 2041-2054. 10.1101/gad.388706.

Ramirez, F., Ryan, D.P., Gruning, B., Bhardwaj, V., Kilpert, F., Richter, A.S., Heyne, S., Dundar, F., and Manke, T. (2016). deepTools2: a next generation web server for deep-sequencing data analysis. Nucleic Acids Res *44*, W160-165. 10.1093/nar/gkw257.

Reed, C.T., Murphy, C., and Fristrom, D. (1975). The ultrastructure of the differentiating pupal leg ofDrosophila melanogaster. Wilehm Roux Arch Dev Biol *178*, 285-302. 10.1007/BF00848064.

Uyehara, C.M., and McKay, D.J. (2019). Direct and widespread role for the nuclear receptor EcR in mediating the response to ecdysone in Drosophila. Proc Natl Acad Sci U S A *116*, 9893-9902. 10.1073/pnas.1900343116.

Uyehara, C.M., Nystrom, S.L., Niederhuber, M.J., Leatham-Jensen, M., Ma, Y., Buttitta, L.A., and McKay, D.J. (2017). Hormone-dependent control of developmental timing through regulation of chromatin accessibility. Genes Dev. 10.1101/gad.298182.117.

Vizcaya-Molina, E., Klein, C.C., Serras, F., Mishra, R.K., Guigo, R., and Corominas, M. (2018). Damage-responsive elements in Drosophila regeneration. Genome Res *28*, 1852-1866. 10.1101/gr.233098.117.

Wilczynski, B., and Furlong, E.E. (2010). Dynamic CRM occupancy reflects a temporal map of developmental progression. Mol Syst Biol *6*, 383. 10.1038/msb.2010.35.

Zhang, Y., Liu, T., Meyer, C.A., Eeckhoute, J., Johnson, D.S., Bernstein, B.E., Nusbaum, C., Myers, R.M., Brown, M., Li, W., and Liu, X.S. (2008). Model-based analysis of ChIP-Seq (MACS). Genome Biol *9*, R137. 10.1186/gb-2008-9-9-r137.

Zhu, L.J., Gazin, C., Lawson, N.D., Pages, H., Lin, S.M., Lapointe, D.S., and Green, M.R. (2010). ChIPpeakAnno: a Bioconductor package to annotate ChIP-seq and ChIP-chip data. BMC Bioinformatics *11*, 237. 10.1186/1471-2105-11-237.

# Chapter 3: Transcriptional Repression and Enhancer Decommissioning at Cell Cycle Genes in Postmitotic Tissues

This chapter was written with:

Elizabeth Fogarty, Elli M. Buchert, Yiqin Ma, Ava Nicely, and Laura Buttitta

EMB contributed to the original writing and final revisions. EMB produced the data shown in Figures 6 – 9

## 3.1 Abstract

The mechanisms that maintain a non-cycling status in postmitotic tissues are still not well understood. Enhancer decommissioning has been observed for rate-limiting cell cycle genes in the short-lived *Drosophila* wing, a tissue where the cells die soon after eclosion. In this study, we observe that long-lived postmitotic tissues decommission enhancers at specific, rate-limiting cell cycle genes to maintain cell cycle exit during terminal differentiation as well. We also find that cell cycle genes with accessible enhancers remain activatable during terminal differentiation, suggesting their repression must be continuously maintained in postmitotic tissues. Here we examine expression of modular enhancers of *e2f1* and *stg* and note that these enhancers show dynamic temporal and spatial expression patterns. These decommissioned enhancers at cell cycle genes include shared and tissue-specific elements that in combination, result in broad gene expression with temporal regulation.

## 3.2 Introduction

The interplay between chromatin and the cell cycle is complex. The cell cycle involves dynamic remodeling of chromatin during DNA replication and mitoses, yet the cell cycle regulators themselves are encoded within the genome where chromatin organization and dynamics influences their expression (Ma et al., 2015). Transcriptional regulation for many genes can be simplified into two categories of gene regulation; broad ubiquitous expression often associated with “housekeeping” genes and developmentally dynamic genes with tissue-specific or cell type-specific expression patterns (Zabidi et al., 2015). Work in *Drosophila* has characterized the transcriptional differences between these modes of gene regulation and shown that housekeeping genes and developmentally dynamic genes have different features of enhancer architecture and preferentially use different types of core promoters. For example, enhancers for housekeeping genes are preferentially overlapping or proximal to the gene transcription start site (TSS) while enhancers for developmentally dynamic genes are predominantly found in introns and intergenic regions (Zabidi et al., 2015).

Most cell cycle genes have been characterized as having features of housekeeping genes, although this designation belies their complex regulation *in vivo* during development, which often exhibits spatial and temporal dynamics (Jones et al., 2000; Lehman et al., 1999; Thacker et al., 2003). This is especially obvious in tissues undergoing cell cycle transitions temporally regulated and coordinated with terminal differentiation programs. Some cells may exit the cell cycle and silence cell cycle genes in a spatially restricted or temporally controlled manner, such as the different cell types in the *Drosophila* larval and pupal eye, the pupal wing during metamorphosis or the

neuroblast stem cells of the larval and pupal brain (Firth and Baker, 2005; Meserve and Duronio, 2017; Milán et al., 1996; Schubiger and Palka, 1987; Siegrist et al., 2010). When cells transition from a proliferating to postmitotic state during development, cell cycle gene transcriptional control switches from activation to repression. This is thought to be largely mediated by the transcription factor complex E2F, which controls the expression of hundreds of cell cycle genes and can form an activating or repressive complex, based on its binding partners and the particular E2F subunit present in the complex. The E2F activator complex in *Drosophila* contains E2F1 with its dimerization partner DP, while the E2F repressive complex contains E2F1 or E2F2 complexed with the inhibitory Retinoblastoma family (Rbf) protein along with components of a conserved complex called dREAM, for dimerization partner (DP), retinoblastoma (RB)-like, E2F and MuvB (Korenjak et al., 2004). Rbf and or DREAM serves a critical function in cell cycle gene silencing during cell cycle exit (Litovchick et al., 2007), but whether this complex maintains cell cycle gene repression over the longer term in postmitotic tissues is unclear.

We previously showed that postmitotic cells in the *Drosophila* wing decommission enhancers at three specific rate-limiting cell cycle genes after cell cycle exit. We suggested this enhancer decommissioning may contribute to the robustness of permanent cell cycle exit, since even bypassing cell cycle exit and keeping cells in a cycling state could not prevent the closing of regulatory elements at the specific rate-limiting cell cycle genes (Ma et al., 2019). The three rate-limiting cell cycle regulators are the G1-S cyclin Cyclin E (CycE), the activator E2F subunit E2F1 and the mitotic Cyclin/Cdk phosphatase that activates mitotic entry, Cdc25c called String (Stg) in flies

(Neufeld et al., 1998). The genomic loci for *cycE*, *stg* and *e2f1* are unique for cell cycle genes in that they contain complex, modular cis-regulatory regions >44kb, more similar in architecture to the category of genes characterized as developmentally dynamic genes (Andrade-Zapata and Baonza, 2014; Jones et al., 2000; Lehman et al., 1999; Lopes and Casares, 2015). Perhaps more surprising though, was our finding that regulatory elements for hundreds of silenced cell cycle genes with enhancer architecture similar to housekeeping genes remain accessible during terminal differentiation, suggesting they require continual repression in the postmitotic phase of life. Thus, our emerging model for a long-term postmitotic state includes stable repression of hundreds of cell cycle genes, perhaps through long-term repression via repressive E2F complexes together with enhancer decommissioning at the cell cycle genes with complex enhancer architecture. But, this model is largely based on chromatin accessibility and gene expression data from the *Drosophila* wing, which is a short-lived tissue, where cells are destined to die by apoptosis shortly post eclosion (Link et al., 2007). One possibility is that short-lived tissues may only selectively decommission specific cell cycle enhancers, or they may use decommissioning instead of stable repression. Here, we address the question of whether long-term postmitotic tissues that persist for the lifetime of the animal follow a similar pattern of long-term repression at most cell cycle genes with enhancer decommissioning at a small subset of rate-limiting cell cycle genes.

### 3.3 Results and Discussion

We have previously shown in the developing wing that most cell cycle gene loci have simple chromatin accessibility profiles, harboring a single region of open chromatin at the promoter near the transcription start site (Ma et al., 2019). By assaying chromatin accessibility at time points before, during and after cell cycle exit, we observed that the chromatin accessibility at these genes is maintained after cell cycle exit. Indeed, even at time points long after cell cycle exit has occurred, cell cycle gene transcripts are no longer expressed, and the tissue has initiated its terminal differentiation program, cell cycle gene promoters remain accessible in the wing. To address whether these findings represent a wing-specific phenomenon or are generalizable to long-lived tissues, we expanded upon our previous work by comparing our findings in the wing to two tissues that persist in the adult fly, the brain and the eye. We chose to compare the eye and brain to the wing because these tissues are composed of diploid cells that persist throughout adulthood and their final cell cycles occur during metamorphosis with roughly similar timing to the wing (Figure 3.1). In the wing epithelial cells undergo a final cell cycle between 10-24h APF (Milán et al., 1996; Schubiger and Palka, 1987). In the eye, cell cycle exit is much less synchronous, as a subset of photoreceptor and cone cells exit from the cell cycle during larval and early pupal stages as the spatiotemporal morphogenetic furrow sweeps across the eye (Firth and Baker, 2005). This is followed by final cell cycles for pigment and bristle precursors in the pupa retina that complete by 24h APF (Buttitta et al., 2007; Meserve and Duronio, 2017). In the brain, neural stem cells termed neuroblasts give rise to ganglion mother cells (GMCs) that divide once and then differentiate into neurons or glia or neuroblasts give rise to transiently proliferating

intermediate neural progenitors (INPs) that give rise to multiple neuronal and glial subtypes (Rajan et al., 2021). Neuroblasts also exit from the cell cycle around 24h APF and, with the exception of a small number of eight central brain neuroblasts termed the “mushroom body” neuroblasts, the brain is nearly fully postmitotic after 24h APF (Homem et al., 2014; Siegrist et al., 2010). To confirm the timing of cell cycle exit in these tissues corresponds with E2F-dependent repression, we assayed for mitotic events as well as the silencing of cell cycle gene expression through a well-characterized E2F transcriptional activity reporter *pcna*-GFP, based upon an E2F regulated enhancer at the *proliferating cell nuclear antigen* (*pcna*) locus (Thacker et al., 2003). In all three tissues, E2F transcriptional activity and mitoses were largely silenced by 24h into metamorphosis, or 24h after puparium formation (APF) and remained silenced at 44h APF and presumably into adulthood.

We next expanded upon our previous work by measuring chromatin accessibility and gene expression in wing, eye and brain at selected time points before, during and after cell cycle exit (Figure 3.2A). Gene expression analysis by RNA-Seq confirmed that expression levels of cell cycle genes decrease in each tissue across this time course (Figure 3.2B), in agreement with the cell cycle exit dynamics that are similar across tissues (Figure 3.1). However, despite the loss of transcript expression during and after cell cycle exit, we observed that chromatin accessibility as measured by ATAC-Seq was maintained at the peaks nearest cell cycle genes in each tissue even at 44 hours APF when terminal differentiation is well underway (Figure 3.2C). This finding supports the idea that what we previously observed in the wing is a general principle of cell cycle

gene regulation in *Drosophila* rather than a peculiarity of wing cells that are destined to die soon after adult eclosion.

The maintenance of accessible chromatin at cell cycle gene promoters during and after cell cycle exit suggests an active repression mechanism whereby some factor(s) continue to occupy these regions to prevent ectopic transcript expression in post-mitotic cells. To investigate what these factors might be, we performed insect and vertebrate motif enrichment analyses on the ATAC peaks nearest to cell cycle genes in each tissue (Figure 3.2D). We found that most of the significantly enriched insect motifs correspond to annotated *Drosophila* promoter sequences. This is unsurprising, given that most of the peaks associated with cell cycle genes fall in promoter regions. Insect transcription factor motifs that were enriched included M1BP, a zinc finger factor which binds the Initiator-like promoter sequence (Baumann and Gilmour, 2017), DREF, a BED-finger factor that is known to regulate proliferation and other developmental processes (Tue et al., 2017) and Trl (GAGA factor). Notably, analysis of vertebrate motifs revealed enrichment for multiple annotated E2F motifs. This is again expected, given that E2F factors are evolutionarily conserved, master transcriptional regulators of the cell cycle, modulating the expression of hundreds of cell cycle genes throughout the genome. E2Fs are known to frequently bind the promoter regions of target genes, and can activate gene expression in a cell cycle phase-dependent manner. E2F activity is regulated based on the binding dynamics of the retinoblastoma (Rb) protein, which binds to E2Fs and hinders their transactivation capabilities in a Cdk-dependent manner. Indeed, it is thought that in postmitotic cells with low Cdk activity levels, Rb-bound E2F complexes continue to occupy binding sites and may actively repress transcript

expression. Therefore, repressive Rb/E2F complexes serve as likely candidates to explain long-term chromatin accessibility maintenance after cell cycle genes have been downregulated.

The finding that many E2F binding sites remain accessible after prolonged cell cycle exit, raised the question of whether ectopically providing E2F activator complexes could re-activate E2F transcriptional targets in postmitotic tissues after cell cycle exit has occurred. To test this, we used the E2F regulated enhancer from the *pcna*-GFP reporter as an E2F transcriptional readout and used the Gal4/UAS system to overexpress and ectopically provide activator E2F complexes in eyes or wings, specifically after 24h APF. To ensure the expression of E2F activator complexes was limited to postmitotic stages, we used the “flipout” approach where a temporally controlled heat-shock is used to induce the flippase enzyme to catalytically remove an intervening stop codon to activate Gal4 expression. By using this system we confirmed with a UAS- driven RFP that there was no Gal4 activity prior to 24h APF and robust Gal4 activity by 40-44h APF after the heatshock (Figure 3.3). We observed that ectopic E2F activator complexes were able to induce the *pcna*-GFP reporter in postmitotic tissues and that this induction could be strengthened by adding in G1 Cyclin/Cdk activity through ectopic Cyclin D and Cdk4, which form a complex to inhibit Rbf to further covert repressive E2F complexes to activator complexes. This suggests that repression of E2F transcriptional targets must be maintained long-term in long-lived postmitotic tissues.

### 3.3.1 Long-lived postmitotic fly tissues decommission enhancers at select, rate-limiting cell cycle genes.

We next compared how chromatin accessibility at the three rate-limiting cell cycle genes changes during and after cell cycle exit across the three tissues. As we previously observed for the wing, we see decommissioning of enhancers at all 3 loci in the eyes and brain after prolonged cell cycle exit at 44h APF (Figure 3.4). Interestingly, we were also able to discern tissue-specific as well as common elements that exhibit closing dynamics, suggesting that enhancer decommissioning is a common mechanism of ensuring cell cycle shut off across terminally differentiating tissues, although the specific enhancers affected may be different.

### 3.3.2 Dynamic chromatin regions within *e2f1* and *stg* show enhancer activity.

To confirm which accessible regions may serve as bona fide enhancers *in vivo* at the *e2f1* and *stg* loci, we crossed a subset of the Janelia Flylight Gal4 collection and one Vienna Tile line that overlaps with dynamic accessible regions in the genome (Kvon et al., 2014; Meissner et al., 2023). To visualize the Gal4 expression, we crossed the lines to a line called G-TRACE (Evans et al., 2009) that allows us to assess the current Gal4 expression using a UAS-responsive RFP, as well as past expression during development by UAS-induced permanent lineage tracing of cells that previously experienced Gal4 expression. By using this line we are able to assess whether elements that do not express in the pupa were active enhancers during larval stages.

Using this method, we examined four or five putative enhancers of *e2f1* in the eye and wing respectively, and seven putative enhancers of *stg* were examined in the

eye and wing (Figures 3.5 – 3.8). We observed that most putative enhancers, if they showed enhancer activity, showed a decrease in expression levels as time into metamorphosis progressed consistent with the decommissioning of these enhancers. Of particular note are the *e2f1* wing enhancers GMR49E02, GMR48C06 and VT045335 and the *stg* wing enhancers GMR31C09, GMR32C11 and GMR32F08 (Figures 3.6, 3.8). In each of these lines, we observe that the current expression intensity peaks between 18h – 36h APF before gradually decreasing at 44h APF. We note that the eye enhancers do not appear to follow this pattern as faithfully. The eye enhancers of interest are the *e2f1* enhancer lines GMR49E02 and GMR48C06 and the *stg* enhancers GM32C12, GMR31C09 and GMR31F07 (Figures 3.5, 3.7). The reason for this is unclear, but we speculate that there may be some factors expressed in the pupal eye at the later 44h APF timepoint that can bind to the synthetic core promoter that is located upstream of the genomic fragments (Jenett et al., 2012; Meissner et al., 2023). Further studies of the pupal eye enhancers, perhaps with different core promoters, will be necessary to resolve the source of the higher enhancer activity at later timepoints.

When comparing the enhancers that were examined in the pupal eyes and wings, we observe that some enhancers show activity in both tissues. For *e2f1*, GMR49E02 and GMR48C06 express in both tissues. Both enhancers show expression at 24h and 44h APF throughout most of the pupal eye, while GMR49E02 expresses at all timepoints in the wing and expression of GMR48C06 is restricted to 24h – 44h APF in the wing (Figure 3.5, 3.6). For *stg*, the enhancers GMR31F05, GMR31C09, GMR31F07 and GMR32F08 show activity in both tissues. In the eye, GMR31F05 shows faint expression in the anterior eye disc, expression of GMR31C09 and GMR31F07 is

observed at 44h APF throughout the eye, while GMR32F08 shows some expression in the larval anterior eye disc and in the antennal disc (Figure 3.7). In the wing, GMR31F05 shows expression in the larval wing disc notum, GMR31C09 expresses in the wing margin from 18h – 44h APF, GMR31F07 expresses faintly in the larval wing disc notum and faint expression in the wing veins from 24h – 44h APF, and GMR32F08 shows high expression from L3 until 24h APF when expression decreases drastically at 36h APF (Figure 3.8). We also note that some enhancers are tissue-specific. For instance, in the eye, we observe tissue-specific activity of the *stg* enhancer GMR32C12 in the lamina, which serves to connect the eye to the brain (Figure 3.7). The *e2f1* VT045335 enhancer only shows activity in the wing, with expression observed from L3 – 44h APF, mostly in the intervein regions (Figure 3.6). The *stg* enhancer GMR32C11 shows activity specifically in the wing, expressing at the ventral-dorsal and anterior-posterior (A-P) boundaries in the larval wing disc, continuing to be expressed along the A-P boundary and wing margin from 6h – 24h APF, before finally showing activity in the anterior wing at 36h – 44h APF (Figure 3.8). These findings indicate that some enhancers are shared between multiple tissues to drive expression of E2F1 and Stg, while others are tissue-specific.

Overall, we observe that over half of the putative enhancer lines tested show enhancer activity. For *e2f1*, two of four lines show activity in the eye while three of five lines show activity in the wing. For *stg*, five of seven lines show activity in the eye and wing, although not the same five lines. Of particular interest is that several enhancers for both *e2f1* and *stg* show expression in discrete compartments of the wing, but the combination of these enhancers cover the entire wing, suggesting that these enhancers

act in a modular fashion to drive expression of *e2f1* and *stg* throughout the wing. It is also important to note that especially for the wing, the activity of these enhancers decreases by 44h APF, which is also when we observe that the chromatin is largely closed, corroborating the possibility that enhancer decommissioning is one mechanism used to ensure these cells maintain a non-cycling, postmitotic state after cell cycle exit.

**3.3.3 Stable repression together with decommissioning of enhancers at rate-limiting cell cycle genes ensures robust cell cycle exit** Our model for genomic control of cell cycle dynamic gene expression is as follows (Figure 3.9): Cell cycle genes with simple enhancer architecture contain promoter proximal enhancers enriched for “housekeeping-associated” motifs such as E2F binding sites and DREF core promoters that exhibit accessibility during proliferation as well as cell cycle exit. The dynamic expression of these genes is controlled through the E2F complex switching from an activating to repressive form, influenced by cyclin/cdk activity and the phosphorylation of Rbf. By contrast, rate-limiting cell cycle genes with complex, modular enhancer architecture such as *cyclin E*, *E2f1* or *string*, may be influenced by E2F complexes, but are also controlled via E2F-idependent mechanisms through enhancers that bind other transcription factors such as Su(H) or bHLH proteins. These genes exhibit enhancer decommissioning after the transition to a postmitotic state to ensure their silencing despite the re-use of signaling pathways such as Notch or EGF in terminal differentiation processes.

## 3.4 Methods

### E2F transcriptional reporter assays:

The PCNA-GFP reporter with characterized E2F binding sites is described in Thacker et al., 2003. For Figure 3.1, genotypes were w; + ; PCNA-GFP with animals aged at 25°C. For Figure 3 genotypes were:

Control: y,w,hs-flp/w; UAS-RFP/+; PCNA-GFP, act>stop>Gal4

+E2F: y,w,hs-flp/w; UAS-RFP/UAS-E2F1, UAS-Dp; PCNA-GFP, act>stop>Gal4/+

E2F+DK4: y,w,hs-flp/w; UAS-RFP/UAS-CycD, UAS-Cdk4; PCNA-GFP, act>stop>Gal4/ UAS-E2F1, UAS-Dp

Animals were heat-shocked for 20 min at 37°C at 24-28h APF and dissected at 40-44h APF.

### Immunofluorescence:

Tissues were fixed in 4% Paraformaldehyde/PBS and stained as described (Ma et al., 2019). Mitoses were assays using rabbit anti phosphohistone H3 (PH3), (Cell Signaling) at 1:1000. Anti-GFP staining was performed with rabbit anti-GFP antibody (Invitrogen) at 1:1000. Secondaries were Alexa-488 or Alexa564 conjugated goat anti-rabbit (Invitrogen) used at 1:2000. DNA was stained with DAPI (Sigma). Tissues were mounted on slides with Vectashield mounting medium and imaged with a Leica DMI6000 epifluorescence system or a Leica SP5 confocal microscope.

### ATAC-seq

ATAC-seq was performed and analyzed as described in Buchert et al., 2023.

**RNA-seq**

Crosses were kept at room temperature. For pupal timepoints, white prepupa were collected and raised at 25ºC until either 24h or 44h APF. Approximately 16 eyes were dissected per sample. Tissues were dissected in filtered 1X PBS, transferred into Trizol containing glycogen, and vortexed. Chloroform was added, samples were vortexed, and then centrifuged for 15 minutes at 12,000xg at 4ºC. The aqueous layer was transferred to a new tube, with Isopropanol added before mixing and storing at -20 ºC overnight. The alcohol layer was removed, and samples were resuspended in RNAse free water. Libraries were produced and sequenced by the University of Michigan Sequencing Core. RNA-seq data was analyzed as described in Buchert et al., 2023, and reads were mapped to the dm6 genome using STAR 2.7.6a (Dobin et al., 2013).

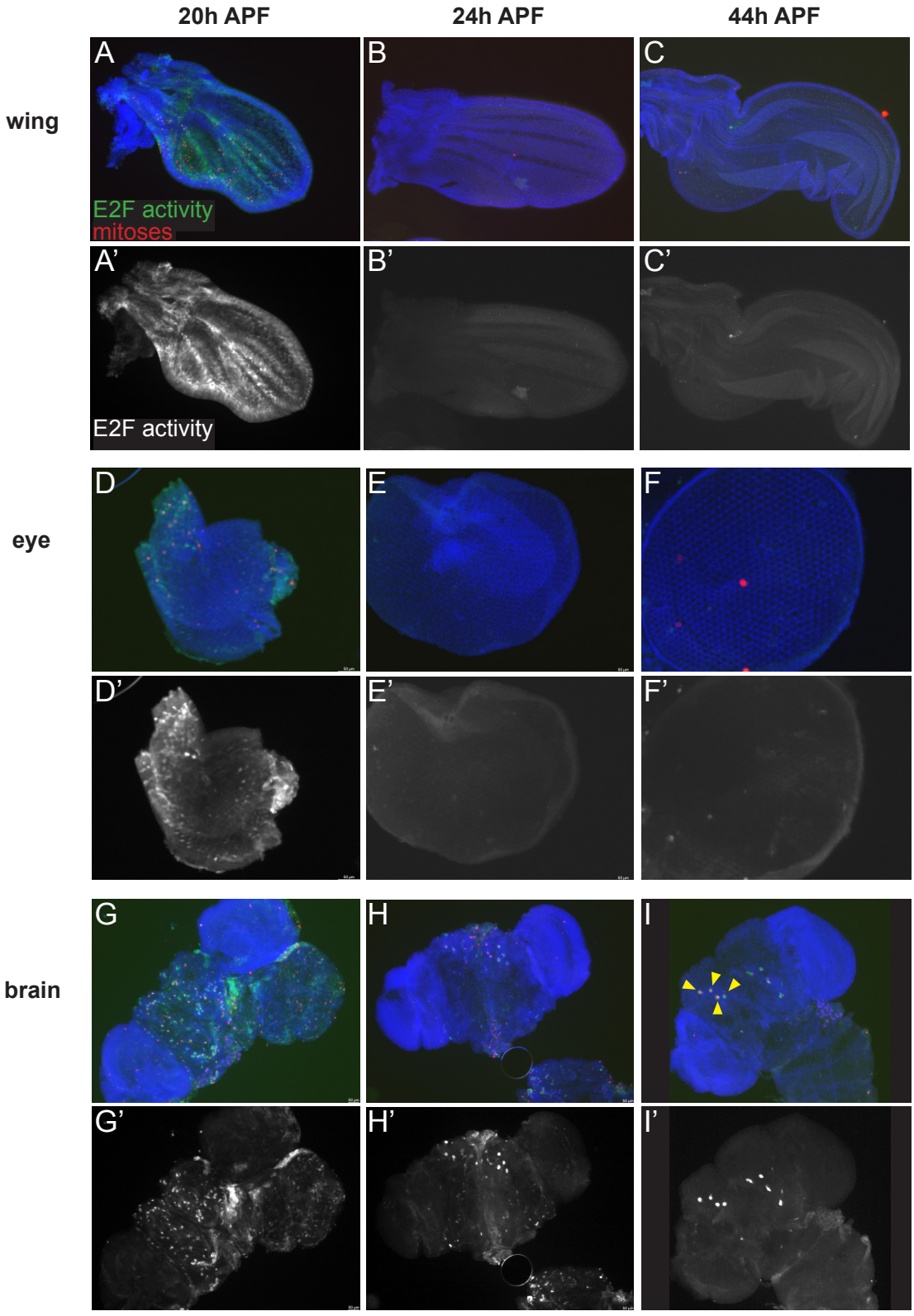
20h APF
24h APF
44h APF
wing
eye
brain
A
B
C
E2F activity
mitoses
A'
B'
C'
E2F activity
D
E
F
D'
E'
F'
G
H
I
G'
H'
I'

**Figure 3.1 The timing of cell cycle exit in the *Drosophila* wing, eye and brain are similar**. Wings (**A-C**), eyes (**D-F**) and brains (**G-I**) were dissected from staged pupa and stained for mitoses (anti-Phosphohistone H3) and E2F transcriptional activity (anti-GFP for PCNA-GFP reporter) at the timepoints indicated. Animals were collected as white pre-pupa (0h APF) and incubated at 25°C to the indicated timepoints. Yellow arrowheads indicate 4 of the 8 mushroom body neuroblasts that continue to cycle until 96h APF (Siegrist et al., 2010).

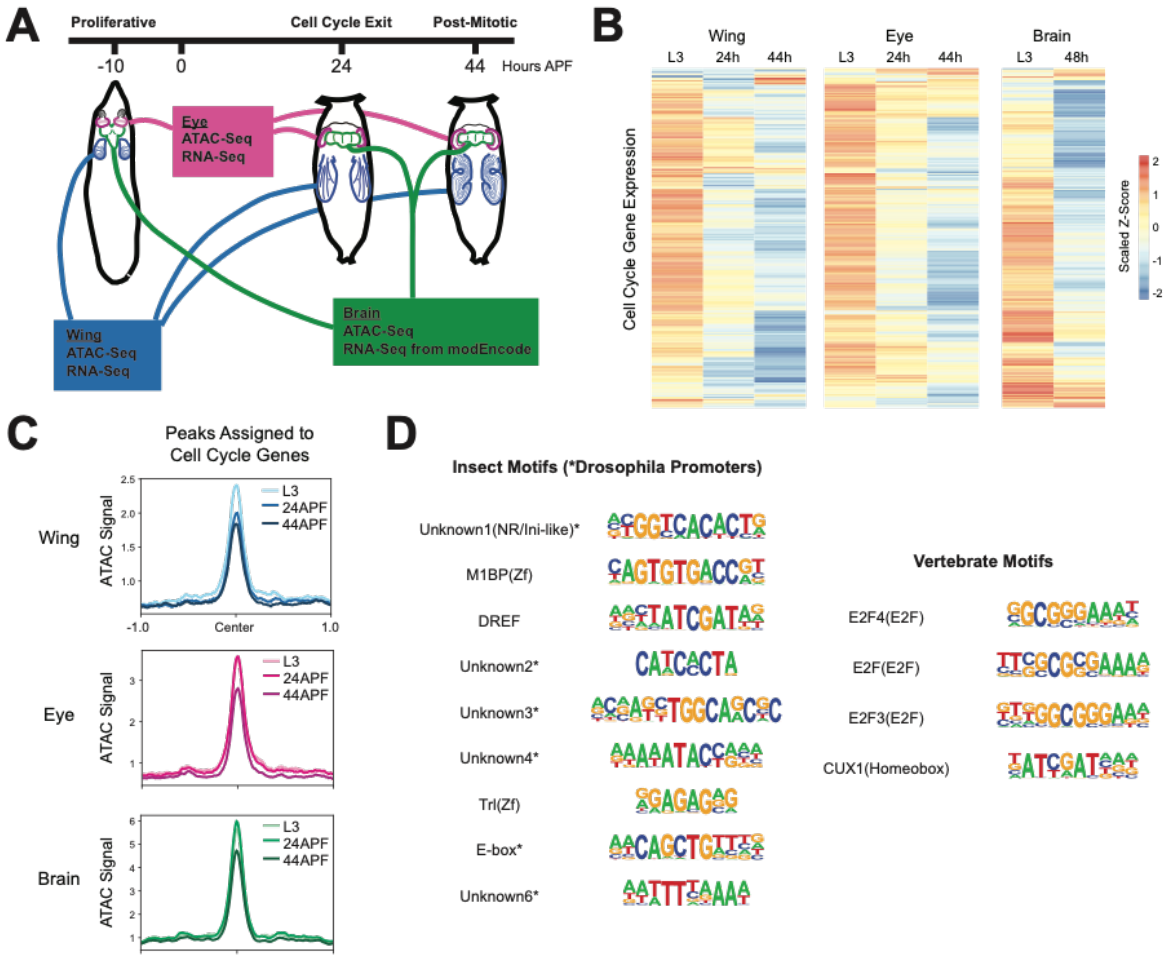


**Figure 3.2 Most cell cycle genes are transcriptionally repressed but retain chromatin accessibility in terminally differentiating fly tissues.** (**A**) Wing, eye, and brain tissue was dissected from third instar larvae (L3, 10 hours prior to puparium formation) and from pupae at 24 hours or 44 hours after puparium formation (APF). ATAC-Seq and RNA-Seq datasets were generated from wing and eye tissues at all three time points. ATAC-Seq data was generated from brain tissue at all three time points. Publicly available RNA-Seq datasets from L3 larva brain and 2-day pupa brain were generated by modEncode. (**B**) Heatmap depicting the average transcript expression values for 284 genes with annotated functions related to the cell cycle. Data are scaled by Z-score and hierarchically clustered. (**C**) Line plots showing the average ATAC-Seq signal across tissues and time points at peaks associated with cell cycle genes (+/- 1 kilobase from peak center). (**D**) Motif enrichment analyses on peaks associated with cell cycle genes in each tissue, including motifs annotated in insects and vertebrates. Table includes motif name and class and position weight matrix (PWM). Each motif received a Benjamini-corrected q-value < 0.05 for at least one tissue.

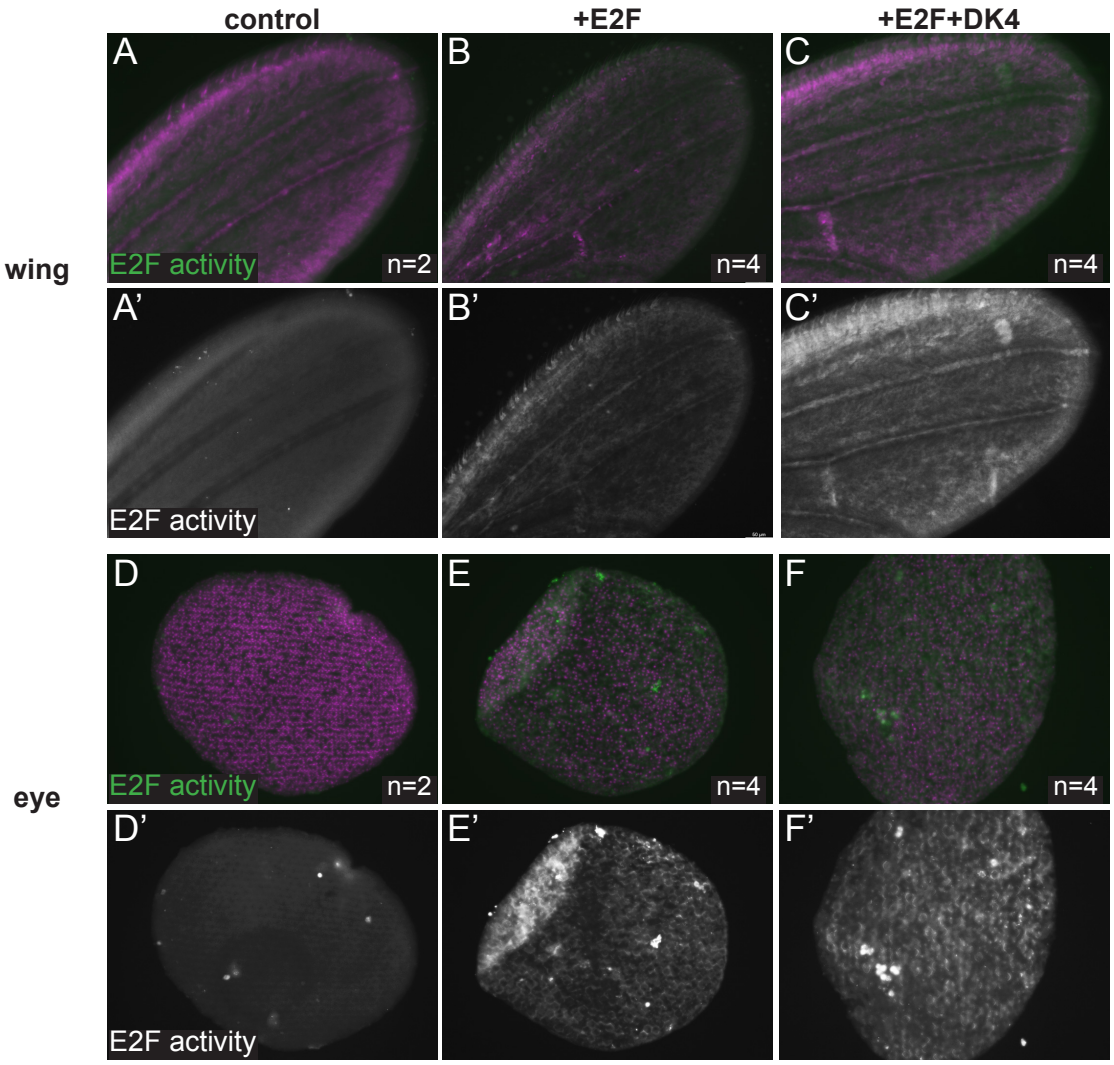


**Figure 3.3 An E2F regulated accessible enhancer remains activatable after 24h APF.** Wings (**A-C**) and eyes (**D-F**) were dissected from staged pupa and stained for E2F transcriptional activity (anti-GFP for PCNA-GFP reporter) at the timepoints indicated. Animals were collected as white pre-pupa (0h APF), staged to a postmitotic stage of 24-28h APF and heat-shocked for 20 min. to induce Gal4 expression driving E2F (UAS-E2F1+UAS-DP) or CycD +E2F (UAS-Cyclin D + UAS-Cdk4 + UAS-E2F1+UAS-DP) postmitotically. Tissues were collected and stained at 40-44h APF.

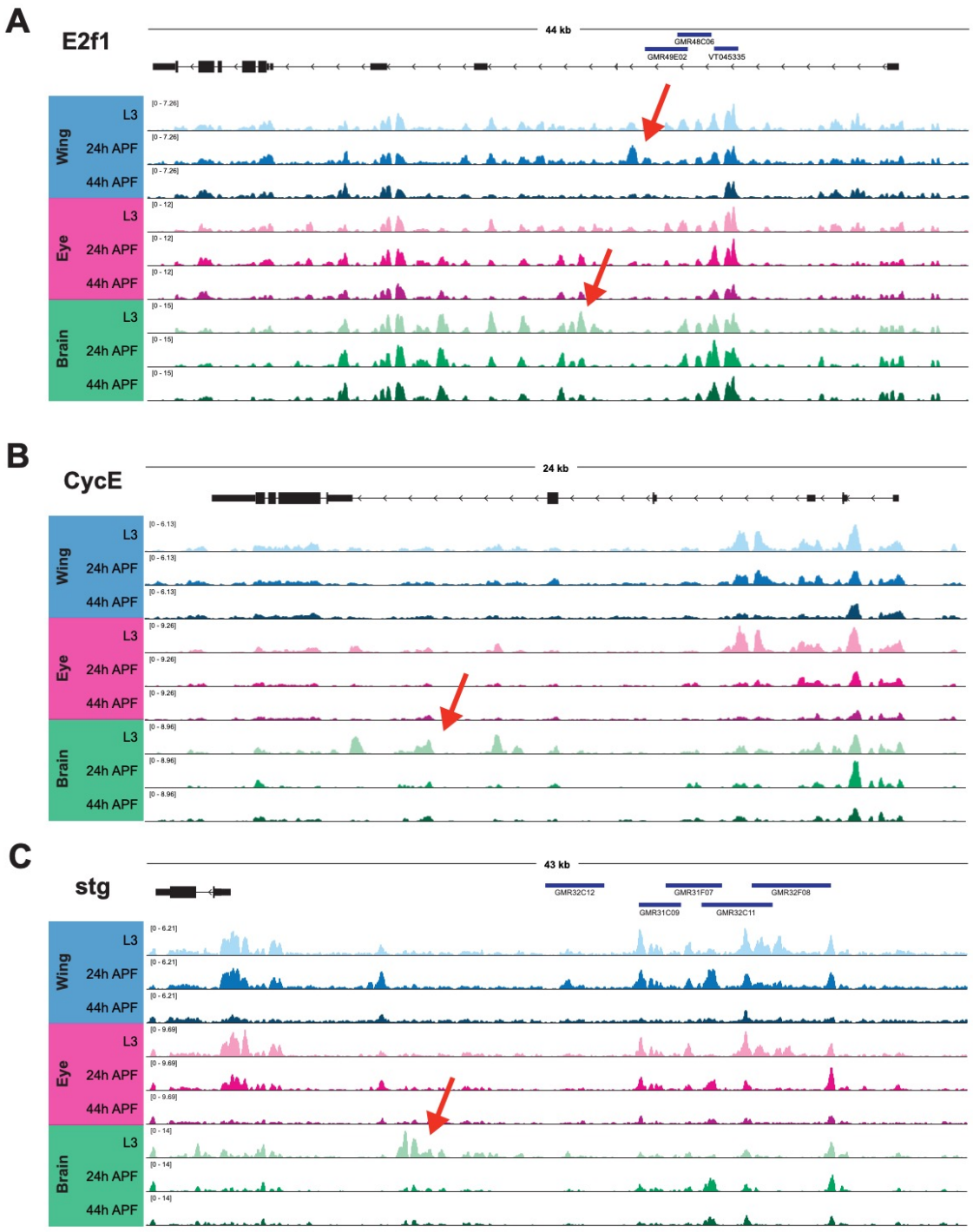


**Figure 3.4 Long-lived postmitotic fly tissues decommission enhancers at select, rate-limiting cell cycle genes.** ATAC-Seq accessibility data at E2f1 (**A**), CycE (**B**) and Stg (**C**) gene loci across tissues and time points. Arrows on gene diagrams indicate the direction of transcription. Y-axes indicate the normalized read counts per million. Red arrows indicate regions of tissue-specific accessibility.

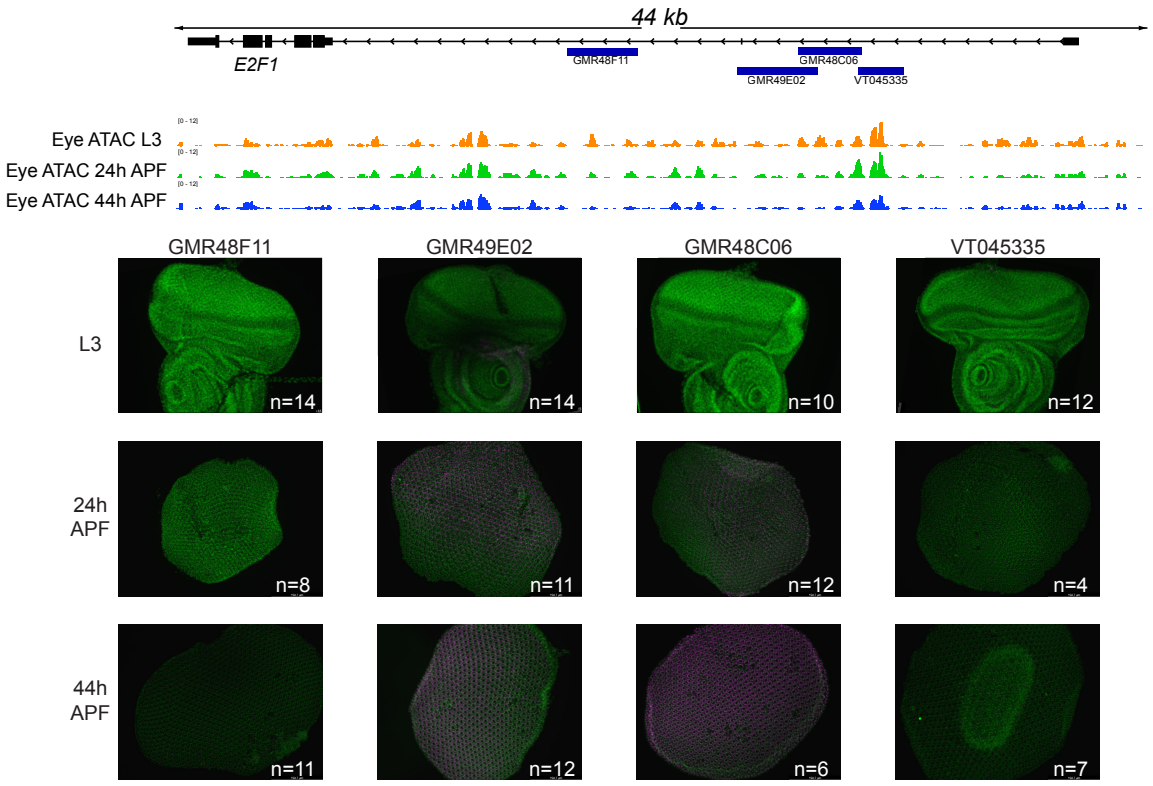


**Figure 3.5: Dynamic chromatin regions within *e2f1* show enhancer activity in the pupal eye.** ATAC-seq data shows chromatin accessibility changes throughout development. Several putative enhancer lines were examined at L3, 24h APF and 44h APF and some show enhancer activity, specifically GMR49E02 and GMR48C06.

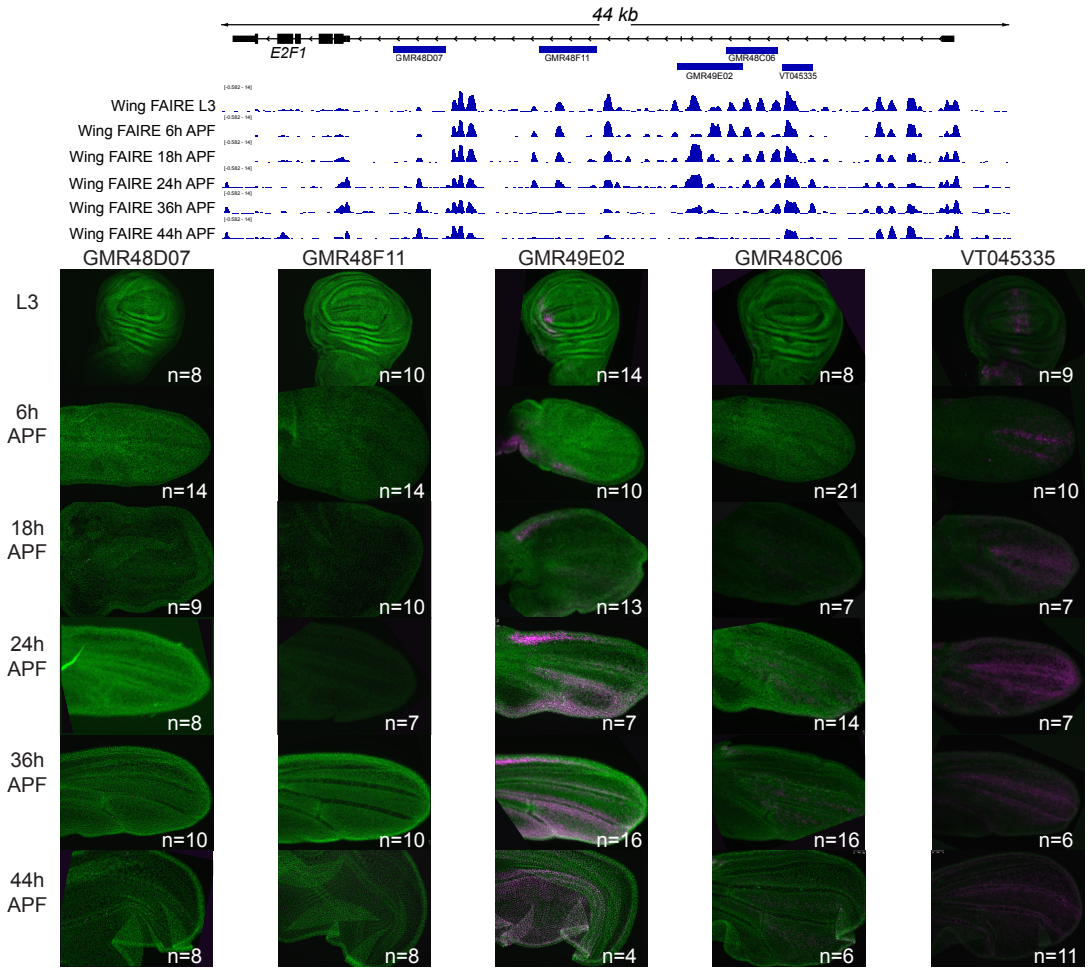


**Figure 3.6: Dynamic chromatin regions within *e2f1* function together to drive expression of E2F1 throughout the wing.** FAIRE-seq shows chromatin accessibility in the wing during development. We observe that a few of these regions show enhancer activity in the wing, specifically GMR49E02, GMR48C06 and VT045335. These enhancers appear to function in a modular fashion, as the sum of their expression patterns drive expression of E2F1 throughout the pupal wing.

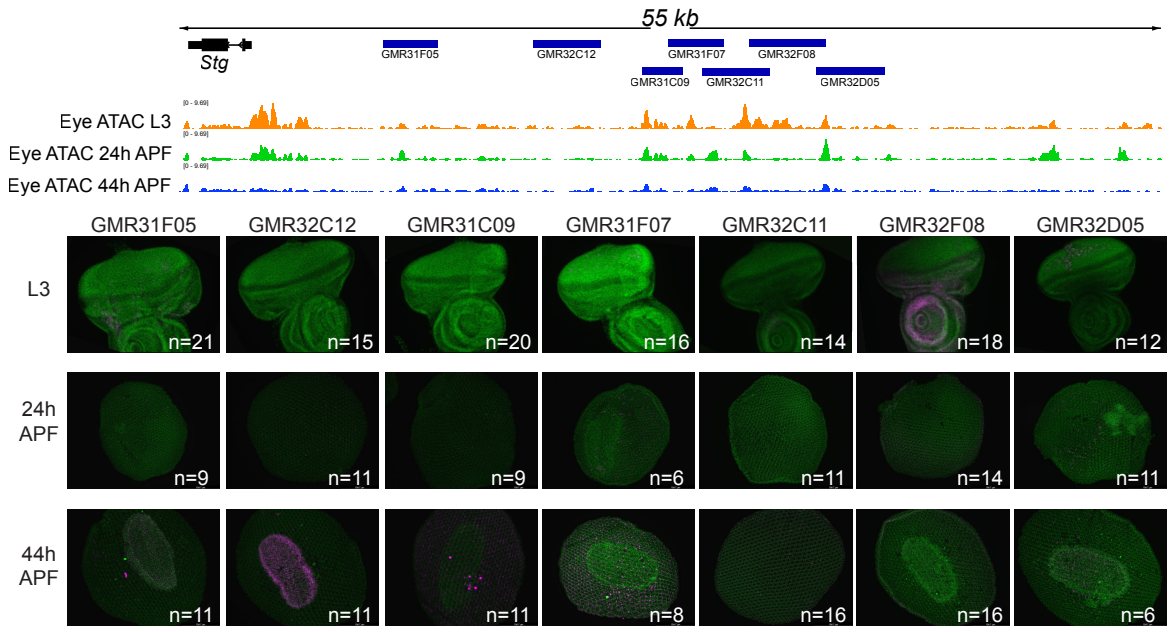


**Figure 3.7: Some dynamic chromatin regions in the *stg cis*-regulatory region have enhancer activity in the larval and pupal eye.** Eye ATAC-seq data shows accessible chromatin throughout metamorphosis. GMR32F08 exhibits enhancer activity in the larval eye-antennal disc, while GMR31C09 and GMR31F07 show enhancer activity in pupal eyes. GMR32C12 shows enhancer activity in the lamina.

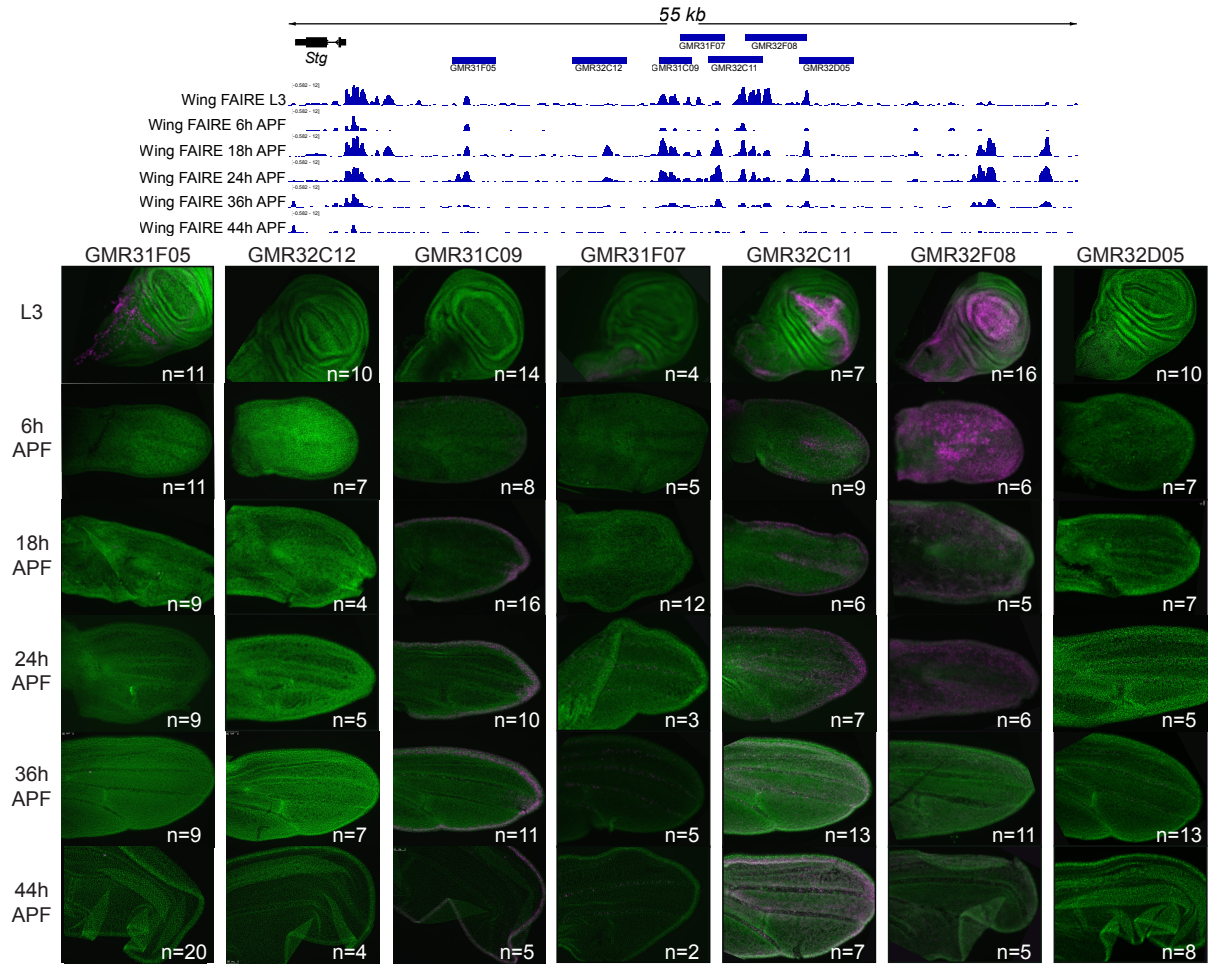


**Figure 3.8: Many modular enhancers function together to drive *stg* expression throughout the larval and pupal wing.** FAIRE-seq data shows dynamic chromatin accessibility changes throughout metamorphosis. Most dynamic chromatin regions show enhancer activity in larval and pupal wings. We observe that several enhancers express in discrete regions of larval and pupal wings, and that the sum of these enhancers drives expression of Stg throughout the entire wing.

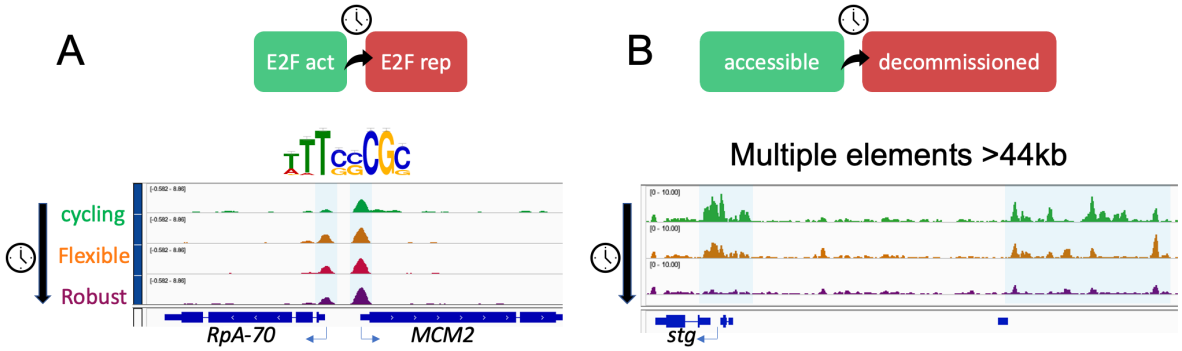


**Figure 3.9: Model. Stable repression together with decommissioning of enhancers at rate-limiting cell cycle genes ensures robust cell cycle exit**
A. Cell cycle genes with simple enhancer architecture contain promoter proximal enhancers enriched for E2F binding sites that exhibit accessibility during proliferation as well as cell cycle exit. B. Rate-limiting cell cycle genes with complex, modular enhancer architecture exhibit enhancer decommissioning after the transition to a postmitotic state.

### 3.5 References


Andrade-Zapata, I., Baonza, A., 2014. The bHLH factors extramacrochaetae and daughterless control cell cycle in Drosophila imaginal discs through the transcriptional regulation of the Cdc25 phosphatase string. PLoS Genet 10. https://doi.org/10.1371/JOURNAL.PGEN.1004233

Baumann, D.G., Gilmour, D.S., 2017. A sequence-specific core promoter-binding transcription factor recruits TRF2 to coordinately transcribe ribosomal protein genes. Nucleic Acids Res 45, 10481–10491. https://doi.org/10.1093/NAR/GKX676

Buchert, E.M., Fogarty, E.A., Uyehara, C.M., McKay, D.J., Buttitta, L.A., 2023. A tissue dissociation method for ATAC-seq and CUT&RUN in Drosophila pupal tissues. Fly (Austin) 17. https://doi.org/10.1080/19336934.2023.2209481

Buttitta, L.A., Katzaroff, A.J., Perez, C.L., de la Cruz, A., Edgar, B.A., 2007. A Double-Assurance Mechanism Controls Cell Cycle Exit upon Terminal Differentiation in Drosophila. Dev Cell 12, 631–643. https://doi.org/10.1016/j.devcel.2007.02.020

Dobin, A., Davis, C.A., Schlesinger, F., Drenkow, J., Zaleski, C., Jha, S., Batut, P., Chaisson, M., Gingeras, T.R., 2013. STAR: Ultrafast universal RNA-seq aligner. Bioinformatics 29, 15–21. https://doi.org/10.1093/bioinformatics/bts635

Evans, C.J., Olson, J.M., Ngo, K.T., Kim, E., Lee, N.E., Kuoy, E., Patananan, A.N., Sitz, D., Tran, P.T., Do, M.T., Yackle, K., Cespedes, A., Hartenstein, V., Call, G.B., Banerjee, U., 2009. G-TRACE: Rapid Gal4-based cell lineage analysis in Drosophila. Nat Methods 6, 603–605. https://doi.org/10.1038/nmeth.1356

Firth, L.C., Baker, N.E., 2005. Extracellular signals responsible for spatially regulated proliferation in the differentiating Drosophila eye. Dev Cell 8, 541–551. https://doi.org/10.1016/j.devcel.2005.01.017

Homem, C.C.F., Steinmann, V., Burkard, T.R., Jais, A., Esterbauer, H., Knoblich, J.A., 2014. Ecdysone and mediator change energy metabolism to terminate proliferation in Drosophila neural stem cells. Cell 158, 874–888. https://doi.org/10.1016/J.CELL.2014.06.024

Jenett, A., Rubin, G.M., Ngo, T.T.B., Shepherd, D., Murphy, C., Dionne, H., Pfeiffer, B.D., Cavallaro, A., Hall, D., Jeter, J., Iyer, N., Fetter, D., Hausenfluck, J.H., Peng, H., Trautman, E.T., Svirskas, R.R., Myers, E.W., Iwinski, Z.R., Aso, Y., DePasquale, G.M., Enos, A., Hulamm, P., Lam, S.C.B., Li, H.H., Laverty, T.R., Long, F., Qu, L., Murphy, S.D., Rokicki, K., Safford, T., Shaw, K., Simpson, J.H., Sowell, A., Tae, S., Yu, Y., Zugates, C.T., 2012. A GAL4-Driver Line Resource for Drosophila Neurobiology. Cell Rep 2, 991–1001. https://doi.org/10.1016/j.celrep.2012.09.011

Jones, L., Richardson, H., Saint, R., 2000. Tissue-specific regulation of cyclin E transcription during Drosophila melanogaster embryogenesis. Development 127, 4619–4630. https://doi.org/10.1242/dev.127.21.4619

Korenjak, M., Taylor-Harding, B., Binné, U.K., Satterlee, J.S., Stevaux, O., Aasland, R., White-Cooper, H., Dyson, N., Brehm, A., 2004. Native E2F/RBF Complexes Contain Myb-Interacting Proteins and Repress Transcription of Developmentally Controlled E2F Target Genes. Cell 119, 181–193. https://doi.org/10.1016/J.CELL.2004.09.034

Kvon, E.Z., Kazmar, T., Stampfel, G., Yáñez-Cuna, J.O., Pagani, M., Schernhuber, K., Dickson, B.J., Stark, A., 2014. Genome-scale functional characterization of Drosophila developmental enhancers in vivo. Nature 512, 91–95. https://doi.org/10.1038/nature13395

Lehman, D.A., Patterson, B., Johnston, L.A., Balzer, T., Britton, J.S., Saint, R., Edgar, B.A., 1999. Cis-regulatory elements of the mitotic regulator, string/Cdc25. Development 126, 1793–803.

Link, N., Chen, P., Lu, W.J., Pogue, K., Chuong, A., Mata, M., Checketts, J., Abrams, J.M., 2007. A collective form of cell death requires homeodomain interacting protein kinase. J Cell Biol 178, 567–574. https://doi.org/10.1083/JCB.200702125

Litovchick, L., Sadasivam, S., Florens, L., Zhu, X., Swanson, S.K., Velmurugan, S., Chen, R., Washburn, M.P., Liu, X.S., DeCaprio, J.A., 2007. Evolutionarily conserved multisubunit RBL2/p130 and E2F4 protein complex represses human cell cycle-dependent genes in quiescence. Mol Cell 26, 539–551. https://doi.org/10.1016/J.MOLCEL.2007.04.015

Lopes, C.S., Casares, F., 2015. Eye Selector Logic for a Coordinated Cell Cycle Exit. PLoS Genet 11, 1–22. https://doi.org/10.1371/journal.pgen.1004981

Ma, Y., Kanakousaki, K., Buttitta, L., 2015. How the cell cycle impacts chromatin architecture and influences cell fate. Front Genet 6. https://doi.org/10.3389/FGENE.2015.00019

Ma, Y., McKay, D.J., Buttitta, L., 2019. Changes in chromatin accessibility ensure robust cell cycle exit in terminally differentiated cells. PLoS Biol 17, e3000378. https://doi.org/10.1371/journal.pbio.3000378

Meissner, G.W., Nern, A., Dorman, Z., Depasquale, G.M., Forster, K., Gibney, T., Hausenfluck, J.H., He, Y., Iyer, N., Jeter, J., Johnson, L., Johnston, R.M., Lee, K., Melton, B., Yarbrough, B., Zugates, C.T., Clements, J., Goina, C., Otsuna, H., Rokicki, K., Svirskas, R.R., Aso, Y., Card, G.M., Dickson, B.J., Ehrhardt, E., Goldammer, J., Ito, M., Kainmueller, D., Korff, W., Mais, L., Minegishi, R., Namiki, S., Rubin, G.M., Sterne, G.R., Wolff, T., Malkesman, O., 2023. A searchable image

resource of Drosophila GAL4 driver expression patterns with single neuron resolution. Elife 12. https://doi.org/10.7554/ELIFE.80660

Meserve, J.H., Duronio, R.J., 2017. A population of G2-arrested cells are selected as sensory organ precursors for the interommatidial bristles of the Drosophila eye. Dev Biol 430, 374–384. https://doi.org/10.1016/J.YDBIO.2017.06.023

Milán, M., Campuzano, S., García-Bellido, A., 1996. Cell cycling and patterned cell proliferation in the Drosophila wing during metamorphosis. Proc Natl Acad Sci U S A 93, 11687–11692. https://doi.org/10.1073/PNAS.93.21.11687

Neufeld, T.P., De La Cruz, A.F.A., Johnston, L.A., Edgar, B.A., 1998. Coordination of growth and cell division in the Drosophila wing. Cell 93, 1183–1193. https://doi.org/10.1016/S0092-8674(00)81462-2

Rajan, A., Ostgaard, C.M., Lee, C.Y., 2021. Regulation of Neural Stem Cell Competency and Commitment during Indirect Neurogenesis. Int J Mol Sci 22. https://doi.org/10.3390/IJMS222312871

Schubiger, M., Palka, J., 1987. Changing Spatial Patterns of DNA Replication in the Developing Wing of Drosophila. Dev Biol 123, 145–153.

Siegrist, S.E., Haque, N.S., Chen, C.H., Hay, B.A., Hariharan, I.K., 2010. Inactivation of both Foxo and reaper promotes long-term adult neurogenesis in Drosophila. Curr Biol 20, 643–648. https://doi.org/10.1016/J.CUB.2010.01.060

Thacker, S.A., Bonnette, P.C., Duronio, R.J., 2003. The Contribution of E2F-Regulated Transcription to Drosophila PCNA Gene Function. Current Biology 13, 53–58.

Tue, N.T., Yoshioka, Y., Mizoguchi, M., Yoshida, H., Zurita, M., Yamaguchi, M., 2017. DREF plays multiple roles during Drosophila development. Biochim Biophys Acta Gene Regul Mech 1860, 705–712. https://doi.org/10.1016/J.BBAGRM.2017.03.004

Zabidi, M.A., Arnold, C.D., Schernhuber, K., Pagani, M., Rath, M., Frank, O., Stark, A., 2015. Enhancer-core-promoter specificity separates developmental and housekeeping gene regulation. Nature 518, 556–559. https://doi.org/10.1038/NATURE13994

# Chapter 4: Mi-2 and E93 Coordinate Robust Cell Cycle Exit With Terminal Differentiation Through Enhancer Decommissioning

Elli M. Buchert, Elizabeth Fogarty, Yiqin Ma, Matthew Neiderhuber, Daniel J. McKay, and Laura A. Buttitta

## 4.1 Abstract

Many postmitotic tissues coordinate robust cell cycle exit with the progression of terminal differentiation. While the signals involved in initiating cell cycle exit during terminal differentiation for some tissues have been described, less is known about the mechanisms that maintain a stable, non-cycling state. We previously found that chromatin accessibility changes at a subset of rate-limiting cell cycle genes occurs during maintenance of cell cycle exit, suggesting chromatin remodelers may play a key role in maintaining a robust postmitotic state during terminal differentiation. Here we show that the chromatin remodeler Mi-2 is required to ensure a stable, postmitotic state in *Drosophila* eyes and wings. Mi-2 alters chromatin accessibility and gene expression during cell cycle exit and terminal differentiation. Mi-2 and a transcription factor involved in tissue maturation, E93, close chromatin accessibility at an overlapping subset of potential enhancers that include the rate-limiting mitotic regulator *string* (*cdc25c*) and genes involved in the progression of terminal differentiation. E93 is also required for a

stable, postmitotic state and we verified *in vivo* that Mi-2 and E93 cooperate to decommission an enhancer for the essential mitotic regulator *string,* to coordinate the transition to a postmitotic state with terminal differentiation. Enhancer decommissioning at the *string* locus provides a molecular explanation for the long-term, nearly irreversible postmitotic state observed in many tissues as terminal differentiation progresses.

### 4.2 Introduction

*Drosophila melanogaster* metamorphosis is a time of dramatic developmental changes, during which many larval tissues are completely remodeled to allow for morphogenesis of the adult structures. The imaginal discs giving rise to the adult eyes, wings, and legs undergo temporally coordinated morphological and cell cycle changes during this time. The temporal coordination occurs in response to a pulse of the steroid hormone ecdysone, which triggers the larval to puparium transition, an event marking the beginning of metamorphosis (Niwa and Niwa, 2016). This transition sets in place a “feed-forward” cascade of ecdysone induced temporal transcriptional changes that coordinate events across tissues. This feed-forward system works by sequential activation of early-responsive targets that induce later targets, concurrent with negative feedback inhibition of the early response, resulting in a unidirectional transcriptional cascade (Thummel, 2002). This ecdysone transcriptional cascade has been best described for the salivary gland, where the large polytene chromosomes provide a visible readout of temporal transcriptional target activation through chromosome “puffs” at the genomic locations of ecdysone target genes (Thummel, 1990). However it is becoming clear that the order and identity of the genes in the ecdysone temporal

transcriptional responses is tissue specific, which is likely essential for shaping tissue-specific responses to the systemic pulses of ecdysone (Guo et al., 2016; Uyehara et al., 2017).

The ecdysone transcriptional cascade coordinates cell cycle changes with tissue remodeling and differentiation during metamorphosis. For example, in abdominal histoblasts, cell proliferation is induced during metamorphosis in response to ecdysone through ecdysone-dependent inhibition of a microRNA suppressor of the mitotic regulator Cdc25c, known as String in flies (Ninov et al., 2009; Verma and Cohen, 2015). By contrast in the wing, the same ecdysone pulse induces the transcriptional repressor Broad which temporarily suppresses String expression to result in a G2 arrest that synchronizes the cell cycle across the tissue during metamorphosis (Guo et al., 2016). By reshaping the response to the hormone in a tissue specific manner, the same systemic pulse of ecdysone can result in opposite outcomes, such as triggering proliferation in one tissue, while inducing cell cycle arrest and differentiation in another.

The imaginal tissues giving rise to the adult eyes, wings, and legs undergo their final cell cycles and a temporally coordinated permanent cell cycle exit during metamorphosis (Buttitta et al., 2007; Graves and Schubiger, 1982; Guo et al., 2016; Milán et al., 1996; Schubiger and Palka, 1987). This final cell cycle arrest is coordinated at 24h into metamorphosis (at standard rearing conditions of 25°C) and is coincident with a second large pulse of ecdysone. The role for ecdysone in promoting permanent cell cycle arrest or entry into a G0 cell cycle state is unclear, although ecdysone targets that are activated at this time such as the E93 transcription factor are known to be involved in tissue maturation and terminal differentiation, suggesting coordination

between the two processes. E93 is required for chromatin accessibility changes associated with wing terminal differentiation during metamorphosis demonstrating the importance of chromatin remodeling in this process (Uyehara et al., 2017).

We performed chromatin accessibility assays in parallel with transcriptomic analysis in pupal eyes and wings during cell cycle arrest and terminal differentiation with a goal to identify gene regulatory networks coordinating the two processes (Ma et al., 2019, Chapter 3). We found that most cell cycle genes maintain accessibility at their promoters despite strong repression after cell cycle exit. By contrast three critical rate-limiting cell cycle regulatory genes have complex, modular enhancers spanning many kilobases. These rate-limiting cell cycle genes exhibit regulatory element closing after cell cycle exit, potentially making them refractory to reactivation after cell cycle exit (Ma et al., 2019). This prompted us to look for chromatin remodelers that may play roles in promoting and maintaining robust cell cycle exit during metamorphosis.

Through a candidate genetic screen, we identified a role for the chromatin remodeler Mi-2 in promoting cell cycle exit during metamorphosis. Mi-2 is a homolog of the mammalian CHD3/4 chromatin remodelers, which are ATP-dependent chromatin remodelers of the Chromodomain-Helicase-DNA (CHD) binding family (Kunert and Brehm, 2009). ATP-dependent chromatin remodelers such as SWI/SNF have been shown to function in not only opening chromatin at differentiation genes to allow for gene expression activation, but they have also been shown to regulate cell cycle exit in other organisms by repressing expression of positive cell cycle regulators (Albini et al., 2015; Ruijtenberg and van den Heuvel, 2016).

Here, we sought to determine how the Mi-2 chromatin remodeler affects cell cycle exit by examining chromatin accessibility and gene expression changes when Mi-2 function is compromised. We show that Mi-2 function is required at a subset of cell cycle and differentiation-associated genes for coordinated chromatin accessibility and gene expression changes during cell cycle exit. Our data suggest that the ecdysone target E93 and Mi-2 act at an overlapping set of cell cycle and terminal differentiation genes to ensure coordination between postmitotic cell cycle exit and terminal differentiation. We validate this *in vivo* identifying a newly defined pupal eye enhancer for the critical mitotic regulator Cdc25c (*string*). Our work on E93 and Mi-2 provides a long-missing molecular pathway linking ecdysone signaling in the pupa to the transition to a postmitotic state and reveals how this is coordinated with terminal differentiation.

## 4.3 Results

### 4.3.1 Enhancers at *e2f1*, *cycE* and *stg* close during robust G0 independent of cell cycling status in the pupal eye.

Three key rate-limiting cell cycle genes, *e2f1*, *cyclin E* and *string,* have uniquely complex modular cis regulatory elements that span ten to >50kb, which control their tissue specific and temporal expression patterns (Andrade-Zapata and Baonza, 2014; Djiane et al., 2013; Jones et al., 2000; Lehman et al., 1999; Lopes and Casares, 2015). E2F1 is a transcriptional activator that works with its binding partner DP to regulate the expression levels of hundreds of cell cycle genes across cell cycle phases and controls the overall timing of the cell cycle (Bradley-Gill et al., 2016; Dimova et al., 2003; Neufeld and Edgar, 1998; Reis and Edgar, 2004). Cyclin E is an activating partner for the S-

phase cyclin-dependent kinase and a rate-limiting factor that regulates the G1-S phase transition, and String (Cdc25c) is a phosphatase that removes an inhibitory phosphorylation on the mitotic Cyclin/Cdk complex and is rate-limiting for entry into mitosis in many *Drosophila* tissues (Neufeld and Edgar, 1998; Ninov et al., 2009; Reis and Edgar, 2004). We previously examined chromatin accessibility dynamics in the *Drosophila* wing using Formaldehyde-Assisted Isolation of Regulatory Elements (FAIRE-seq) and Assay for Transposase-Accessible Chromatin (ATAC-seq) in the eye and brain. We observed thousands of chromatin accessibility changes coordinated with morphogenesis, cell cycle exit and terminal differentiation (Ma et al., 2019, Chapter 3). We found that verified enhancers at these three specific rate-limiting cell cycle genes close after cell cycle exit, while the vast majority of other cell cycle genes show no loss of chromatin accessibility, even after prolonged exit from the cell cycle (Ma et al., 2019). Furthermore, in the wing, we showed that verified and putative distal cis regulatory elements at these three rate-limiting cell cycle genes continue to close, even when wings are forced to continue ectopic proliferation during stages of metamorphosis that are normally post-mitotic (Ma et al., 2019). This demonstrates that the closing of these regulatory elements in the wing is developmentally controlled and independent of the tissue cell cycling status. This led us to a model where chromatin closing at three rate-limiting cell cycle genes may be critical to ensure and maintain a robust non-cycling state. We therefore next sought to identify the chromatin remodeler(s) responsible for these chromatin accessibility changes.

We have identified new regulators of cell cycle exit using a sensitized genetic background where specific cell types in the *Drosophila* eye undergo 1-2 extra rounds of

cell division. This background results in enlarged adult eyes amenable to forward genetic or candidate screening for enhancers that cause additional proliferation and increase eye size, as well as suppressors that reduce proliferation and decrease eye size (Pulianmackal et al., 2022). However, before we could perform an eye-based screen to identify chromatin remodelers involved in cell cycle exit, we first needed to establish whether distal cis regulatory elements also close at the rate-limiting cell cycle genes in the eye under conditions of ectopic proliferation, as they do in the wing. To test this we characterized genetic backgrounds that delay cell cycle exit in the eye vs. bypass cell cycle exit, causing sustained continued proliferation for more than 24h after normal cell cycle exit. To delay cell cycle exit we used the *Glass Multimer Repeat* (*GMR*)-Gal4 driver to express cell cycle regulators during the final cell cycle for the photoreceptors R1, R6, and R7, cone, pigment cell and bristle cell precursors (Freeman, 1996; Treisman, 2013). GMR-driven expression of the G1-S regulator CycE causes 1-2 rounds of additional cell cycles that stop by 44h APF, constituting a delay of cell cycle exit (Figure S4.1). When we simultaneously combine overexpression of CycE, with the G1 Cyclin Cyclin D (CycD) and its Cdk partner Cdk4, which promotes E2F1 activation through phosphorylation of the E2F inhibitor RB (Rbf in *Drosophila*, Meyer et al., 2000; Xin et al., 2002), we observe continued mitoses beyond 44h APF, constituting a sustained bypass of cell cycle exit (Figure S4.1). Importantly, the delay and bypass of cell cycle exit in the fly eye did not alter the timing of developmental hallmarks in the fly, including the onset of pigmentation in the eye or time to eclosion, confirming that developmental temporal regulation remained intact. However, we did observe about a 20% reduction in overall animal viability (Figure S4.1).

We next examined chromatin accessibility in the eye under cell cycle exit delay and bypass conditions using ATAC-Seq. Similar to the wing, we observed that distal regulatory elements at the rate-limiting cell cycle genes *e2f1*, *cycE* and *stg* continued to close after cell cycle exit, regardless of whether or not the eyes were still proliferating (Figure 4.1A, B). This suggested that these tissues use similar developmentally controlled mechanisms to close chromatin at the rate-limiting cell cycle genes. We therefore proceeded to use our sensitized eye background to screen for chromatin remodelers that are required for establishing or maintaining cell cycle exit.

### 4.3.2 Mi-2 is required for stable cell cycle exit in the *Drosophila* eye and wing.

We performed an RNAi-based candidate screen for chromatin modifiers or remodelers that enhance a large eye phenotype when knocked down in a sensitized background expressing the G1-S regulator CycE and an apoptosis inhibitor P35 (Hay et al., 1994). As internal screening controls, we included a known suppressor background, overexpression of the G1-S and mitotic Cyclin/Cdk inhibitors Dacapo and Wee, as well as the known positive regulator that causes extra proliferation, CycD+Cdk4+E2F overexpression (Figure 4.2A). We focused on one chromatin remodeler Mi-2, because both Mi-2$^{RNAi}$, as well as loss of one allele (*Mi-2$^{4}$*/+), resulted in reproducibly larger eyes (Figure 4.2A). We stained these eyes for Discs Large (DLG), a cell boundary marker, to visualize whether the enlarged eyes resulted from increases in cell size or cell number. As expected, suppression with Dacapo + Wee reduced interommatidial cell density and cone cell numbers, while Mi-2$^{RNAi}$ elevated interommatidial cell density and cone cell numbers, indicating that additional cell cycles had occurred (Figure 4.2B). We next

examined whether inhibition of Mi-2 alone in a non-sensitized background affected cell cycle exit. We expressed a control RNAi (*white*$^{RNAi}$) or *Mi-2*$^{RNAi}$ in eyes during the final cell cycle using *GMR*-Gal4. Eyes expressing the control RNAi exhibit very few mitoses and little E2F activity as revealed by expression of an E2F1 transcriptional reporter, PCNA-GFP (Thacker et al., 2003) while expression of Mi-2$^{RNAi}$ increases E2F activity and mitoses (Figure S4.2A). We next examined whether Mi-2 inhibition also delayed cell cycle exit in pupal wings. Overexpression of Mi-2$^{RNAi}$ alone in the posterior pupal wing using *engrailed*-Gal4 with a temperature sensitive Gal80 repressor Gal80$^{TS}$ (*en*$^{TS}$) to activate the Gal4 at L3, delays cell cycle exit and causes additional mitoses at 28h APF, that resolve by 36h APF (Figure S4.2B). This demonstrates that inhibition of Mi-2 temporarily delays cell cycle exit. To test whether inhibition of Mi-2 might further delay cell cycle exit in wings undergoing extra proliferation, as it did in the eye screen, we co-overexpressed E2F1 and its partner DP (hereafter referred to as E2F complex) in the posterior pupal wing using *en*$^{TS}$. E2F expression in the wing increases nuclear density by driving additional cell cycles from 24-36h APF but cannot sustain cell cycling at later timepoints such as 42h APF (Buttitta et al., 2007). By contrast, co-expression of E2F+ Mi-2$^{RNAi}$ allows for continued mitotic cycling at 42h APF (Figure 4.2C), demonstrating that in the wing Mi-2 also promotes cell cycle exit at later timepoints under conditions where cell cycle exit is delayed.

Mi-2 is a component of multiple chromatin remodeling complexes such as the NuRD and dMec complexes (Ahringer, 2000; Aughey et al., 2023; Kunert et al., 2009). In addition, Mi-2 can form NuRD and dMec independent complexes (Kim et al., 2017; Kreher et al., 2017; Kunert and Brehm, 2009) where its knockdown could result in

phenotypes simply by altering stoichiometries. To test whether the chromatin remodeling ATPase function of Mi-2 function was required for proper cell cycle exit, we expressed a dominant-negative form Mi-2 (Mi-$2^{DN}$) in which the ATPase domain has been deleted, which can bind nucleosomes but cannot hydrolyze ATP for chromatin remodeling (Fasulo et al., 2012). Overexpression of Mi-$2^{DN}$ but not wild type Mi-2 (Mi-$2^{WT}$) in eyes resulted in a double layer of interommatidial cells indicative of extra cell cycles in the pupal eye, demonstrating that the ATPase activity of Mi-2 is required for proper cell cycle exit (Figure S4.2D). In the sensitized background, we observed additional mitoses with overexpression of either Mi-$2^{WT}$ and Mi-$2^{DN}$ at 30h APF, 6 hours beyond the normal timing of cell cycle exit (Figure 4.2D, E). However only Mi-$2^{DN}$ resulted in extra cone and interommatidial cells (Figure 4.2F), suggesting the Mi-$2^{WT}$ may delay cell cycle exit by slowing the final cell cycle rather than by causing extra cell cycles. Consistent with this Mi-$2^{WT}$ suppressed eye size in the sensitized screening background suggesting overexpression of Mi-$2^{WT}$ reduces cell cycling, perhaps due to altered stoichiometry of Mi-2 complexes involved in DNA damage repair and chromosome condensation (Fasulo et al., 2012; Polo et al., 2010). As in the eye, Mi-$2^{DN}$ under the control of $en^{TS}$, is sufficient to delay cell cycle exit in the pupal wing (Figure 4.2G), demonstrating that Mi-2 ATPase activity is required for proper cell cycle exit in the *Drosophila* pupal eye and wing.

### 4.3.3 Mi-2 is required for chromatin remodeling at a subset of genes involved in coordinating terminal differentiation and cell cycle exit.

We performed parallel ATAC-seq and RNA-seq on 24h APF and 44h APF eyes to capture chromatin accessibility and gene expression data at the time of cell cycle exit and when the cells have become post-mitotic (Figure 4.1A). Using the GMR driver to manipulate Mi-2 during the final cell cycle and postmitotically, we compared three conditions, GMR-Gal4, UAS-P35 crossed to $w^{1118}$, UAS-Mi-$2^{WT}$ and UAS-Mi-$2^{DN}$. We included the UAS-Mi-$2^{RNAi}$ condition in the studies, but only observed a ~6-7% knockdown of the Mi-2 RNA transcript at both 24h APF and 44h APF. We also observed that the Mi-$2^{RNAi}$ ATAC-seq data clustered closely with the $w^{1118}$ condition at both 24h and 44h APF in the RNA-seq dataset (Figure S4.3), suggesting the Mi-2 knockdown during the final cell cycle is limited. Therefore we did not analyze the Mi-$2^{RNAi}$ data further.

We first compared Mi-$2^{WT}$ and Mi-$2^{DN}$ to $w^{1118}$ for ATAC-seq and RNA-seq. We observed little separation of these conditions in the 24h APF ATAC-seq and RNA-seq, but by 44h APF the Mi-$2^{DN}$ and Mi-$2^{WT}$ cluster separately in the RNA-seq, while only Mi-$2^{DN}$ clusters separately in the ATAC-seq (Figure S4.3). This suggests Mi-$2^{WT}$ expression has effects on gene expression that are not reflected in coordinated chromatin accessibility changes. Of over 45,000 peaks called by MACS2, 1893 peaks are significantly upregulated and 391 significantly downregulated in the Mi-$2^{DN}$ 44h APF time point compared to $w^{1118}$, while there were only 64 peaks significantly upregulated and 379 peaks significantly downregulated in the Mi-$2^{WT}$ 44h APF condition compared to $w^{1118}$ (Figure S4.3, Table 4.1). This suggests that the primary function of Mi-2 during the final cell cycle is to close accessible chromatin. Therefore, we focused further analysis on the Mi-$2^{DN}$ condition at 44h APF.

To validate our Mi-2$^{DN}$ dataset, we examined genes previously shown to be mis-regulated in *Drosophila* brains expressing Mi-2$^{RNAi}$ (Aughey et al., 2023). We observe that from the top 30 upregulated and top 30 downregulated genes in the Mi-2 brain study, the vast majority are affected in a similar manner by Mi-2$^{DN}$ in the eye (Figure S4.4). Of note, we see de-repression of several germline genes, which the *C. elegans* homolog of Mi-2, LET-418 has been shown to regulate (Unhavaithaya et al., 2002) as well as accessibility changes at the male germline gene *kumgang (kmg)*, which was previously shown to interact with Mi-2 to repress somatic gene expression in the germline (Kim et al., 2017). We also identify enriched motifs for transcription factors in our Mi-2$^{DN}$ accessibility data that overlap with motifs identified in the Mi-2$^{RNAi}$ brain study (Figure S4.4, Aughey et al., 2023).

Chromatin accessibility changes with Mi-2$^{DN}$ expression from 24-44h APF include three categories – regions that fail to close, regions that open ectopically or fail to close prior to 24h APF, and regions that close prematurely. We find that the majority of significant peaks fall into the 'peaks that fail to close' category. Genes such as *stg, blimp-1*, *vrille* (*vri*), *shadow* (*sad)*, and *hedgehog* (*hh*) fall into this category (Figure 4.3A, Figure S4.5). Most notably at the *broad* (*br*) locus a large peak that opens either ectopically or prior to 24h APF, is coordinated with upregulation of *br* expression (1.80-fold) at 44h APF (Figure S4.5). In the Mi-2$^{DN}$ 44h APF RNA-seq dataset, 2231 genes were significantly upregulated and 2068 genes were significantly downregulated (Table 4.1). When examining specific gene lists, clusters of cell cycle genes, EcR response genes, and compound eye development genes, exhibited mis-regulation in both directions (Figure 4.3B). Our data suggests the primary function of Mi-2 during terminal

differentiation is to close chromatin, but these regions could include both repressive and activating elements.

### 4.3.4 Mi-2 and E93 regulate accessibility at a subset of overlapping genes

General chromatin remodelers such as Mi-2 are thought to be recruited to specific genomic locations at the right times during development through interactions with specific transcription factors (Kim et al., 2017; Kreher et al., 2017). Ecdysone signaling is known to promote cell cycle exit at 24h APF and the levels of the Ecdysone-induced protein Eip93F transcription factor (E93) peak during cell cycle exit (Guo et al., 2016). We previously showed that E93 is essential for chromatin accessibility changes during metamorphosis, including both opening and closing of chromatin in regions where E93 binds, as assayed by ChIP-seq (Uyehara et al., 2017). To identify interacting partners of E93 we performed a proximity labeling assay in *Drosophila* cell culture S2 cells, which identified Mi-2 as a top hit. This suggested E93 and Mi-2 may coordinately regulate closing of chromatin at overlapping locations during cell cycle exit.

To identify chromatin regions coordinately regulated by Mi-2 and E93 we compared datasets of E93 mutant (E93MUT) FAIRE-seq from 24h and 44h APF pupal wings, E93 overexpression gain of function (E93GOF) FAIRE-seq and ChIP-seq studies in larval wings and $E93^{mimicGFP}$ ChIP-seq data from 24h APF pupal wings (Nystrom et al., 2020; Uyehara et al., 2017). By comparing staged-matched E93MUT wing FAIRE-seq significant peaks to our $Mi\text{-}2^{DN}$ eye ATAC-seq dataset, we identified overlap at a subset of genes (Figure 4.4A, B). At several of the $Mi\text{-}2^{DN}$ significant peaks, we observed E93GOF and E93MUT significant peaks that changed in the same direction,

suggesting a co-regulatory function of E93 and Mi-2 at these loci (Figure 4.4C, Figure S4.6). Of particular interest is overlap of E93 significant peaks at the promoter and a distal region of the *stg* regulatory locus, several peaks within the *broad* (*br)* locus and peaks upstream of the hedgehog (*hh)* gene. This suggests that E93 and Mi-2 may be coordinately regulating accessibility and possibly gene expression during cell cycle exit at a subset of genes in a manner shared between the eye and wing.

### 4.3.5 E93 knockdown delays cell cycle exit and disrupts terminal differentiation

While E93 is known to play a role in wing maturation, it is unclear whether E93 plays a role in eye development, or any role in cell cycle exit. To examine E93 function in eyes, we expressed UAS-E93$^{RNAi}$ during the final cell cycle in the eye using the same GMR-Gal4 line that was used for our Mi-2 ATAC-seq and RNA-seq experiments. We observed eye shape and pigment defects in adults demonstrating that E93 indeed plays a role in eye development (Figure 4.5A). We stained the eyes for DLG to look at cone cell and interommatidial cell boundaries, and we observed that the E93 knockdown pupal eyes have a highly disorganized structure, where we were unable to accurately assess cone or interommatidial cell number. Although the adult E93$^{RNAi}$ eyes appear smaller than controls, we noted that the pupal eye disc is much thicker in the E93 knockdown condition (Figure S4.7), suggesting there could be defects in cell cycle exit that do not result in a larger adult eye. Indeed, in the sensitized eye background that causes 1-2 rounds of additional cell cycles, we observed even more mitoses between 30h – 44h APF suggesting cell cycle exit is further compromised when E93 is knocked down (Figure 4.5B, C). E93 knockdown in the wing and eyes also delayed cell cycle exit,

demonstrating that E93, like Mi-2 plays a shared role in eyes and wings to promote proper cell cycle exit (Figure S4.7). Finally, to assay eye terminal differentiation, we stained 44h APF eyes for Chaoptin (Chp), a marker for photoreceptor boundaries and axons, and Elav, a postmitotic neuronal cell marker. At the apical photoreceptor layer of the eye, there is severely reduced Elav in $E93^{RNAi}$-expressing eyes, and at the basal layer closer to the lamina photoreceptor axons appear shorter and less organized, demonstrating E93 loss in eyes causes severe defects in terminal differentiation (Figure 4.5D).

We performed RNA-seq on $E93^{RNAi}$ eyes at 44h APF, using $mCherry^{RNAi}$ as a negative RNAi control and the GMR driver line used in the Mi-2 experiments. We observed a failure to shut off a subset of cell cycle genes at 44h and a mixture of mis-regulated genes involved in eye development and ecdysone response. Some of these genes fail to be downregulated, while others failed to be properly induced at 44h (Figure 4.5E). The gene expression profile is consistent with a failure to exit the cell cycle and a block in the eye temporal terminal differentiation process. As evidence of this, we observe a failure to shut down expression of Broad, and this correlates with a block in the ecdysone cascade, with some genes failing to turn off and others failing to activate (Figure 4.5E, Table 4.2). This suggests that E93 coordinates cell cycle exit with temporal progression through terminal differentiation.

### 4.3.6 Mi-2 is required to shut off a known *stg* enhancer after cell cycle exit

We began this study with the goal of identifying a chromatin remodeler that may be responsible for closing chromatin at rate-limiting cell cycle genes after cell cycle exit

occurs. While examining the chromatin accessibility datasets, we observed a peak distal to *stg* that failed to close in the Mi-2$^{DN}$ ATAC-seq and E93MUT FAIRE-seq, and opened prematurely in the E93GOF FAIRE-seq (Figure 4.6A). E93 also binds this region in both E93GOF and E93$^{mimicGFP}$ ChIP-seq datasets suggesting it may recruit Mi-2 to this region. This peak is in close proximity to a known eye *stg* enhancer, called *stg-Visual System* (*stg-VS*) (Lopes and Casares, 2015). Within the *stg-VS* region there are two identified regulatory elements, *stg*-FMW and *stg*-EO known to express in the larval eye. However it remained unknown whether these elements can drive expression in the pupal eye and whether they are shut off at cell cycle exit. We therefore examined the expression patterns for these elements in a timecourse from the larval to pupal eye, during cell cycle exit. We found that these enhancers express in pupal eyes, with *stg*-FMW expression peaking at 24h APF and then being shut off within a few hours after cell cycle exit, and *stg*-EO plummeting at 24h APF during cell cycle exit and remaining low thereafter (Figure 4.6A). This suggested that these elements may be repressed by Mi-2 chromatin remodeling at the nearby E93-bound region. To test this, we next examined the expression of the *stg*-FMW and *stg*-EO reporters in the presence and absence of Mi-2$^{DN}$, using both the GMR driver line in our RNA-seq experiments, as well as the sensitized background line with delayed cell cycle exit. We see in both conditions that shut off the *stg*-FMW and *stg*-EO reporters is delayed when Mi-2$^{DN}$ is expressed, with higher reporter levels observed at both 24h and 36h APF for *stg*-FMW and higher levels of *stg*-EO at 24h APF (Figure 4.6B, C, Figure S4.8). This demonstrates that Mi-2 can regulate *stg* enhancers *in vivo*.

To determine whether Mi-2 and/or E93 may regulate the other rate-limiting cell cycle genes, we examined accessibility at *cycE* and *e2f1* loci. We observed no significant effect of Mi-$2^{DN}$ on chromatin accessibility at *cycE* and only minor effects at *e2f1*, consistent with a lack of change in gene expression when Mi-2 is inhibited. However, when examining the E93MUT wing FAIRE-seq data, we observe several peaks that show differential accessibility at 24h and/or 44h APF (Figure S4.9), suggesting E93 may coordinate with other chromatin remodelers to modulate specific elements at *e2f1* and *cycE*.

## 4.4 Discussion

### 4.4.1 Mi-2 and E93 alter chromatin accessibility and gene expression to coordinate cell cycle exit with progression of terminal differentiation.

Our data supports a model for how the high levels of ecdysone signaling at the second pulse around 24h APF promotes cell cycle exit in coordination with the progression of terminal differentiation in wings and eyes. The ecdysone target E93 is upregulated in response to a high threshold of ecdysone signaling and works cooperatively with the chromatin remodeler Mi-2 to co-regulate enhancer and promoter accessibility at various genes during the final cell cycle, including cell cycle and terminal differentiation genes (Figure 4.7). In particular, pupal tissue-specific enhancers at the key mitotic regulator *string* as well as genes involved in early eye differentiation are decommissioned to facilitate their downregulation (e.g. *Hh*, *Blimp-1*) to ensure a postmitotic state along with progression from early to later terminal differentiation (Wang et al., 2022). Although we compared chromatin accessibility data between wings and eyes, we find many

temporally regulated elements to be shared between these tissues including at cell cycle genes, suggesting they use similar mechanisms to regulate tissue-specific differentiation targets and cell cycle exit (McKay and Lieb, 2013, Chapter 3).

Over 15 years ago, the existence of exit elements was postulated – regulatory elements that mediate the robust transcriptional shut down of cell cycle genes during cell cycle exit and terminal differentiation (Buttitta and Edgar, 2007). Exit elements could mediate transcriptional repression through binding repressors or through recruiting chromatin remodelers leading to a repressive chromatin state (Ma et al., 2015). For most cell cycle genes, the regulatory elements involved in repression are also involved in gene activation. This is best resolved for targets of RB/E2F regulation where the same promoter-proximal element mediates E2F-dependent gene activation as well as RB or DREAM-mediated repression (Thacker et al., 2003). But the rate-limiting cell cycle genes with more complex cis regulatory modules could be subject to the control of exit elements to maintain repression during stable postmitotic states. Our work demonstrates that the stable repression of rate-limiting cell cycle genes likely involves enhancer decommissioning through nucleosome movement, rather than formation of repressive chromatin via heterochromatin-mediated repression (Ma and Buttitta, 2017). While the work here shows a role for the remodeler Mi-2 in the proper shut down of the mitotic regulator *string*, future work will be needed to identify the remodeler(s) responsible for decommissioning regulatory elements in the critical G1-S regulatory gene *cyclin E*.

Mi-2 remodels nucleosomes by moving end nucleosomes towards the center of a DNA fragment and is known to bind to nucleosomal DNA through its chromodomains

(Bouazoune et al., 2002; Brehm et al., 2000). Mi-2 is also known to function as a member of two complexes in *Drosophila melanogaster*, the Nucleosome Remodeling and Deacetylase complex (NuRD) and the *Drosophila* MEP-1 complex (dMec). Both complexes are thought to serve mostly transcriptional repressive functions, with the NuRD complex having a histone deacetylase function while dMec uses a histone deacetylase-independent mechanism (Kunert et al., 2009; Xue et al., 1998). In our RNAi screen for cell cycle exit regulators we tested HDAC1, the main HDAC in the NuRD complex, as well as Caf1-55 and MBD-like. None of these NuRD knockdowns resulted in any obvious cell cycle exit phenotype, despite robust accumulation of H3K27 acetylation with the HDAC1 knockdown. We therefore suggest that the functions of Mi-2 described here may be NuRD independent, although we cannot rule out the possibility that NuRD plays a role in maintaining cell cycle exit at timepoints later than those examined here.

### 4.4.2 Disruption of E93/Mi-2 function leads to a block in the ecdysone feed-forward cascade

Inhibition of either E93 or Mi-2 led to a disruption of the normal ecdysone feed-forward transcriptional cascade in eye and wings (Uyehara et al., 2017). E93 expression is activated around 12h APF, around the time of transition from prepupal to pupal stages (Baehrecke EH and Thummel CS, 1995). The E93 binding motif is enriched in chromatin accessibility peaks that close between third larval instar (L3) and 24h APF as well as peaks that open between 24h and 44h APF (Uyehara et al., 2017). This suggests that E93 may play a role in not only activating gene expression at later

developmental stages, but may aid in closing chromatin at genes expressed earlier in development. E93 expressed ectopically at earlier stages of development has also been shown to prematurely turn off early stage enhancers while binding to and opening late stage enhancers (Nystrom et al., 2020). In the case of E93 loss, the early ecdysone targets Broad and Ftz-F1 remain high, presumably leading to subsequent temporal effects in the execution of the proper cascade. In the case of blocking Mi-2 function, Broad and Ftz-F1 also remain high, although with milder temporal cascade defects. Interestingly, when Mi-2 function is inhibited, E93 is upregulated (Fold Change 1.71) and we observe two significant sites of chromatin accessibility upstream of E93 that fail to close. This suggests E93 is upregulated in response to Mi-2 loss of function, which may compensate to correct the chromatin accessibility changes and gene expression changes through E93 acting in concert with other chromatin remodelers. Consistent with this the wing and eye phenotypes and effects on cell cycle exit are much stronger for E93 inhibition than Mi-2 inhibition. There is abundant evidence of redundancies and chromatin remodelers acting in concert (Martin et al., 2023), which may be uncovered through additional manipulations during cell cycle exit.

### 4.5 Acknowledgements

We thank Dr. Fernando Casares for providing the Stg-EO and FMW lines, along with reporters for many other Stg regulatory elements. We thank Dr. John Tamkun for kindly providing the UAS-Mi2$^{WT}$ and UAS-Mi2$^{DN}$ lines. We thank Dr. Helena Richardson for kindly providing the GMR-Gal4, UAS-CycE; GMR-P35 line. We thank the UM Advanced Genomics Core for assistance with sample quality control, RNA-seq library preparation

and sequencing. Additional fly stocks used here were obtained from the Bloomington Drosophila Stock Center (BDSC). Antibodies were obtained from the Developmental Studies Hybridoma Bank, created by the NICHD of the NIH and maintained at The University of Iowa, Department of Biology, Iowa City, IA 52242. EMB was supported by the U.Michigan Genetics Training Grant (T32GM007544).

**4.6 Methods**

Fly Stocks

Figure 4.1 ATAC-seq genotypes:

Control: *GMR-P35; +; +*

Delay: *w;GMR-Gal4, UAS-CycE/+; GMR-P35/+* (GMR>UAS-CycE+P35 from Helena Richardson)

Bypass: *w; GMR-Gal4, UAS-CycE/UAS-CycD, Cdk4; GMR-P35/+*

All crosses were kept at room temperature. White prepupa were collected and raised at 25ºC until dissection.

Figure 4.2 genotypes:

Fig 4.2A and B Sensitized: *w; GMR-Gal4, UAS-CycE/+; GMR-P35/UAS-GFP$^{RNAi}$* (UAS-GFP$^{RNAi}$ from BDSC 9330)

Suppressed: *w; GMR-Gal4, UAS-CycE/+; GMR-P35/UAS-Wee, UAS-Dap* (UAS-Wee+Dap described in Flegel et al., 2016)

Enhanced: *w; GMR-Gal4, UAS-CycE/+; GMR-P35/UAS-Mi-2$^{RNAi}$* (Mi-2$^{RNAi}$ BDSC 51774) and *w; GMR-Gal4, UAS-CycE/+; GMR-P35/Mi2$^{4}$* (Mi2$^{4}$ allele BDSC 26170)

CycD/Cdk4/ E2F: *w; GMR-Gal4, UAS-CycE/UAS-CycD, UAS-Cdk4; GMR-P35/UAS-E2F1, UAS-Dp* (UAS-CycD, UAS-Cdk4; UAS-E2F1, UAS-Dp described in Ma et al., 2019).

Fig. 4.2C: *w; en-Gal4, UAS-GFP/UAS-E2F1, UAS-DP; tub-Gal80$^{TS}$/UAS-white$^{RNAi}$ or Mi-2$^{RNAi}$* (white$^{RNAi}$ BDSC BL35573). Animals were shifted from 18 deg to 28deg at early L3. Wings are 28h APF (corrected for relative timing at 25ºC as described in Buttitta et al., 2007).

Fig 4.2D-F: *w; GMR-Gal4, UAS-CycE/+; GMR-P35/+ or GMR-Gal4, UAS-CycE/+; GMR-P35/ UAS Mi-2$^{WT}$ or Mi-2$^{DN}$* (Mi-2 lines kindly provided by J. Tamkun, described in Fasulo et al., 2012)

Fig 4.2G *w; en-Gal4, UAS-GFP; tub-Gal80$^{TS}$/UAS-Mi-2$^{DN}$* Animals were shifted as described in C.

Supplemental Figure 4.2 genotypes:

Fig S4.2A: *w; GMR-Gal4/+; UAS-white$^{RNAi}$* or *UAS-Mi-2$^{DN}$/ PCNA-GFP* (white$^{RNAi}$ BDSC BL35573, PCNA-GFP from B. Duronio described in Thacker et al., 2003)

Fig S4.2B: *w; en-Gal4, UAS-GFP; tub-Gal80TS/UAS-white$^{RNAi}$* or *Mi-2$^{RNAi}$*. Animals were shifted from 18ºC to 28ºC at early L3. Wings are 28h APF (corrected for relative timing at 25ºC as described in Buttitta et al., 2007).

Fig S4.2C: *w; GMR-Gal4, UAS-CycE/+; GMR-P35/+* or *GMR-Gal4, UAS-CycE/+; GMR-P35/UAS-Mi-2$^{WT}$* and genotypes described in Fig. 4.2 A.

Fig S4.2D: *w$^{1118}$;GMR-Gal4/+;+* or *w$^{1118}$;GMR-Gal4/+; UAS-Mi2$^{WT}$ or $^{DN}$* as described for Fig.4.2.

Sensitized Background genotypes:

*w$^{1118}$/+; GMR-Gal4, UAS-CycE/+;GMR-P35/+*

*+; GMR-Gal4,UAS-CycE/+; GMR-P35/UAS-Mi-2$^{WT}$*

*+; GMR-Gal4,UAS-CycE/+; GMR-P35/UAS-Mi-2$^{DN}$*

*+; GMR-Gal4,UAS-CycE/UAS-E93$^{RNAi}$; GMR-P35/+* (E93$^{RNAi}$ Vienna *Drosophila* Resource Center, #104390)

All crosses were kept at 25ºC.

ATAC-seq and/or RNA-seq were performed using the following lines:

*GMR-P35/w$^{1118}$; GMR-Gal4/+; +/+*

*GMR-P35/+; GMR-Gal4/+; UAS-Mi-2$^{WT}$-FLAG/+*

*GMR-P35/+; GMR-Gal4/+; UAS-Mi-2$^{DN}$-FLAG/+*

*GMR-P35/+; GMR-Gal4/+; UAS-Mi-2$^{RNAi}$/+*

*GMR-P35/+; GMR-Gal4/+; UAS-mCherry$^{RNAi}$/+* (mCherry$^{RNAi}$ BDSC BL35785)

*GMR-P35/+; GMR-Gal4/UAS-E93$^{RNAi}$/+; +*

All crosses were kept at 25ºC.

Mi-2 manipulations with *stg* reporters:

*GMR-P35/+; GMR-Gal4/stgFMW; UAS-Mi-2$^{DN}$/+*

*GMR-P35/+; GMR-Gal4/stgEO; UAS-Mi-2$^{DN}$/+*

All crosses were kept at 25ºC.

Supplemental Figure 4.7 genotypes:

Fig S4.7A: *w1118;+;E93$^{mimicGFP}$* (E93$^{mimicGFP}$ BDSC BL43675)

Fig S4.7B: *GMR-P35/+; GMR-Gal4/UAS-E93$^{RNAi}$;* + or *GMR-P35/+; GMR-Gal4/+ UAS-mCherry$^{RNAi}$/+*

Fig S4.7C: $w^{1118}$; *en-Gal4/UAS-E93*$^{RNAi}$; *tub-Gal80*$^{TS}$/*E93*$^{mimicGFP}$ Wings are 26h APF (eggs were laid and raised at 18ºC, Wpp were collected and raised at 29ºC until an equivalent of 26h APF)

Fig S4.7D: $w^{1118}$/*GMR-P35; GMR-Gal4/UAS-E93*$^{RNAi}$; +

Immunohistochemistry and imaging

For pupal tissues, white prepupae were collected and raised at 25ºC until the appropriate age for dissection unless otherwise noted above. Tissues were dissected in 1X PBS and fixed for 30 min in 1X PBS + 4% paraformaldehyde. Primary antibodies were diluted in PAT (1X PBS containing 0.1% Triton X-100 + 1% BSA) and incubated for 4 hours at room temperature or overnight at 4ºC. Secondary antibodies were diluted in PBT-X + 2% normal goat serum (1X PBS containing 0.3% Triton X-100 with 0.1% BSA) and incubated for 4 hours at room temperature or overnight at 4ºC. DAPI was diluted 1:1000 in 1X PBS + 0.1% Triton X-100, then incubated with tissues for 10 minutes at room temperature in the dark. Samples were mounted onto glass slides using Vectashield mounting medium (Vector Laboratories). Slides were imaged on a Leica SP5 or SP8 confocal microscope.

Antibodies

Mouse Anti-Discs large (4F3), DSHB, 1:100

Rabbit Anti-Phosphohistone H3 (serine 10) (D2C8), Cell Signaling, cat#33775, 1:1000

Rat Anti-Elav (7E8A10), DSHB, 1:100

Mouse Anti- Chaoptin (24B10-S), DSHB, 1:100

Rabbit Anti-GFP, Invitrogen, cat#A11122, 1:1000

Goat Anti-Mouse Plus (488), AlexaFluor, cat#A32723, 1:2000

Goat Anti-Rabbit (488), AlexaFluor, cat#A11034, 1:2000

Goat Anti-Rabbit (568), AlexaFluor, cat#A11036, 1:2000

Goat Anti-Rat (568), AlexaFluor, cat#A11077, 1:2000

Image quantifications

Images were quantified in FIJI. PH3 was quantified using max projections of z stacks, and using a minimum threshold of 20 to count spots. Average total GFP intensity was measured to assess expression of *stg* reporters with and without Mi-$2^{DN}$.

ATAC-seq & RNA-seq

For both ATAC-seq and RNA-seq, crosses were kept at 25ºC. White prepupa were collected, sexed, and aged at 25ºC until dissection at either 24h or 44h APF.

ATAC-seq was performed on 24h and 44h APF eyes using pupal tissue dissociation and ATAC-seq protocol as described in Buchert et al., 2023. Approximately 16 eyes were used per sample, with 2-3 replicates per genotype and timepoint. White prepupae were collected and sexed, then housed at 25°C until the appropriate time for dissection.

For RNA-seq, 16 eyes were used per sample, with three replicates for GMR x $w^{1118}$, Mi-$2^{WT}$ and Mi-$2^{DN}$ genotypes 24h and 44h APF timepoints, and four replicates for GMR x mCherry$^{RNAi}$ and E93$^{RNAi}$ 44h APF samples. Pupal eyes were dissected in filtered 1X PBS, then transferred to 400 µL Trizol containing 0.5 µL of 20mg/mL glycogen. Samples were vortexed for 2 minutes, then 80 µL of chloroform was added, and samples were

vortexed, then centrifuged for 15 minutes at 12,000xg at 4ºC. Aqueous layer was transferred to a new Eppendorf tube, then 250 µL of Isopropanol was added. Samples were mixed, then frozen overnight at -20ºC. The next day, samples were centrifuged for 5 minutes at 12,000xg at 4ºC. Alcohol was removed and samples were resuspended in 50 µL of RNAse free water. Libraries were generated by the University of Michigan Sequencing Core. Total RNA was sequenced for GMR x $w^{1118}$, Mi-$2^{WT}$ and Mi-$2^{DN}$ samples, and polyA selection was performed for GMR x mCherry$^{RNAi}$ and E93$^{RNAi}$ samples.

Sequencing platform and read depth

All sequencing was performed at the University of Michigan Sequencing Core. An Agilent Tape Station was used to assess library quality. All ATAC-seq and RNA-seq samples were sequenced using Illumina NovaSeq S4 300 cycles, paired-end 150bp reads with a target depth of 90-100 million reads.

Data Analysis

ATAC-seq and RNA-seq data was analyzed as described in Buchert et al., 2023 with the following changes. Statistics were performed and ATAC-seq multidimensional scaling plots were generated using R package edgeR (Robinson et al., 2010). RNA-seq reads were mapped to the dm6 genome was performed using STAR 2.7.6a (Dobin et al., 2013).

Data Access

Previously published larval wing E93 gain of function FAIRE-seq and ChIP-seq data was accessed from GSE141738.

Previously published 24h and 44h APF wing E93 mutant FAIRE-seq and 24h APF wing $E93^{mimicGFP}$ ChIP-seq data was accessed from GSE97956.

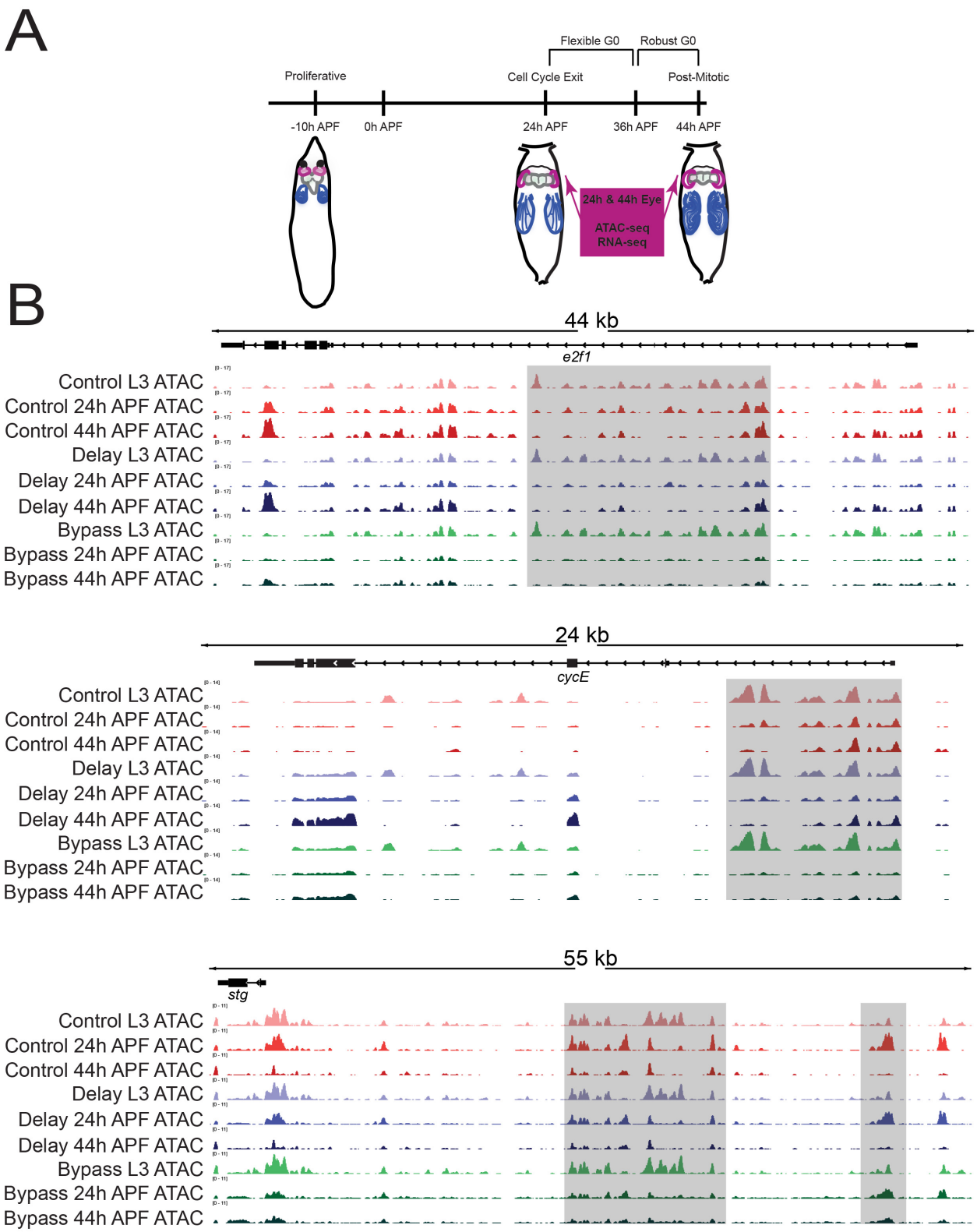


**Figure 4.1 Enhancers at cell cycle genes close independent of cell cycling status in the pupal eye. (A)** Diagram of experimental design describing the timeline of GMR

expression, Flexible G0 and Robust GO relative to hours after puparium formation (APF). Pink indicates imaginal and pupal eyes, blue indicates imaginal and pupal wings, and green indicates larval and pupal brains. (**B**) Browser tracks of cell cycle exit control, delay, and bypass conditions in the *Drosophila* eye at *e2f1*, *cycE*, and *stg*. Shaded regions show predicted and verified enhancer regions that continue to close after cell cycle exit, regardless of proliferative status.

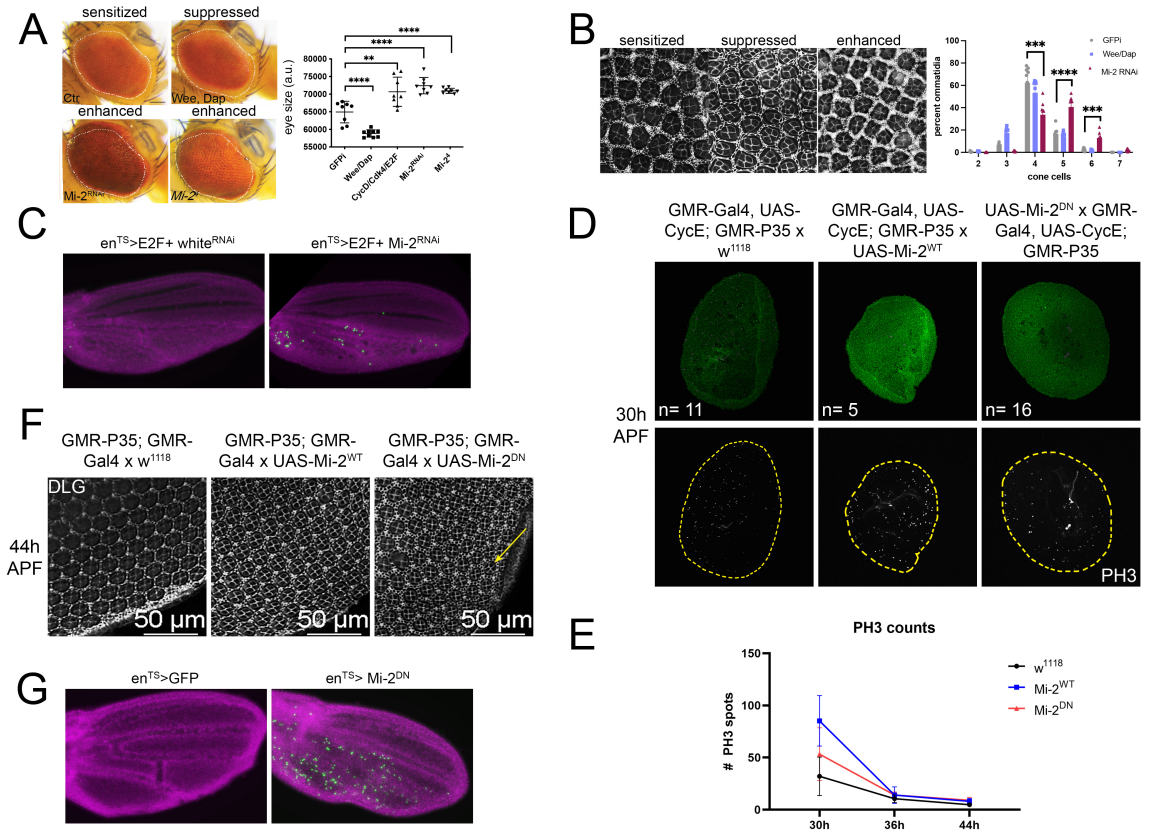


**Figure 4.2 Mi-2 is required for stable cell cycle exit in the *Drosophila* eye. (A)** Adult eyes from a sensitized screen to identify remodelers that impact cell cycle exit. Sensitized eyes express CyclinE + P35 under the control of *GMR*-Gal during the final cell cycle and during the postmitotic stage. Overexpression of the cell cycle inhibitors Dacapo and Wee suppress eye size, while positive cell cycle regulators (CycD/Cdk4+E2F) enhance eye size. Inhibition of Mi-2 via RNAi under the control of GMR-gal or loss of function of one allele (*Mi-2$^{4}$/+)* enhances eye size. **(B)** Pupal eyes (44h APF) stained for Discs Large (Dlg) reveal changes in cone cell number consistent with suppression or enhancement of the number of cell cycles in the differentiating eye. Sensitized eyes express CyclinE + P35 under the control of GMR-Gal and exhibit 1-2 extra cell cycles in cone cells and interommatidial cells. Suppression via Dacapo + Wee reduces cell number. Enhancement by Mi-2 RNAi expression results in increased cone cells and interommatidial cells. Quantifications of cone cell numbers are shown at right. **(C)** Overexpression of E2F (E2F1+DP) in the posterior pupal wing using temperature sensitive *engrailed*-Gal4 (*en$^{TS}$*) increases nuclear density by driving additional cell cycles from 24-36h APF but cannot sustain cell cycling at 42h APF, while co-expression of E2F+ Mi-2 RNAi allows for continued mitotic cycling at 42h APF. **(D)** PH3 staining of w$^{1118}$ control, (Mi-2$^{WT}$) control, and (Mi-2$^{DN}$) experimental 30h APF eyes in a sensitized background that causes 1-2 additional rounds of cell division, showing mitoses beyond the normal cell cycle exit time of 24h APF. **(E)** Quantification of PH3 counts shown in D.

**(F)** DLG staining of $w^{1118}$ control, Mi-$2^{WT}$ control, and Mi-$2^{DN}$ experimental 44h APF eyes, marking the boundaries of cone cells and interommatidial cells. Yellow arrow indicates ommatidia with five cone cells. Extra cone cells are only observed in the Mi-$2^{DN}$ condition. **(G)** Overexpression of Mi-$2^{DN}$ in the posterior pupal wing using $en^{TS}$ delays cell cycle exit at 28h APF.

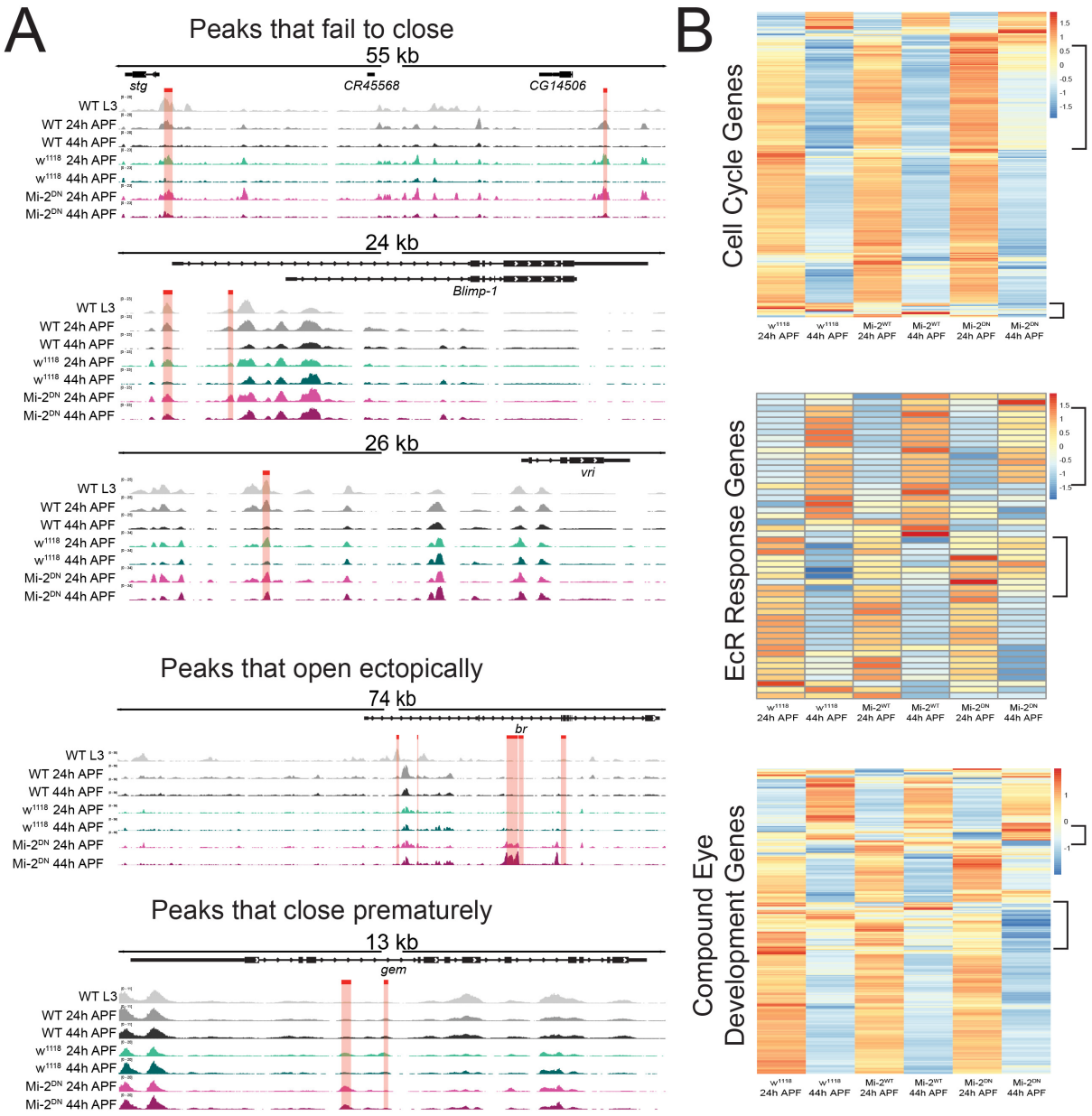


**Figure 4.3 ATAC-seq and RNA-seq show that a subset of genes involved in coordinating terminal differentiation and cell cycle are affected by loss of Mi-2 function. (A)** ATAC-seq browser tracks showing larval and pupal eye wildtype, $w^{1118}$ control and Mi-$2^{DN}$ experimental conditions. We observe differentially accessible peaks falling into three categories, peaks failing to close, peaks that open ectopically, and peaks that close prematurely. Red bars show significant peaks called in the 24h and 44h APF Mi-$2^{DN}$ conditions. **(B)** RNA-seq heatmaps for Cell Cycle Genes, EcR Response Genes, and Compound Eye Development Genes. Brackets highlight clusters of genes where differential expression is observed compared to the $w^{1118}$ control.

A

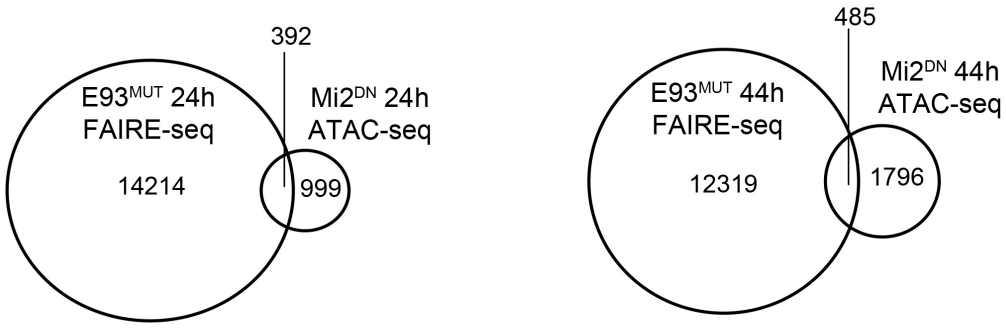


B

| 24h APF Genes with Overlapping Peaks | 44h APF Genes with Overlapping Peaks |
|---|---|
| Blimp-1, Broad, CycB3, Eip93F. Fruitless, Grainy head, Shadow, Shade, Zelda | Blimp-1, Broad, Fizzy-related, Hedgehog, String, Vrille, Wingless |

C

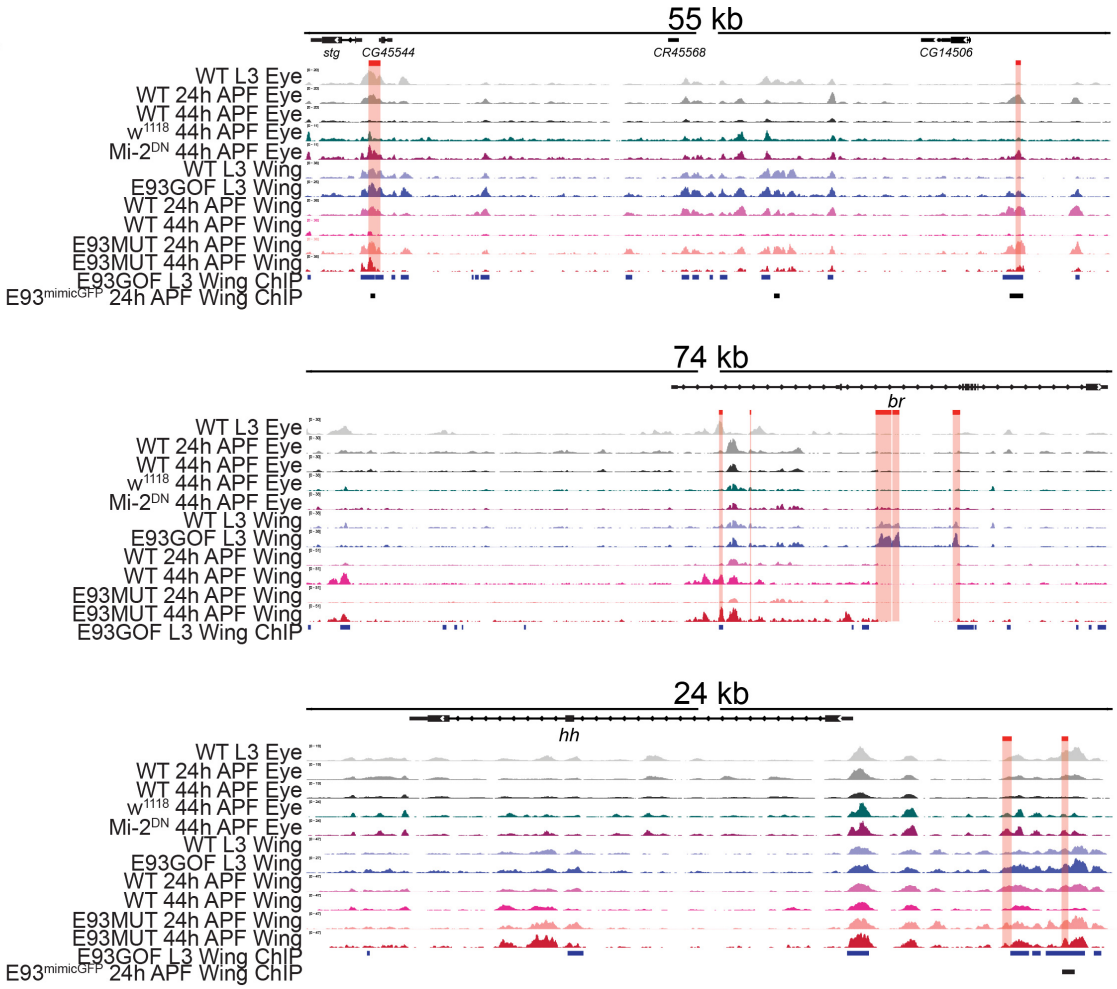


**Figure 4.4 Comparison of E93 ChIP-seq and FAIRE-seq datasets with Mi-2$^{DN}$ ATAC-seq reveals overlapping peaks at a subset of genes. (A)** Venn Diagrams showing time-matched overlap of E93 mutant FAIRE and Mi-2$^{DN}$ ATAC significant

peaks. **(B)** Table listing genes where overlapping significant peaks were found in both the E93 mutant FAIRE-seq and Mi-$2^{DN}$ ATAC-seq datasets. **(C)** ATAC-seq and FAIRE-seq browser tracks at *stg*, *br* and *hh* showing Mi-$2^{DN}$, E93 gain of function and E93 mutant conditions. Blue bars at the bottom of each set of tracks shows significant ChIP-seq peaks for larval E93 gain of function and black bars show significant ChIP-seq peaks for 24h APF wing $E93^{mimicGFP}$. Red bars indicate significant peaks in the Mi-$2^{DN}$ condition.

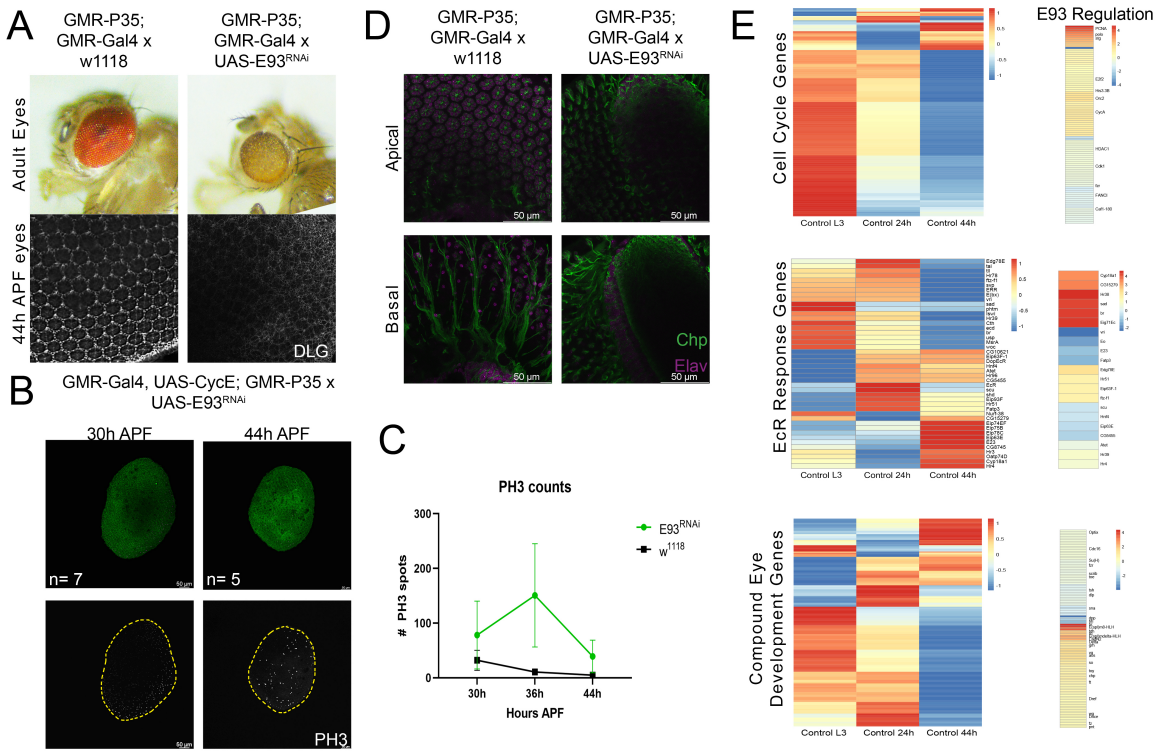


**Figure 4.5 E93 knockdown delays cell cycle exit and disrupts terminal differentiation**. **(A)** Adult eyes and 44h APF eyes with DLG in $w^{1118}$ control and $E93^{RNAi}$ conditions. $w^{1118}$ DLG image is a different view of the same eye as shown in figure 2. **(B)** PH3 staining of 30h and 44h APF eyes in a sensitized background with expression of $E93^{RNAi}$. **(C)** Quantification of eyes shown in B. $w^{1118}$ data is the same as shown in Figure 4.2. **(D)** Chaoptin (Chp) and Elav staining of $w^{1118}$ and $E93^{RNAi}$ 44h APF eyes. The apical layer is showing photoreceptors marked by Elav and outlined by Chp. The basal layer shows the lamina attached underneath the eye where Chp marks photoreceptor axons. **(E)** RNA-seq heatmaps for logCPM of Cell Cycle Genes, EcR Response Genes and Compound Eye Development Genes showing Control eye RNA-seq time course. The $log_2FC$ of $E93^{RNAi}$ significant genes, relative to $mCherry^{RNAi}$ controls, within the gene lists shown to the right.

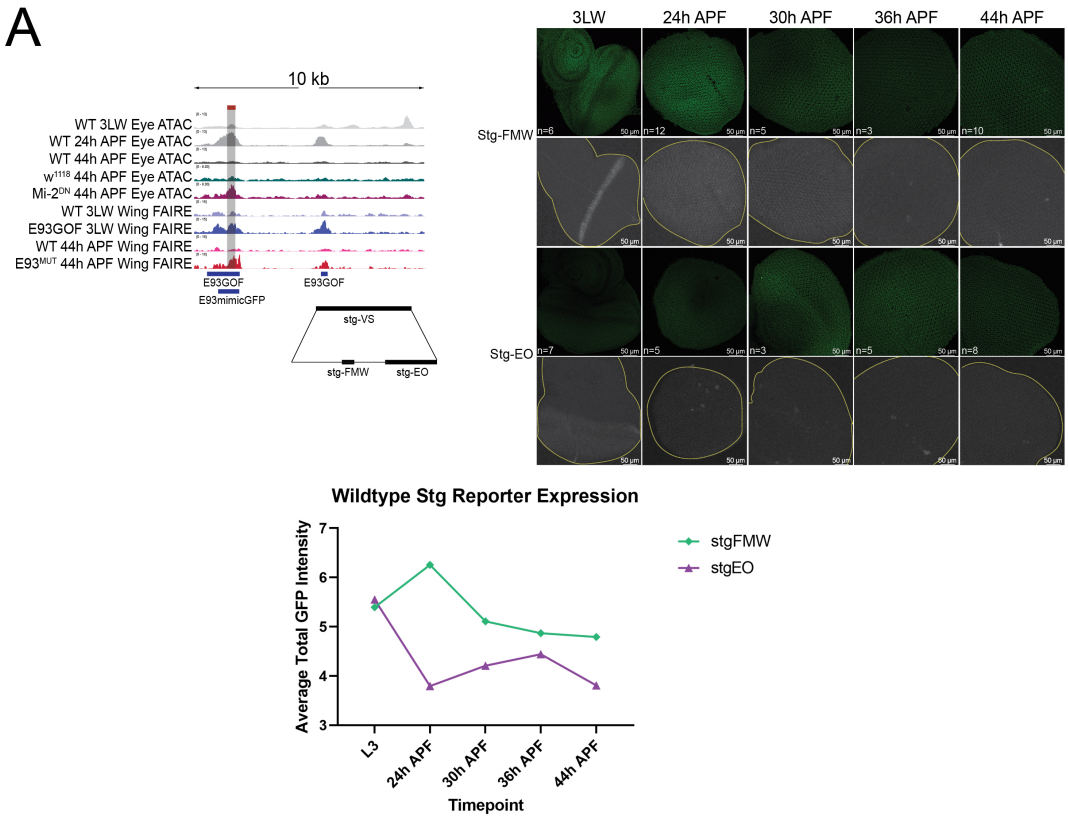


**Figure 4.6 Inhibition of Mi-2 function delays shut off of a known eye *stg* enhancer.** **(A)** Browser tracks of the stg-VS locus showing proximity to a significant peak in the Mi-

$2^{DN}$ condition as well as wild type expression of the stg-FMW and stg-EO reporters. Grey bar highlights Mi-$2^{DN}$ significant ATAC-seq peak. Images shown in figure have been brightened to show stg-FMW and stg-EO expression patterns. Quantification of total GFP intensity for both reporter lines shown below, and unmodified images were used for quantification. **(B)** Images of stg-FMW expressed with Mi-$2^{DN}$ showing delayed shut off when Mi-$2^{DN}$ is expressed. Quantification of stg reporter with and without Mi-$2^{DN}$ shown below. Quantifications performed in the sensitized background that causes an additional 1-2 rounds of cell division. Images shown in figure have been brightened to show expression patterns, but quantifications were performed on images taken at the same intensity. **(C)** Same as B for stg-EO reporter.

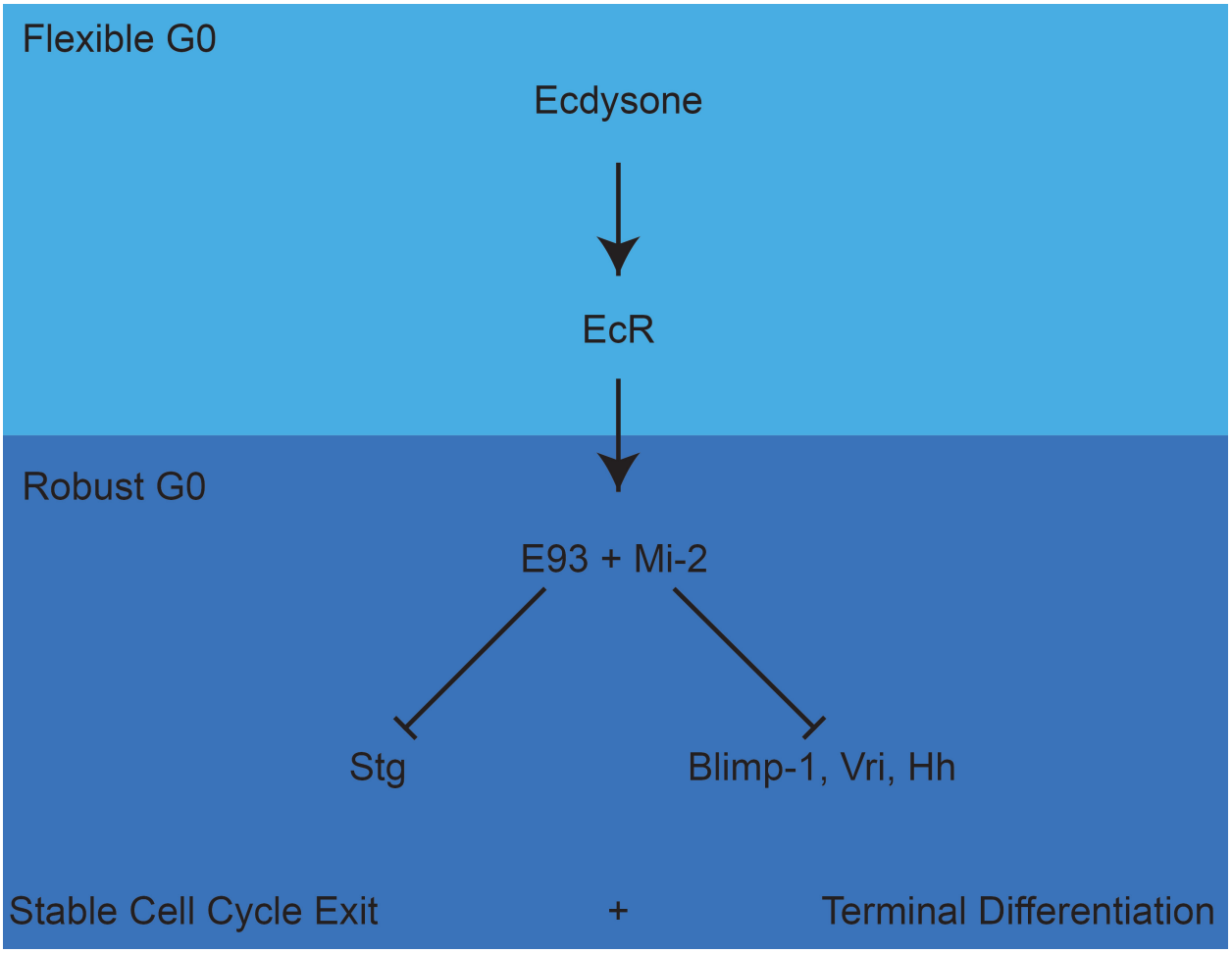


**Figure 4.7 Mi-2 and E93 work cooperatively at a subset of cell cycle and differentiation genes to coordinate termination of the cell cycle with initiation of differentiation programs.** Working model for how Mi-2 and E93 may be working to co-regulate genes to coordinate the shut off of the cell cycle with initiation of terminal differentiation programs.

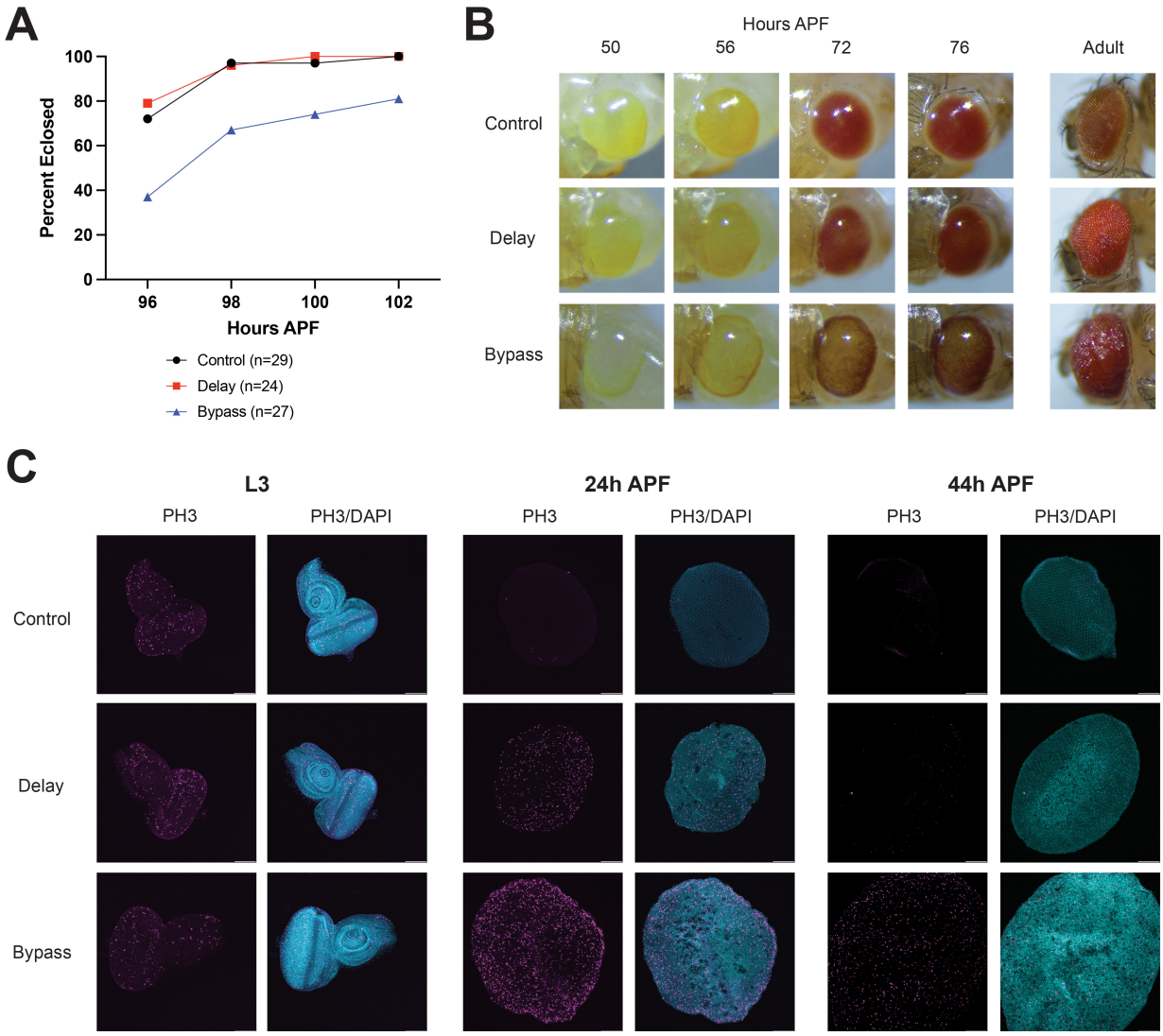


**Figure S4.1 Phenotypes of Control, Delay and Bypass eyes. (A)** Timing and percent of flies eclosed in the control, delay, and bypass conditions. **(B)** Time course of eye pigmentation of control, delay, and bypass eyes with adult eye phenotypes. Of note is the delayed pigmentation of the bypass eyes. **(C)** PH3 staining of control, delay, and bypass eyes at L3, 24h and 44h APF. Control eyes show mitoses at L3, but very few at 24h APF and none at 44h APF. Delay eyes have mitoses at L3 and 24h APF, and none at 44h APF. Bypass eyes show continued cycling, with mitoses observed at all three timepoints.

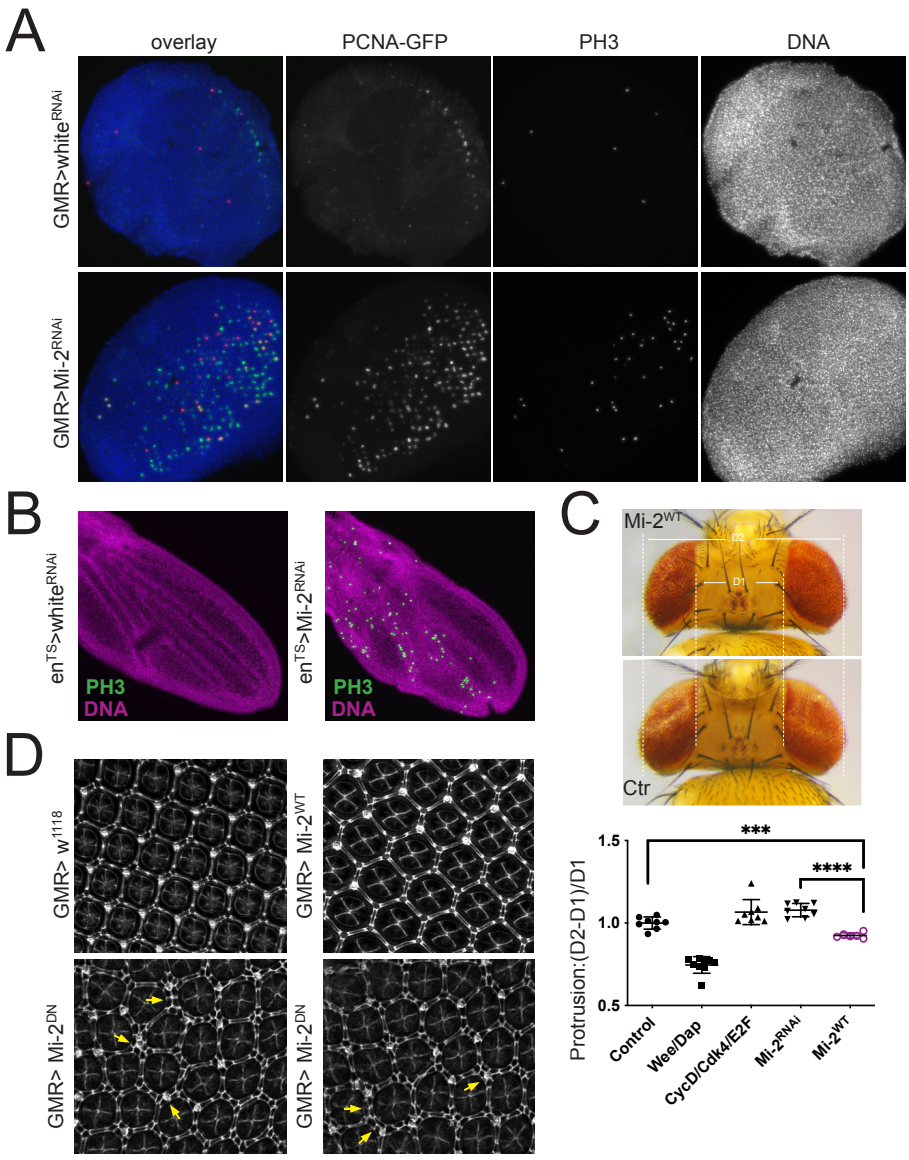


**Figure S4.2 Verification of Mi-2$^{RNAi}$ and Mi-2$^{DN}$ effects in the eye and wing. (A)** Pupal eyes at 24h APF expressing a control (*white$^{RNAi}$*) or *Mi-2*$^{RNAi}$ during the final cell cycle under the control of *GMR*-Gal during the final cell cycle. Control eyes exhibit very few mitoses and little E2F activity as revealed by expression of the PCNA-GFP reporter (Thacker and Duronio 2003) while expression of Mi-2$^{RNAi}$ increases E2F activity and mitoses. **(B)** Overexpression of Mi-2$^{RNAi}$ in the posterior pupal wing using *en$^{TS}$* delays cell cycle exit and causes additional mitoses at 28h APF. **(C)** Adult eyes for eye

protrusion measurements. Control (Ctrl) eyes express CyclinE + P35 under the control of *GMR*-Gal during the final cell cycle and during the postmitotic stage. Overexpression of wild-type Mi-2 (Mi-$2^{WT}$) suppressed eye size and folding, suggesting Mi-$2^{WT}$ delays the cell cycle and causes reduced cycling. Quantifications of eye protrusion measurements for enhancers and suppressors are shown below. **(D)** DLG staining of 44h APF pupal eyes expressing GMR-Gal4 crossed to $w^{1118}$ (control), UAS-Mi-$2^{WT}$, or UAS- Mi-$2^{DN}$. Dlg marks cell-cell junctions for cone and interommatidial cells at this optical section. Extra interommatidial cells (e.g. double layers of cells between cone cell clusters) are only observed in UAS- Mi-$2^{DN}$.

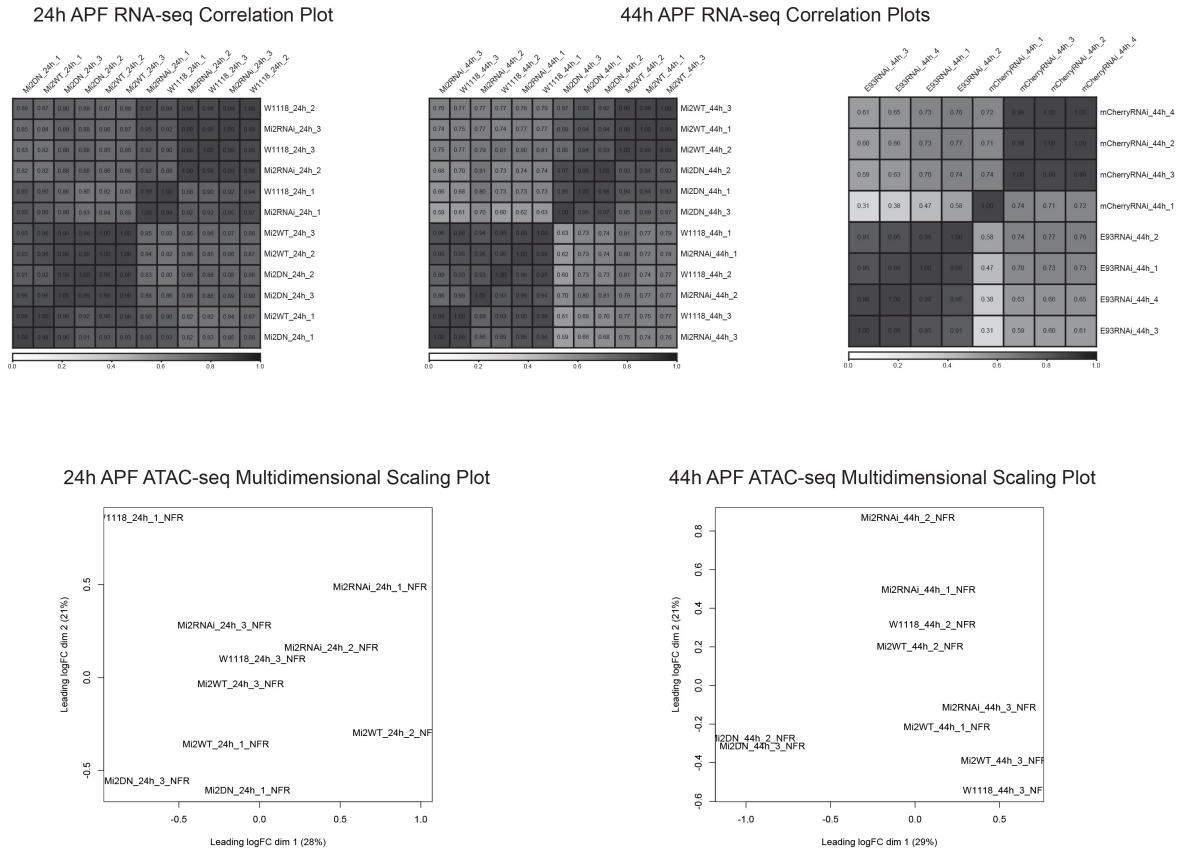


**Figure S4.3 RNA-seq Correlation Plots and ATAC-seq Multidimensional Scaling Plots.** Correlation plots and multidimensional scaling plots show how individual RNA-seq and ATAC-seq replicates cluster.

## ATAC-seq EdgeR Statistics

| Sample | Peaks called by MACS2 | Significantly Upregulated Peaks | Significantly Downregulated Peaks |
|---|---|---|---|
| Mi-2$^{RNAi}$ 24h APF eyes | 46640 | 40 | 55 |
| Mi-2$^{WT}$ 24h APF eyes | 46640 | 30 | 60 |
| Mi-2$^{DN}$ 24h APF eyes | 46640 | 648 | 749 |
| Mi-2$^{RNAi}$ 44h APF eyes | 45028 | 158 | 66 |
| Mi-2$^{WT}$ 44h APF eyes | 45028 | 64 | 379 |
| Mi-2$^{DN}$ 44h APF eyes | 45028 | 1893 | 391 |

## RNA-seq EdgeR Statistics

| Sample | Total number of genes | Significantly Upregulated Genes | Significantly Downregulated Genes |
|---|---|---|---|
| Mi-2$^{RNAi}$ 24h APF eyes | 12963 | 477 | 530 |
| Mi-2$^{WT}$ 24h APF eyes | 12963 | 1405 | 1182 |
| Mi-2$^{DN}$ 24h APF eyes | 12963 | 1954 | 1695 |
| Mi-2$^{RNAi}$ 44h APF eyes | 12632 | 503 | 413 |
| Mi-2$^{WT}$ 44h APF eyes | 12632 | 1240 | 833 |
| Mi-2$^{DN}$ 44h APF eyes | 12632 | 2231 | 2068 |
| E93$^{RNAi}$ 44h APF eyes | 11071 | 1782 | 2033 |

**Table S4.1 EdgeR Statistics for ATAC-seq and RNA-seq datasets.**

| Gene | Fold Change at 24h APF (Mi-2$^{DN}$) | Fold Change at 44h APF (Mi-2$^{DN}$) | False Discovery Rate 44h APF (Mi-2$^{DN}$) | Fold Change at 44h APF (E93$^{RNAi}$) | False Discovery Rate 44h APF (E93$^{RNAi}$) |
|---|---|---|---|---|---|
| stg | 1.38 | 1.32 | 0.0171 | 6.15 | 2.54E-49 |
| vri | 1.20 | 7.92 | 0.0014 | 0.19 | 0.0001 |
| hh | 0.98 | 1.58 | 2.40E-12 | 0.17 | 1.58E-45 |
| br | 1.02 | 1.80 | 3.40E-09 | 20.83 | 2.66E-43 |
| gem | 1.55 | 1.11 | 8.42E-08 | 0.80 | 0.5137 |
| zld | 1.65 | 3.36 | 1.29E-16 | 2.45 | 0.0011 |
| sad | 11.32 | 7.33 | 2.05E-12 | 19.88 | 6.51E-27 |
| Blimp-1 | 1.06 | 2.10 | 8.33E-05 | 0.97 | 0.9603 |
| shd | 0.61 | 0.97 | 0.9274 | 0.64 | 0.1367 |
| so | 1.38 | 1.21 | 0.00545 | 2.00 | 3.87E-05 |
| eya | 1.26 | 1.02 | 0.8461 | 0.87 | 0.3503 |
| toy | 1.02 | 0.79 | 0.0149 | 1.66 | 1.79E-05 |
| ey | 1.06 | 1.50 | 3.69E-09 | 1.02 | 0.9193 |
| E2F1 | 1.14 | 0.81 | 0.0133 | 1.10 | 0.6981 |
| E2F2 | 1.17 | 1.25 | 0.0056 | 1.36 | 0.0011 |
| CycE | 1.14 | 0.99 | 0.9310 | 0.86 | 0.3943 |

**Table S4.2 RNA-seq fold changes and False Discovery Rates (FDRs) of various genes of interest in Mi-2$^{DN}$ and E93$^{RNAi}$ conditions.** Significant FDRs are shown in black, non-significant FDRs are indicated in grey.

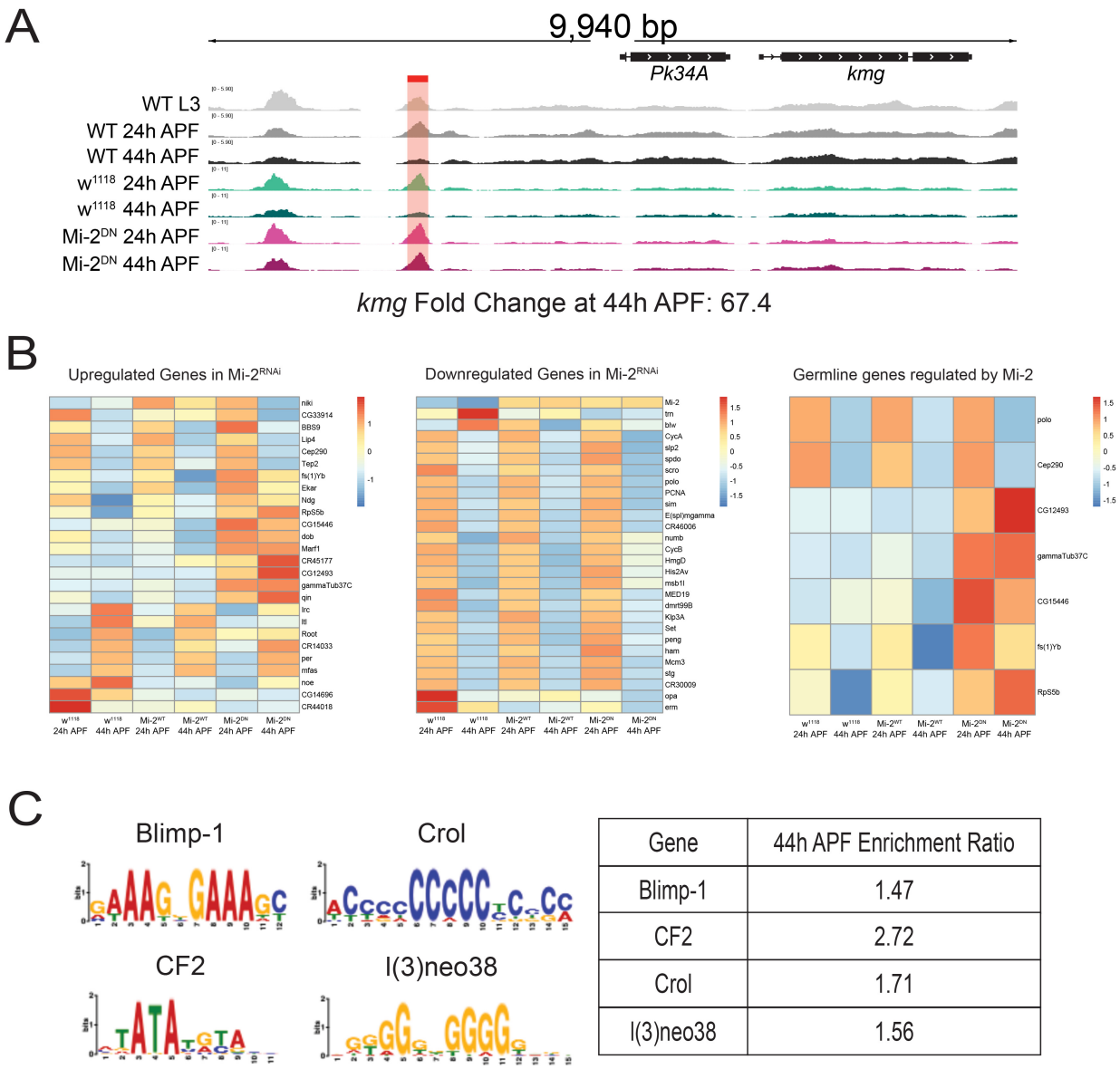


| Gene | 44h APF Enrichment Ratio |
|---|---|
| Blimp-1 | 1.47 |
| CF2 | 2.72 |
| Crol | 1.71 |
| l(3)neo38 | 1.56 |

**Figure S4.4 Validation of Mi-2$^{DN}$ datasets. (A)** *kmg* locus showing a peak upstream that fails to close upon disrupted Mi-2 function. **(B)** Genes known to be dysregulated by knockdown of Mi-2 RNAi show similar changes in Mi-2$^{DN}$ expressing eyes **(C)** Motifs predicted within significantly differentially accessible peaks in the Mi-2$^{DN}$ expressing 44h APF eyes and their corresponding enrichment ratios.

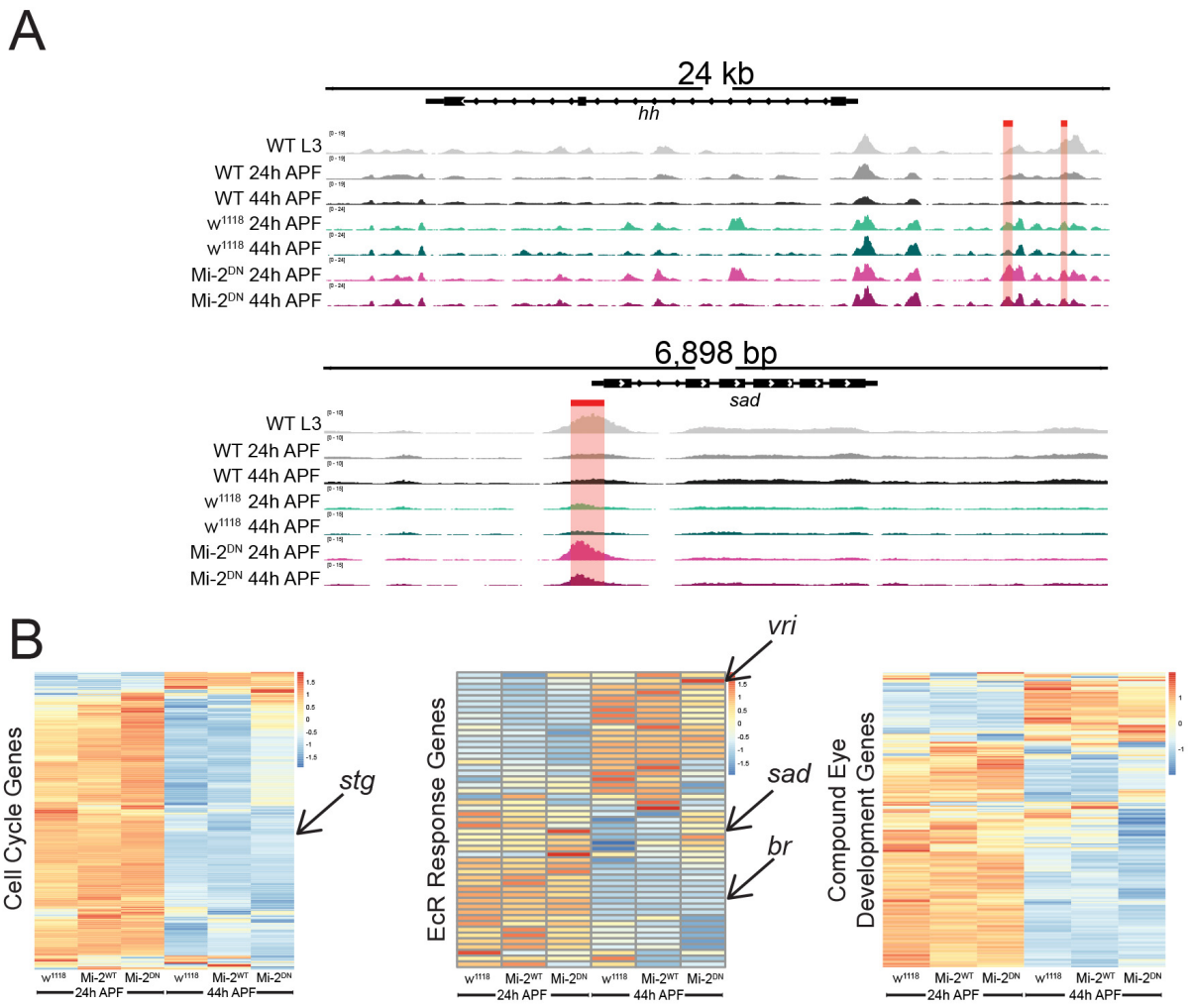


**Figure S4.5 Mi-2$^{DN}$ affects many genes of interest. (A)** Hedgehog and Shadow also contain chromatin peaks that fail to close with inhibition of Mi-2 function. **(B)** Alternate grouping of RNA-seq conditions for heatmaps of Cell Cycle Genes, EcR Response Genes, and Compound Eye Development Genes. Several of our genes of interest are shown to have affected gene expression levels.

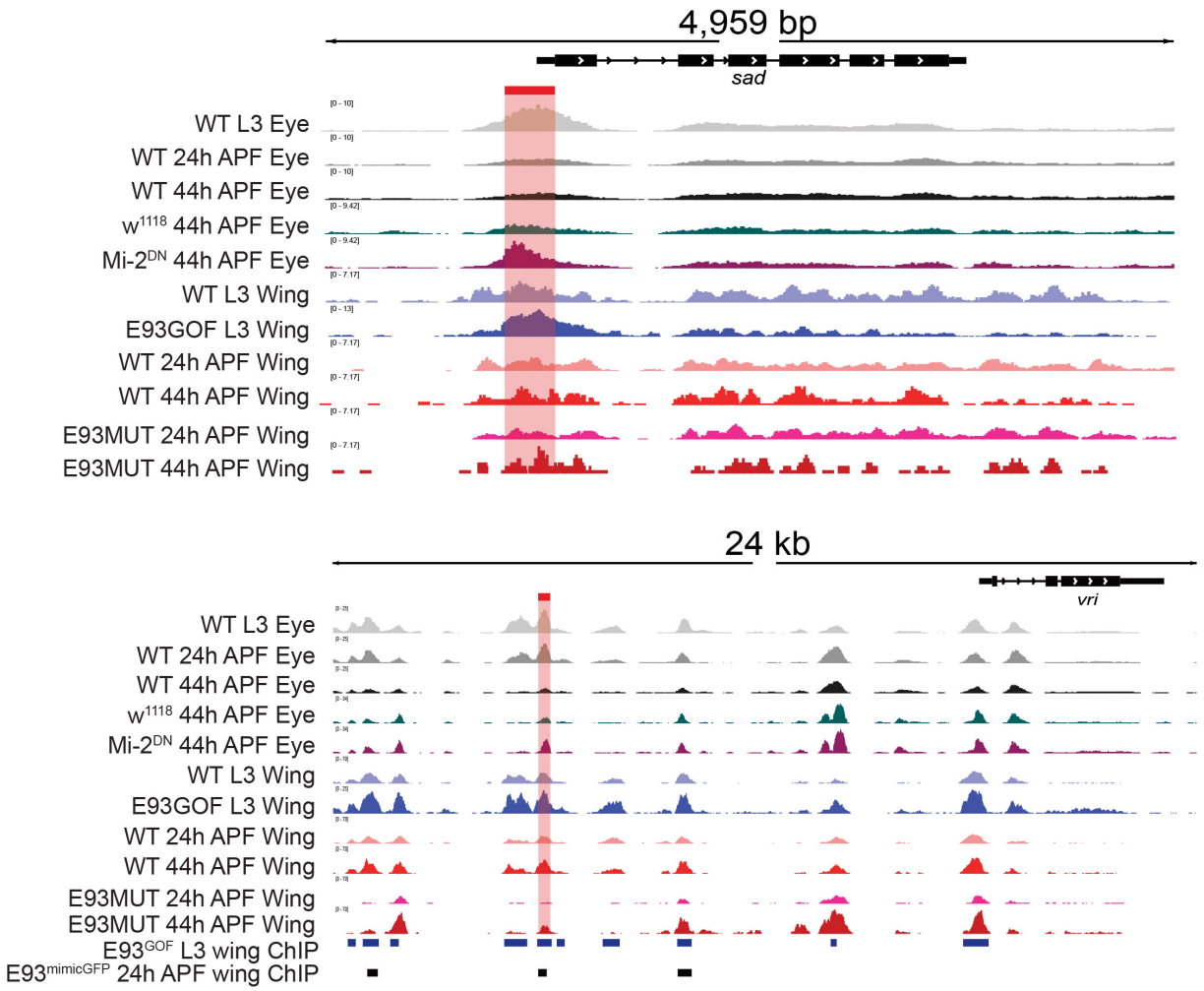


**Figure S4.6 Additional Genes that show overlap between E93 and Mi-2$^{DN}$ datasets.** Shadow and Vrille show affected chromatin accessibility in the E93 manipulations at peaks also affected by Mi-2

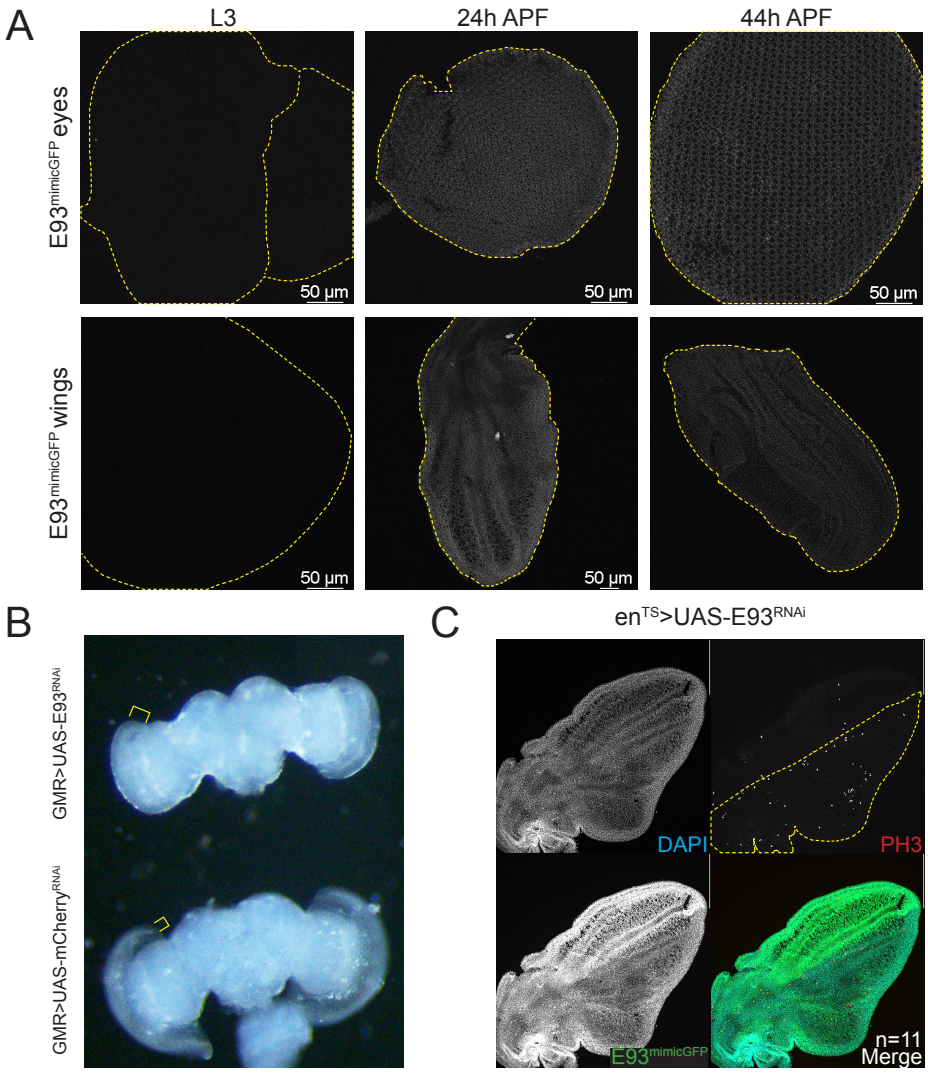
A
L3
24h APF
44h APF
E93mimicGFP eyes
E93mimicGFP wings
50 µm
B
GMR>UAS-E93RNAi
GMR>UAS-mCherryRNAi
C
enTS>UAS-E93RNAi
DAPI
PH3
E93mimicGFP
n=11
Merge
D
GMR-P35;GMR-Gal4 x UAS-E93RNAi
28h APF
44h APF
n= 4
n= 5
PH3

**Figure S4.7 Characterization of E93$^{RNAi}$ expressing eyes and wings. (A)** E93$^{mimicGFP}$ eyes and wings showing endogenous expression of E93. Image brightness was increased to show the E93 expression patterns. **(B)** Eye-brain complex at 45h APF in the E93 knockdown and mCherry$^{RNAi}$ conditions. The eye discs in the E93 knockdown condition appear to be smaller in diameter but thicker when compared to control eyes. **(C)** E93$^{mimicGFP}$ 26h APF wings expressing UAS-E93$^{RNAi}$ under the control of *en*-Gal4, *tub*-gal80$^{TS}$. White prepupa were collected and shifted to the non-permissive temperature of *tub*-gal80$^{TS}$, allowing expression of E93$^{RNAi}$ in the posterior wing during the final cell cycle. PH3 staining shows that mitoses are largely restricted to the posterior domain of the wing. **(D)** 28h and 44h APF eyes expressing E93$^{RNAi}$. Many mitoses are observed at 28h APF, and a few are observed at 44h APF. PH3 images have been brightened to highlight mitoses spots.

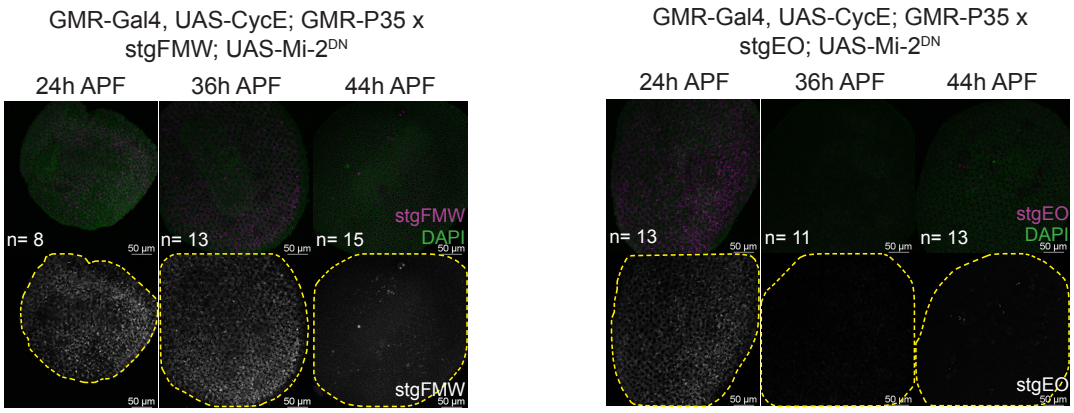


**Figure S4.8 Example eyes that were used for quantifications in Figure 4.6.** *stg-VS* reporters show delayed shut off when Mi-2 function is inhibited. The stgFMW and stgEO greyscale panels have been brightened to show expression patterns. Same intensity and unaltered images of these eyes were used for quantification is Figure 4.6B and C.

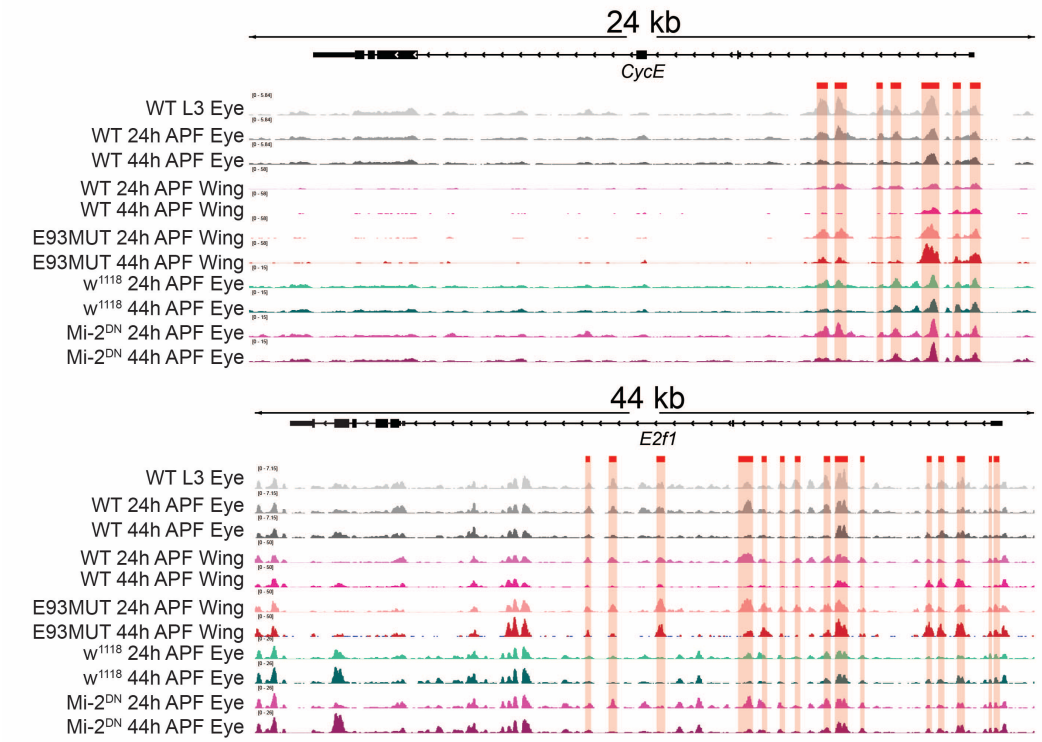


**Figure S4.9 E93 mutants show accessibility changes at *e2f1* and *cycE.*** E93MUT FAIRE-seq datasets have several significant peaks that localize within the regulatory regions of *cycE* and *e2f1*.

## 4.7 References


Ahringer, J., 2000. NuRD and SIN3 histone deacetylase complexes in development. Trends Genet 16, 351–356. https://doi.org/10.1016/S0168-9525(00)02066-7

Albini, S., Coutinho Toto, P., Dall'Agnese, A., Malecova, B., Cenciarelli, C., Felsani, A., Caruso, M., Bultman, S.J., Puri, P.L., 2015. Brahma is required for cell cycle arrest and late muscle gene expression during skeletal myogenesis. EMBO Rep 16, 1037–1050. https://doi.org/10.15252/EMBR.201540159

Andrade-Zapata, I., Baonza, A., 2014. The bHLH factors extramacrochaetae and daughterless control cell cycle in Drosophila imaginal discs through the transcriptional regulation of the Cdc25 phosphatase string. PLoS Genet 10. https://doi.org/10.1371/JOURNAL.PGEN.1004233

Aughey, G.N., Forsberg, E., Grimes, K., Zhang, S., Southall, T.D., 2023. NuRD-independent Mi-2 activity represses ectopic gene expression during neuronal maturation. EMBO Rep 24. https://doi.org/10.15252/embr.202255362

Baehrecke EH, Thummel CS, 1995. The Drosophila E93 Gene from the 93F Early Puff Displays Stage and Tissue Specific Regulation by 20-Hydroxyecdysone. Dev Biol 171, 85–97. https://doi.org/10.1006/dbio.1995.1262

Bouazoune, K., Mitterweger, A., Längst, G., Imhof, A., Akhtar, A., Becker, P.B., Brehm, A., 2002. The dMi-2 chromodomains are DNA binding modules important for ATP-dependent nucleosome mobilization. EMBO J 21, 2430–2440. https://doi.org/10.1093/emboj/21.10.2430

Bradley-Gill, M.R., Kim, M., Feingold, D., Yergeau, C., Houde, J., Moon, N.S., 2016. Alternate transcripts of the Drosophila "activator" E2F are necessary for maintenance of cell cycle exit during development. Dev Biol 411, 195–206. https://doi.org/10.1016/j.ydbio.2016.02.004

Brehm, A., Längst, G., Kehle, J., Clapier, C.R., Imhof, A., Eberharter, A., Müller, J., Becker, P.B., 2000. dMi-2 and ISWI chromatin remodeling factors have distinct nucleosome binding and mobilization properties. EMBO J 19, 4332–4341. https://doi.org/10.1093/emboj/19.16.4332

Buttitta, L.A., Edgar, B.A., 2007. Mechanisms controlling cell cycle exit upon terminal differentiation. Curr Opin Cell Biol 19, 697–704. https://doi.org/10.1016/J.CEB.2007.10.004

Buttitta, L.A., Katzaroff, A.J., Perez, C.L., de la Cruz, A., Edgar, B.A., 2007. A Double-Assurance Mechanism Controls Cell Cycle Exit upon Terminal Differentiation in Drosophila. Dev Cell 12, 631–643. https://doi.org/10.1016/j.devcel.2007.02.020

Dimova, D.K., Stevaux, O., Frolov, M. V., Dyson, N.J., 2003. Cell cycle-dependent and cell cycle-independent control of transcription by the Drosophila E2F/RB pathway. Genes Dev 17, 2308–2320. https://doi.org/10.1101/GAD.1116703

Djiane, A., Krejci, A., Bernard, F., Fexova, S., Millen, K., Bray, S.J., 2013. Dissecting the mechanisms of Notch induced hyperplasia. EMBO J 32, 60. https://doi.org/10.1038/EMBOJ.2012.326

Dobin, A., Davis, C.A., Schlesinger, F., Drenkow, J., Zaleski, C., Jha, S., Batut, P., Chaisson, M., Gingeras, T.R., 2013. STAR: Ultrafast universal RNA-seq aligner. Bioinformatics 29, 15–21. https://doi.org/10.1093/bioinformatics/bts635

Fasulo, B., Deuring, R., Murawska, M., Gause, M., Dorighi, K.M., Schaaf, C.A., Dorsett, D., Brehm, A., Tamkun, J.W., 2012. The Drosophila Mi-2 Chromatin-Remodeling Factor Regulates Higher-Order Chromatin Structure and Cohesin Dynamics In Vivo. PLoS Genet 8. https://doi.org/10.1371/journal.pgen.1002878

Flegel, K., Grushko, O., Bolin, K., Griggs, E., Buttitta, L., 2016. Roles for the Histone Modifying and Exchange Complex NuA4 in Cell Cycle Progression in Drosophila melanogaster. Genetics 203, 1265–1281. https://doi.org/10.1534/GENETICS.116.188581

Freeman, M., 1996. Reiterative use of the EGF receptor triggers differentiation of all cell types in the Drosophila eye. Cell 87, 651–660. https://doi.org/10.1016/S0092-8674(00)81385-9

Graves, B.J., Schubiger, G., 1982. Cell cycle changes during growth and differentiation of imaginal leg discs in Drosophila melanogaster. Dev Biol 93, 104–110. https://doi.org/10.1016/0012-1606(82)90243-3

Guo, Y., Flegel, K., Kumar, J., McKay, D.J., Buttitta, L.A., 2016. Ecdysone signaling induces two phases of cell cycle exit in Drosophila cells. Biol Open 5, 1648–1661. https://doi.org/10.1242/bio.017525

Hay, B.A., Wolff, T., Rubin, G.M., 1994. Expression of baculovirus P35 prevents cell death in Drosophila. Development 120, 2121–2129. https://doi.org/10.1242/DEV.120.8.2121

Jones, L., Richardson, H., Saint, R., 2000. Tissue-specific regulation of cyclin E transcription during Drosophila melanogaster embryogenesis. Development 127, 4619–4630. https://doi.org/10.1242/dev.127.21.4619

Kim, J., Lu, C., Srinivasan, S., Awe, S., Brehm, A., Fuller, M.T., 2017. Blocking promiscuous activation at cryptic promoters directs cell type-specific gene expression. Science 356, 717–721. https://doi.org/10.1126/SCIENCE.AAL3096

Kreher, J., Kovač, K., Bouazoune, K., MačInković, I., Ernst, A.L., Engelen, E., Pahl, R., Finkernagel, F., Murawska, M., Ullah, I., Brehm, A., 2017. EcR recruits dMi-2 and increases efficiency of dMi-2-mediated remodelling to constrain transcription of hormone-regulated genes. Nat Commun 8. https://doi.org/10.1038/ncomms14806

Kunert, N., Brehm, A., 2009. Novel Mi-2 related ATP-dependent chromatin remodelers. Epigenetics 4, 209–211. https://doi.org/10.4161/epi.8933

Kunert, N., Wagner, E., Murawska, M., Klinker, H., Kremmer, E., Brehm, A., 2009. dMec: A novel Mi-2 chromatin remodelling complex involved in transcriptional repression. EMBO Journal 28, 533–544. https://doi.org/10.1038/emboj.2009.3

Lehman, D.A., Patterson, B., Johnston, L.A., Balzer, T., Britton, J.S., Saint, R., Edgar, B.A., 1999. Cis-regulatory elements of the mitotic regulator, string/Cdc25. Development 126, 1793–803.

Lopes, C.S., Casares, F., 2015. Eye Selector Logic for a Coordinated Cell Cycle Exit. PLoS Genet 11, 1–22. https://doi.org/10.1371/journal.pgen.1004981

Ma, Y., Buttitta, L., 2017. Chromatin organization changes during the establishment and maintenance of the postmitotic state. Epigenetics Chromatin 10. https://doi.org/10.1186/S13072-017-0159-8

Ma, Y., Kanakousaki, K., Buttitta, L., 2015. How the cell cycle impacts chromatin architecture and influences cell fate. Front Genet 6. https://doi.org/10.3389/FGENE.2015.00019

Ma, Y., McKay, D.J., Buttitta, L., 2019. Changes in chromatin accessibility ensure robust cell cycle exit in terminally differentiated cells. PLoS Biol 17, e3000378. https://doi.org/10.1371/journal.pbio.3000378

Martin, B.J.E., Ablondi, E.F., Goglia, C., Mimoso, C.A., Espinel-Cabrera, P.R., Adelman, K., 2023. Global identification of SWI/SNF targets reveals compensation by EP400. Cell 186. https://doi.org/10.1016/J.CELL.2023.10.006

McKay, D.J., Lieb, J.D., 2013. A Common Set of DNA Regulatory Elements Shapes Drosophila Appendages. Dev Cell 27, 306–318. https://doi.org/10.1016/j.devcel.2013.10.009

Meyer, C.A., Jacobs, H.W., Datar, S.A., Du, W., Edgar, B.A., Lehner, C.F., 2000. Drosophila Cdk4 is required for normal growth and is dispensable for cell cycle progression. EMBO J 19, 4533–4542. https://doi.org/10.1093/EMBOJ/19.17.4533

Milán, M., Campuzano, S., García-Bellido, A., 1996. Cell cycling and patterned cell proliferation in the Drosophila wing during metamorphosis. Proc Natl Acad Sci U S A 93, 11687–11692. https://doi.org/10.1073/PNAS.93.21.11687

Neufeld, T.P., Edgar, B.A., 1998. Connections between growth and the cell cycle. Curr Opin Cell Biol 10, 784–790. https://doi.org/10.1016/S0955-0674(98)80122-1

Ninov, N., Manjón, C., Martín-Blanco, E., 2009. Dynamic control of cell cycle and growth coupling by ecdysone, EGFR, and PI3K signaling in Drosophila histoblasts. PLoS Biol 7, 0892–0903. https://doi.org/10.1371/JOURNAL.PBIO.1000079

Niwa, Y.S., Niwa, R., 2016. Transcriptional regulation of insect steroid hormone biosynthesis and its role in controlling timing of molting and metamorphosis. Dev Growth Differ. https://doi.org/10.1111/dgd.12248

Nystrom, S.L., Niederhuber, M.J., McKay, D.J., 2020. Expression of E93 provides an instructive cue to control dynamic enhancer activity and chromatin accessibility during development. Development (Cambridge) 147. https://doi.org/10.1242/dev.181909

Polo, S.E., Kaidi, A., Baskcomb, L., Galanty, Y., Jackson, S.P., 2010. Regulation of DNA-damage responses and cell-cycle progression by the chromatin remodelling factor CHD4. EMBO J 29, 3130–3139. https://doi.org/10.1038/EMBOJ.2010.188

Pulianmackal, A.J., Kanakousaki, K., Flegel, K., Grushko, O.G., Gourley, E., Rozich, E., Buttitta, L.A., 2022. Misregulation of Nucleoporins 98 and 96 leads to defects in protein synthesis that promote hallmarks of tumorigenesis. Dis Model Mech 15. https://doi.org/10.1242/DMM.049234

Reis, T., Edgar, B.A., 2004. Negative regulation of dE2F1 by cyclin-dependent kinases controls cell cycle timing. Cell 117, 253–264. https://doi.org/10.1016/S0092-8674(04)00247-8

Robinson, M.D., McCarthy, D.J., Smyth, G.K., 2010. edgeR: a Bioconductor package for differential expression analysis of digital gene expression data. Bioinformatics 26, 139. https://doi.org/10.1093/BIOINFORMATICS/BTP616

Ruijtenberg, S., van den Heuvel, S., 2016. Coordinating cell proliferation and differentiation: Antagonism between cell cycle regulators and cell type-specific gene expression. Cell Cycle. https://doi.org/10.1080/15384101.2015.1120925

Schubiger, M., Palka, J., 1987. Changing Spatial Patterns of DNA Replication in the Developing Wing of Drosophila. Dev Biol 123, 145–153.

Thacker, S.A., Bonnette, P.C., Duronio, R.J., 2003. The Contribution of E2F-Regulated Transcription to Drosophila PCNA Gene Function. Current Biology 13, 53–58.

Thummel, C.S., 2002. Ecdysone-regulated puff genes 2000. Insect Biochem Mol Biol 32, 113–120.

Thummel, C.S., 1990. Puffs and gene regulation--molecular insights into the Drosophila ecdysone regulatory hierarchy. Bioessays 12, 561–568. https://doi.org/10.1002/BIES.950121202

Treisman, J.E., 2013. Retinal differentiation in Drosophila. Wiley Interdiscip Rev Dev Biol 2, 545–557. https://doi.org/10.1002/WDEV.100

Unhavaithaya, Y., Shin, T.H., Miliaras, N., Lee, J., Oyama, T., Mello, C.C., 2002. MEP-1 and a Homolog of the NURD Complex Component Mi-2 Act Together to Maintain Germline-Soma Distinctions in C. elegans. Cell 111, 991–1002.

Uyehara, C.M., Nystrom, S.L., Niederhuber, M.J., Leatham-Jensen, M., Ma, Y., Buttitta, L.A., McKay, D.J., 2017. Hormone-dependent control of developmental timing through regulation of chromatin accessibility. Genes Dev 31, 862–875. https://doi.org/10.1101/gad.298182.117

Verma, P., Cohen, S.M., 2015. miR-965 controls cell proliferation and migration during tissue morphogenesis in the Drosophila abdomen. Elife 4. https://doi.org/10.7554/ELIFE.07389

Wang, H., Morrison, C.A., Ghosh, N., Tea, J.S., Call, G.B., Treisman, J.E., 2022. The Blimp-1 transcription factor acts in non-neuronal cells to regulate terminal differentiation of the Drosophila eye. Development 149. https://doi.org/10.1242/DEV.200217

Xin, S., Weng, L., Xu, J., Du, W., 2002. The role of RBF in developmentally regulated cell proliferation in the eye disc and in Cyclin D/Cdk4 induced cellular growth. Development 129, 1345–1356. https://doi.org/10.1242/DEV.129.6.1345

Xue, Y., Wong, J., Moreno, G.T., Young, M.K., Cô, J., Wang, W., 1998. NURD, a Novel Complex with both ATP-Dependent Chromatin-Remodeling and Histone Deacetylase Activities. Mol Cell 2, 851–861.

## Chapter 5: Conclusions and Future Directions

In the *Drosophila melanogaster* eye and wing, cell cycle exit occurs at 24h APF during metamorphosis and correlates with the initiation of terminal differentiation programs. The mechanism(s) controlling this coordination are largely unknown, and my thesis work has focused on gaining an understanding of this coordination. In Chapter 2, I developed a dissociation protocol that allowed us to perform enzymatic genomic techniques such as ATAC-seq and CUT&RUN with reduced input material. These techniques help us determine the open chromatin profile and genome binding profiles respectively, which were previously difficult to perform due to the major tissue quantities needed to perform mechanical techniques like FAIRE-seq and ChIP-seq. In Chapter 3, I examined modular enhancer patterns of the rate-limiting cell cycle genes *e2f1* and *stg*. This work not only verified that these dynamic chromatin regions are in fact larval and pupal enhancers of *e2f1* and *stg*, but also provides insight into how these enhancers are expressed over time as well as within the *Drosophila* eye and wing. We also note that these expression from these enhancers largely decreases after cell cycle exit occurs at 24h APF, suggesting that closing of chromatin is a mechanism by which expression of rate-limiting cell cycle genes is terminated. In Chapter 4, I investigate the role of the chromatin remodeler Mi-2 and the ecdysone-responsive transcription factor E93 in coordinating cell cycle exit with initiation of terminal differentiation programs. We observe that while Mi-2 and E93 largely affect different genes, they do affect the

expression of a shared subset of genes, including cell cycle genes, compound eye development genes, and ecdysone response genes. We focus on their effect on the previously studied larval eye enhancer of *stg* called *stg-VS*. We find that this enhancer also functions as a pupal eye enhancer. Expression of a dominant-negative Mi-2 and various manipulations of E93 cause a neighboring chromatin region to remain open beyond the normal time of closing. We also observed that expression of the dominant-negative Mi-2 during the final cell cycle in the eye causes the *stg*-VS reporters to express for several hours beyond what is observed in wild type eyes. We speculate that the chromatin region that remains open upon disruption of Mi-2 and E93 function regulates the *stg-VS* region, but the manner of regulation is still unclear. We believe that Mi-2 and E93 are only one piece of the mechanism that coordinates cell cycle exit with terminal differentiation, so additional work is needed to further our understanding of this process.

### 5.1 Further investigation into the chromatin region near stg-VS

In Chapter 4 we identified a chromatin accessibility peak near the stg-VS locus that fails to close after cell cycle exit when Mi-2 function is disrupted. We also observed that this peak opened prematurely in response to precocious E93 expression and failed to close in E93 mutant pupal wings. Unfortunately, there are no publicly available fly reporter lines that cover this region, so we must generate our own lines to determine whether this region behaves as an enhancer. The first step will be to clone multiple fragments that encompass various parts of this chromatin region (Figure 5.1). We plan to clone individual accessible regions, with the particular peak of interest contained

within what we are calling the *stg* proximal line. We will also clone larger fragments, ~6kb and ~10kb, that will encompass the peak of interest as well as portions of the stg-VS region. Because we have not tested the *stg* proximal peak yet, we do not know if it contains any activator sequences, or if it is only able to modify expression of other chromatin regions. When we test the *stg* proximal line alone, we may or may not observe enhancer activity. By including portions of the nearby stg-VS region, which is known to act as an eye enhancer for *stg*, we will be able to observe any effects this larger region may have on the stg-VS enhancer. These fragments will be cloned upstream of a destabilized Green Fluorescent Protein (GFP), so that we can compare to the established stg-VS reporters which are also upstream of a destabilized GFP.

Once we have reporter fly lines in hand, we will first look at normal expression of these constructs in the *Drosophila* larval and pupal eye and wing to observe their normal expression patterns. We will then follow up on any lines that show enhancer activity. We will perform multi-step crosses to eventually produce progeny that contain the new reporter construct, the GMR-Gal4 driver, GMR-P35, and UAS-Mi-2$^{DN}$. This will allow us to dissect pupal eyes and observe any effects that Mi-2$^{DN}$ expression has on the reporter constructs. If pupal wing enhancer activity is also observed, we will perform multi-step crosses to produce progeny that contain the reporter construct, *en*-Gal4 driver, *tub*-Gal80$^{TS}$, and UAS-Mi-2$^{DN}$. This will allow us to raise the progeny at 18ºC, keeping the *en*-Gal4 activity suppressed due to *tub*-Gal80$^{TS}$ expression, until the progeny reach the white prepupa stage. White prepupa will be collected and raised at 29ºC to degrade *tub*-Gal80$^{TS}$, until they reach the equivalent age of 24h and 44h APF, when pupal wings will be dissected. This cross also allows for an internal control, due to

*en*-Gal4 expression only in the posterior wing, limiting Mi-2$^{DN}$ activity to the posterior wing. To examine the effects of E93 on these constructs, we can perform the same experiments as above using UAS-E93$^{RNAi}$ in place of Mi-2$^{DN}$. These experiments will provide in vivo validation of whether or not these regions act as enhancers of *stg* and whether or not their activity is affected by Mi-2$^{DN}$ and knockdown of E93.

**5.2 Determining Mi-2 and E93 genomic localization**

In Chapter 2, I describe a dissociation protocol that is compatible with CUT&RUN (Cleavage Under Targets & Release Using Nuclease) (Skene and Henikoff, 2017). We have performed preliminary CUT&RUN studies in the *Drosophila* larval wing to determine localization of the Mi-2 chromatin remodeler. We tested overexpression of Mi-2$^{WT}$ and Mi-2$^{DN}$, using *apterous*-Gal4 with a temperature sensitive *tub*-Gal80. This allows us to control the timing of Mi-2$^{WT}$ and Mi-2$^{DN}$ overexpression with the *tub*-Gal80$^{TS}$, and the *apterous*-Gal4 restricts their expression to the dorsal half of the wing. Both Mi-2$^{WT}$ and Mi-2$^{DN}$ contain FLAG tags, so we used an Anti-FLAG antibody to isolate only those chromatin regions that were bound by FLAG-tagged proteins. From these studies, we observed that the binding profile of Mi-2$^{DN}$ largely overlaps with accessible chromatin (Figure 5.2). We also observed that Mi-2$^{WT}$ appears to bind non-specifically all over the genome, a pattern seen with SWI/SNF remodelers termed as “recreational binding” (Gelbart et al., 2005). Our hypothesis is that the Mi-2$^{DN}$ binds to accessible chromatin but lacks ATPase activity and cannot release, while Mi-2$^{WT}$ may exhibit dynamic binding with a remodeling activity that is too rapid to be reliably detected by CUT&RUN. To follow up on these preliminary experiments, we have several

options. We can use the same GMR crosses described in Chapter 4 and look at localization of Mi-2$^{WT}$ and Mi-2$^{DN}$ in the pupal eye with newer CUT&RUN protocols designed to capture dynamic binding to chromatin, that use low volume, crosslinkers and denaturation (Bai et al., 2022; Zambanini et al., 2022). We have also validated a fly line containing an endogenously tagged allele of Mi-2, Mi-2$^{mimicGFP}$, that not only localizes correctly, but also rescues a mutant Mi-2 allele and a deficiency line, where the entire Mi-2 locus has been removed (Figure 5.3). The Mi-2$^{mimicGFP}$ line also contains a FLAG tag, so we can use the same Anti-FLAG antibody that was used in the preliminary studies to detected where the FLAG-tagged proteins are localized. We can also explore localization of E93 using an E93$^{mimicGFP}$ fly line, which similarly contains a FLAG tag. Performing CUT&RUN in the *Drosophila* pupal eye would allow us to determine if there are any regions where Mi-2 and E93 co-localize and would corroborate our hypothesis that Mi-2 and E93 are co-regulating a subset of genes at cell cycle exit and initiation of terminal differentiation. Having E93 CUT&RUN data in the pupal eye would allow for a comparison to the published E93 wing ChIP-seq datasets that were discussed in chapter 4, and give insight into whether or not there are any eye-specific or wing-specific binding events.

### 5.3 Identifying larval and pupal eye and wing enhancers for *cycE*

In chapter 3 we investigated the modular enhancers of *stg* and *e2f1* in the pupal eye, wing and brain to identify shared and tissue-specific enhancers as well as their spatial and temporal expression patterns. We performed these studies using readily available Gal4 lines from the Janelia and ViennaTile collections (Jenett et al., 2012;

Kvon et al., 2014). Unfortunately, none of the available Gal4 lines cover the dynamic chromatin regions of the *cycE* locus that we suspect may be enhancers, and only one line overlapping the dynamic chromatin at the cycE locus has been generated (Djiane et al., 2013). As expected based on the accessibility, this line does express in pupal wings and eyes and shows reduced expression after 36h APF (Figure 5.4). We observe that when the known Su(H) binding sites are mutated, the enhancer fails to turn off, especially in pupal wings (Figure 5.4, Figure 5.5). Su(H) is a transcription factor that directly binds to DNA, and it acts as a transcriptional activator when bound by Notch and a transcriptional repressor when it is not bound by Notch (Morel and Schweisguth, 2000). Deletion of the Su(H) binding sites may prevent Su(H) from acting as a transcriptional repressor of CycE in the absence of Notch signaling, resulting in failure to turn off the enhancer.

To perform similar studies of the *cycE* locus, it will be necessary to clone 1-3kb fragments that cover the regulatory regions where we observe dynamic opening and closing of chromatin during metamorphosis (Figure 5.5). We can create plasmids containing these fragments upstream of a *Drosophila* synthetic core promoter and Gal4 coding sequence, and have these p-elements injected into flies. We can then perform similar experiments to those performed in Chapter 3, using GTRACE to observe any past and present expression from the putative enhancer fragments in the *Drosophila* larval and pupal eyes, wings and brain (Evans et al., 2009). These experiments will allow us to identify the enhancers of *cycE* and allow for future studies to gain an understanding of how *cycE* expression is turned off after cell cycle exit.

### 5.4 Determining how *cycE* and *e2f1* enhancers are remodeled after cell cycle exit

In chapter 4, I discuss the chromatin accessibility and gene expression changes that occurred as a result of overexpressing a dominant-negative Mi-2 (Mi-$2^{DN}$) in the developing pupal eye. While we observed chromatin accessibility and gene expression changes at a subset of cell cycle genes including *stg*, *cycB3*, *cdc14* and FANCI, we observed very minor changes at *e2f1* and *e2f2*, but none at *cycE*. This suggests that other chromatin remodelers besides Mi-2 function at these loci to promote the closing of chromatin after cell cycle exit.

### 5.5 Examining the roles of chromatin remodelers Brahma & Osa in coordinating cell cycle exit with terminal differentiation

Previous work in the Buttitta Lab identified Mi-2, Brahma (Brm) and Osa as chromatin remodelers that have a role in cell cycle exit through a screen performed in the *Drosophila* eye (Ma, 2018). Brahma belongs to the SWI/SNF family of chromatin remodelers and is the ATPase domain of the chromatin remodeling complexes BAP and PBAP (Elfring et al., 1998; Moshkin et al., 2007). Osa is a DNA-binding protein, and it is a subunit of the BAP chromatin remodeling complex (Moshkin et al., 2007; Vázquez et al., 1999). We have now confirmed further that Mi-2 coordinates the timing of cell cycle exit with initiation of terminal differentiation by affecting chromatin accessibility and gene expression of cell cycle genes, compound eye development genes and ecdysone response genes. However, we did not see major chromatin accessibility and gene expression changes at all cell cycle genes including *e2f1, e2f2,* and *cycE*. We have performed preliminary experiments in the pupal eye to observe the effects of two

$Osa^{RNAi}$ lines and a $Brm^{RNAi}$ line. As shown in Figure 5.6, we observe additional mitoses at 24h APF, indicating that cell cycle exit is delayed when Osa and Brm are knocked down. Additionally, we have a dominant-negative Brahma (UAS-$Brm^{DN}$) line that requires validation but is expected to behave similarly to the UAS-Mi-$2^{DN}$ used in Chapter 4. With these fly lines, we can repeat the ATAC-seq and RNA-seq experiments performed in Chapter 4 to observe any chromatin accessibility and gene expression changes that occur as a result of disrupting Brm and Osa function. With these new datasets, particular attention will be paid to *e2f1* and *cycE*, to determine if Brm and Osa are the chromatin remodelers responsible for closing chromatin at these loci.

Due to the importance of chromatin remodeler function, we expect that redundancies between chromatin remodelers exist, in that chromatin remodelers can "substitute" for one another when a particular remodeler is not functioning properly. We have considered recombining the Mi-$2^{DN}$ and $Brm^{DN}$ lines, so that using the Gal4-UAS system, we can selectively overexpress these dominant-negative remodelers together in the fly eye. We will perform staining for phospho-histone H3 (PH3), a mitosis marker, and discs-large (DLG), which marks the apical region of lateral cell membranes. This will show us whether or not cell cycle exit is delayed and will also mark extra cells of the fly eye, including cone cells and interommatidial cells. We can observe the adult eyes of these flies to look for pigmentation or differentiation defects. To further examine differentiation defects, we can stain pupal eyes for Elav, which marks neuronal cells, and chaoptin (Chp), which marks photoreceptor plasma membranes and axons in the pupal eye. Depending upon the state of these Mi-$2^{DN}$ and $Brm^{DN}$ expressing eyes, we could perform ATAC-seq and RNA-seq to observe chromatin accessibility and gene

expression changes. This may allow us to observe regions that can be remodeled by both chromatin remodelers, even though they may be preferentially remodeled by one of the two. The redundancy of chromatin remodelers in silencing rate-limiting cell cycle genes may be essential for the permanent cell cycle exit associated with terminal differentiation. These redundancies are likely to be the molecular mechanism underlying permanent exit.

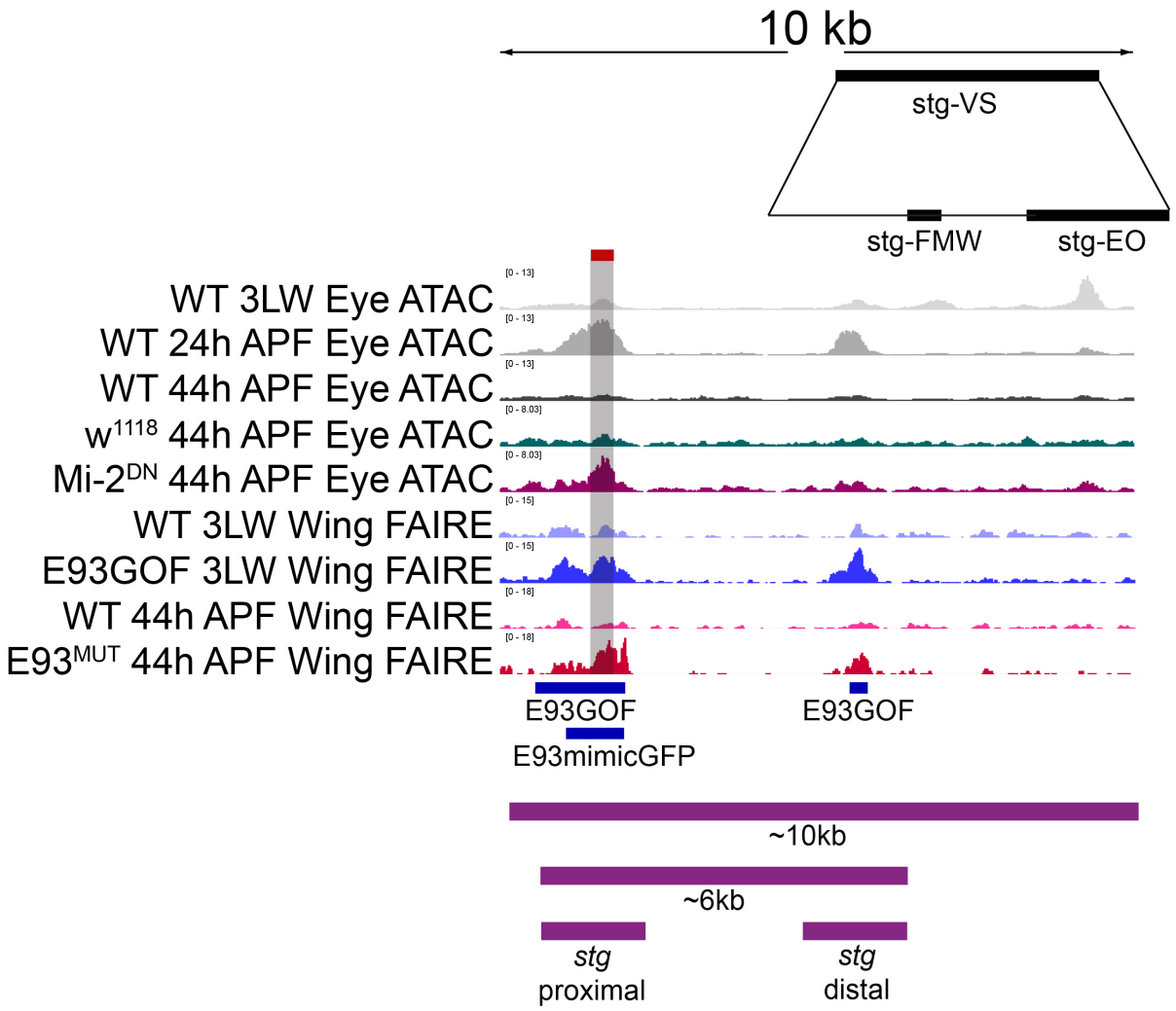


**Figure 5.1 Chromatin peak near *stg-VS*.** The grey box highlights the chromatin peak that fails to close in the Mi-2$^{DN}$ ATAC-seq dataset. The black bars show the approximate location of *stg-VS, stg-FMW* and *stg-EO*. The purple bars below indicate regions that we are in the process of cloning to examine whether or not they function as *stg* eye enhancers.

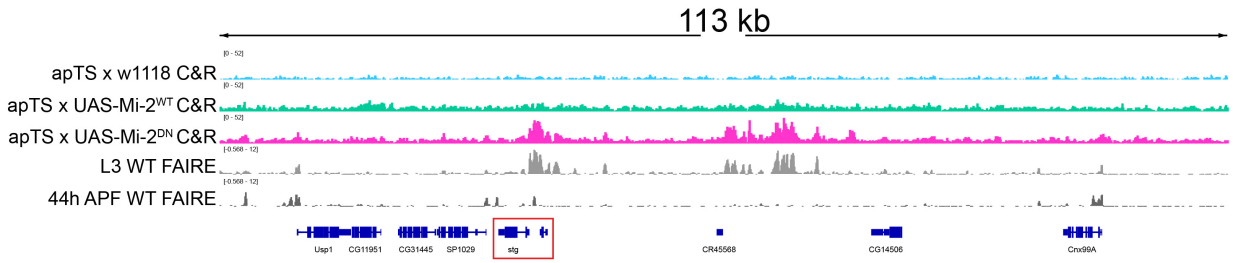


**Figure 5.2 Preliminary Mi-2 CUT&RUN.** Preliminary CUT&RUN data performed in *Drosophila* larval wing discs, focused on *stg*, highlighted by the red box. Mi-2DN appears to primarily bind to open chromatin regions, while Mi-2$^{WT}$ appears to bind evenly across the region.

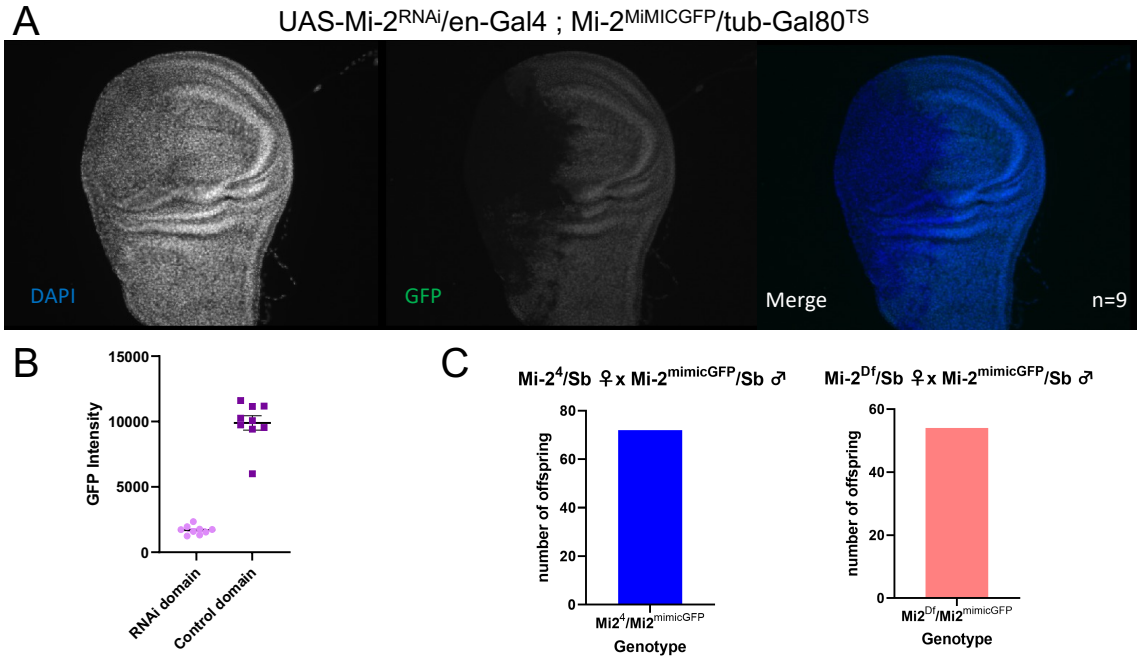


**Figure 5.3 Mi-2$^{mimicGFP}$ is a functional allele of Mi-2. (A)** In third instar larval wings, Mi-2$^{mimicGFP}$ is successfully knocked down by UAS-Mi-2$^{RNAi}$. **(B)** Quantification of GFP intensity in RNAi-expressing and control domains. **(C)** Quantification of offspring from rescue crosses. Mi-2$^{mimicGFP}$ also rescues Mi-2$^{4}$, a truncated allele of Mi-2, and Mi-2$^{Df}$, a deficiency line where the entire Mi-2 locus has been deleted.

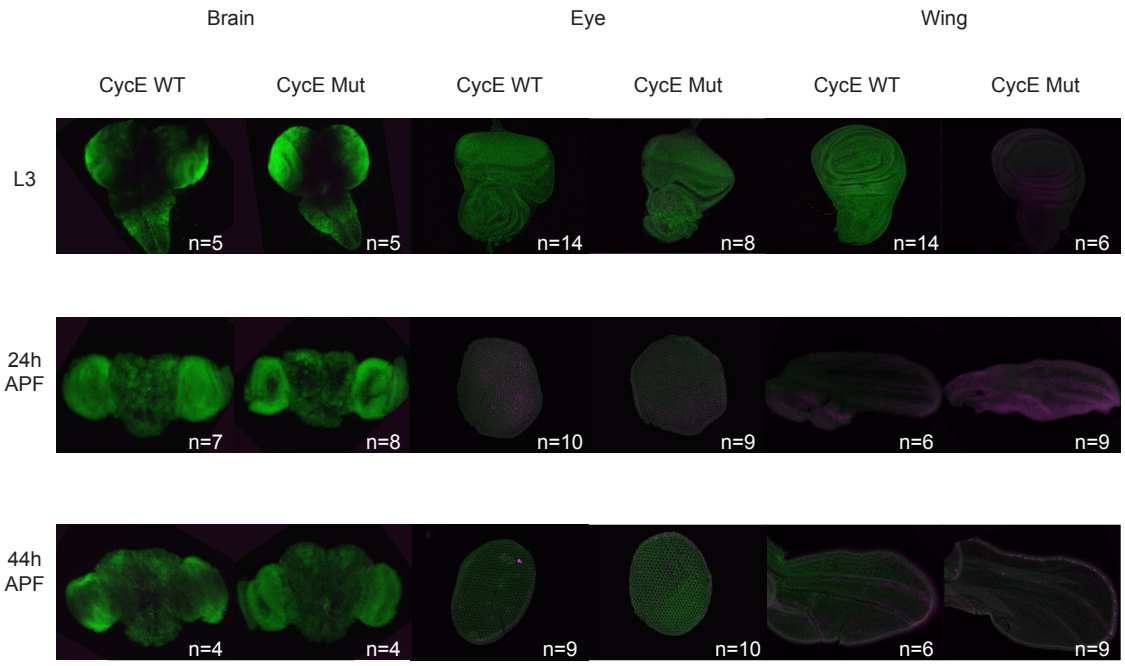


**Figure 5.4 Characterization of wildtype and mutant CycE reporters.** Brains, eyes and wings with wildtype and mutant CycE reporter constructs. CycE Mut reporter contains two Su(H) binding sites that have been mutated. DAPI is shown in green and reporter expression is shown in magenta.

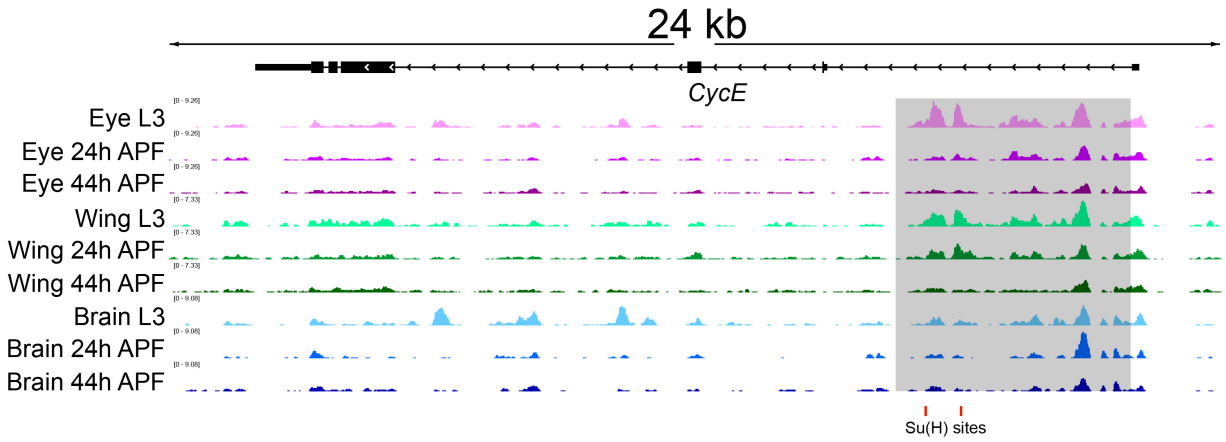


**Figure 5.5 ATAC-seq data for the *cycE* locus in the *Drosophila* eye, wing and brain.** The grey box indicates chromatin where dynamic accessibility changes are observed during metamorphosis, and these regions are largely inaccessible at 44h APF. This is the region that we will clone and make reporter constructs for. The red vertical bars along the bottom are known *suppressor of hairless* (*Su(H)*) sites known to affect expression of *cycE* when mutated (Djiane et al., 2013).

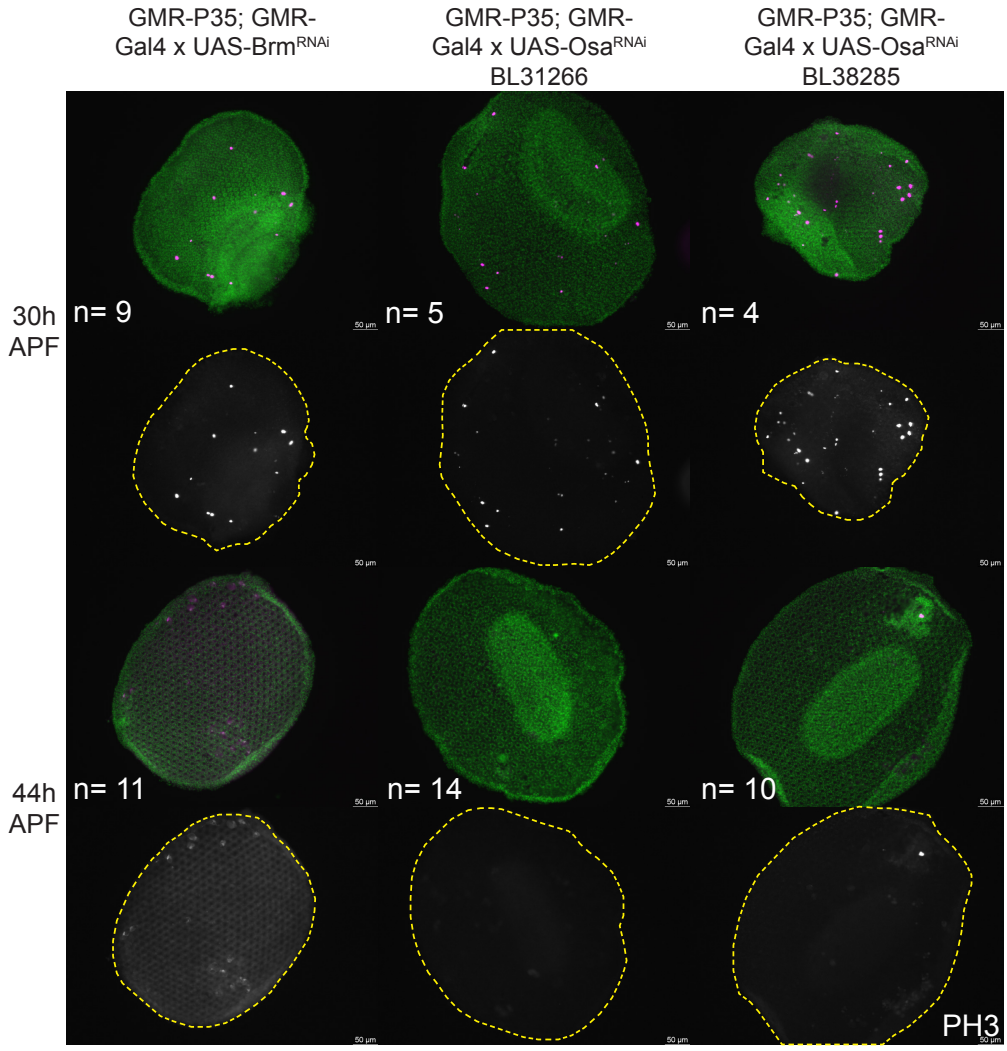


**Figure 5.6 Cell cycle exit is delayed with knockdown of Brm and Osa.** PH3 staining in 30h and 44h APF eyes shows mitoses occurring beyond the normal timing of cell cycle exit. One RNAi line for Brm and two RNAi lines for Osa were tested.

## 5.6 References


Bai, Huiru, Lin, M., Meng, Y., Bai, Huiyuan, Cai, S., 2022. An improved CUT&RUN method for regulation network reconstruction of low abundance transcription factor. Cell Signal 96. https://doi.org/10.1016/J.CELLSIG.2022.110361

Djiane, A., Krejci, A., Bernard, F., Fexova, S., Millen, K., Bray, S.J., 2013. Dissecting the mechanisms of Notch induced hyperplasia. EMBO J 32, 60. https://doi.org/10.1038/EMBOJ.2012.326

Elfring, L.K., Daniel, C., Papoulas, O., Deuring, R., Sarte, M., Moseley, S., Beek, S.J., Ross Waldrip, W., Daubresse, G., Depace, A., Kennison, J.A., Tamkun, J.W., Tamkun, J., 1998. Genetic Analysis of brahma : The Drosophila Homolog of the Yeast Chromatin Remodeling Factor SWI2/SNF2. Genetics 148, 251–265. https://doi.org/10.1093/genetics/148.1.251

Evans, C.J., Olson, J.M., Ngo, K.T., Kim, E., Lee, N.E., Kuoy, E., Patananan, A.N., Sitz, D., Tran, P.T., Do, M.T., Yackle, K., Cespedes, A., Hartenstein, V., Call, G.B., Banerjee, U., 2009. G-TRACE: Rapid Gal4-based cell lineage analysis in Drosophila. Nat Methods 6, 603–605. https://doi.org/10.1038/nmeth.1356

Gelbart, M.E., Bachman, N., Delrow, J., Boeke, J.D., Tsukiyama, T., 2005. Genome-wide identification of Isw2 chromatin-remodeling targets by localization of a catalytically inactive mutant. Genes Dev 19, 942–954. https://doi.org/10.1101/GAD.1298905

Jenett, A., Rubin, G.M., Ngo, T.T.B., Shepherd, D., Murphy, C., Dionne, H., Pfeiffer, B.D., Cavallaro, A., Hall, D., Jeter, J., Iyer, N., Fetter, D., Hausenfluck, J.H., Peng, H., Trautman, E.T., Svirskas, R.R., Myers, E.W., Iwinski, Z.R., Aso, Y., DePasquale, G.M., Enos, A., Hulamm, P., Lam, S.C.B., Li, H.H., Laverty, T.R., Long, F., Qu, L., Murphy, S.D., Rokicki, K., Safford, T., Shaw, K., Simpson, J.H., Sowell, A., Tae, S., Yu, Y., Zugates, C.T., 2012. A GAL4-Driver Line Resource for Drosophila Neurobiology. Cell Rep 2, 991–1001. https://doi.org/10.1016/j.celrep.2012.09.011

Kvon, E.Z., Kazmar, T., Stampfel, G., Yáñez-Cuna, J.O., Pagani, M., Schernhuber, K., Dickson, B.J., Stark, A., 2014. Genome-scale functional characterization of Drosophila developmental enhancers in vivo. Nature 512, 91–95. https://doi.org/10.1038/nature13395

Ma, Y., 2018. Chromatin Structure Changes During Terminal Differentiation and Cell Cycle Exit in Drosophila melanogaster. University of Michigan - Ann Arbor.

Morel, V., & Schweisguth, F. 2000. Repression by Suppressor of Hairless and activation by Notch are required to define a single row of single-minded expressing cells in the Drosophila embryo. Genes & Development, 14, 377–388. www.genesdev.org

Moshkin, Y.M., Mohrmann, L., van Ijcken, W.F.J., Verrijzer, C.P., 2007. Functional Differentiation of SWI/SNF Remodelers in Transcription and Cell Cycle Control. Mol Cell Biol 27, 651–661. https://doi.org/10.1128/mcb.01257-06

Skene, P.J., Henikoff, S., 2017. An efficient targeted nuclease strategy for high-resolution mapping of DNA binding sites. Elife 6, 1–35. https://doi.org/10.7554/eLife.21856

Vázquez, M., Moore, L., Kennison, J.A., 1999. The trithorax group gene osa encodes an ARID-domain protein that genetically interacts with the Brahma chromatin-remodeling factor to regulate transcription. Development 126, 733–742. https://doi.org/10.1242/DEV.126.4.733

Zambanini, G., Nordin, A., Jonasson, M., Pagella, P., Cantù, C., 2022. A new CUT&RUN low volume-urea (LoV-U) protocol optimized for transcriptional co-factors uncovers Wnt/β-catenin tissue-specific genomic targets. Development 149. https://doi.org/10.1242/DEV.201124